UNIVERSITÀ DEGLI STUDI DI SASSARI

DOTTORATO DI RICERCA IN SCIENZE E TECNOLOGIE CHIMICHE

INDIRIZZO: SCIENZE CHIMICHE

"Synthesis of amides from aldehydes and amines via C-H bond activation and discovery and development of novel and selective carbonic anhydrase inhibitors"

COORDINATORE:

Prof. Stefano Enzo

SUPERVISORI:

Dott. Mario Sechi

Dott.ssa Lidia De Luca

DOTTORANDO:

Dott.ssa Roberta Cadoni

XXVII CICLO

(Triennio 2011-2014)

Citazione

"Sia la meta cui giungi il punto onde tu muovi per tendere a nuova meta."

Arturo Graf, **Ecce Homo**, 1908

Dedica

A Pietro,
perché mi incoraggia ogni giorno.

Introduction

The present thesis reports ideas, experiences, experimental work and results pursued during the PhD course. In the first chapter is described the work done during the first year of my PhD experience in the laboratory of organic chemistry, under the supervision of Dr. Lidia De Luca. More precisely, it details on the methodology developed for the synthesis of amides from aldehydes and amines by proper activation of the aldehydic C-H bond. The technique involves the formation *in situ* of *N*-chloro amines, followed by addition the appropriate aldehyde, which mixture in the presence of TBHP and $Cu(OAc)_2$, leads to the formation of a new CN bond. The method has been proposed as a facile synthesis of amides variously substituted and in good yields.

The second chapter reports the projects carried out under the supervision of Dr. Sechi in the laboratory of medicinal chemistry, during the second and the third year of my PhD internships. During this period, I focused on the development of novel and selective carbonic anhydrase inhibitors (CAIs). This chapter is divided into four subchapters including a) the application of the "click chemistry" as a powerful synthetic approach for the generation of sulfonamide-based inhibitors; b) the synthesis of a set of derivatives belonging to a previously indentified *hit* compound bearing the trifluorodihydroxypropanone moiety, and the strategy adopted for its biological optimization; c) the design and development of novel pyrazole-carboxylic acids derived from a previously identified *lead compound,* as well as its pharmacobiological optimization; d) the synthesis of potential

carbonic anhydrase inhibitors carrying a benzoxaborole scaffold, carried out during the last year of my PhD at the laboratory of Prof. Jean-Yves Winum, at the Institut des Biomolecules Max Mousseron University of Montpellier II (France) within the program “Erasmus placement”.

INDEX

CHAPTER 1:

CHAPTER 2:

Chapter 1:

Synthesis of amides from aldehydes and amines via C-H bond activation

1.1 Introduction

Amides are prevalent structural motifs that are found in biological systems, such proteins, as well as in natural products and synthetic intermediates.[1]

Amide bonds are not limited to biological systems and are indeed present in an immense array of drugs. In fact, more than 25% of known pharmaceutical compounds contain the amide group.[2]

In **Fig. 1** are shown some amide-bond containing drugs actually widely present in the market: Atorvastatin (**1**), used for lowering blood cholesterol and for prevention of the events associated with cardiovascular diseases; Lisinoprin (**2**) used for the treatment of hypertension; Valsartan (**3**), which blocks the action of angiotensin, dilates blood vessels and reduces blood pressure; Diltiazem (**4**), a calcium channel blocker, used to treat hypertension, angina and certain heart rhythm disorders.

Fig. 1 Examples of top drugs containing an amide bond.

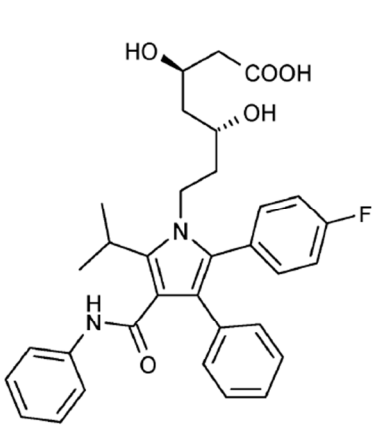

1 Atorvastatin

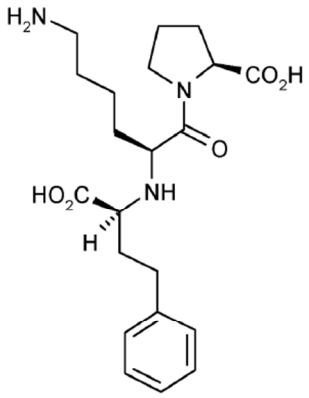

2 Lisinopril

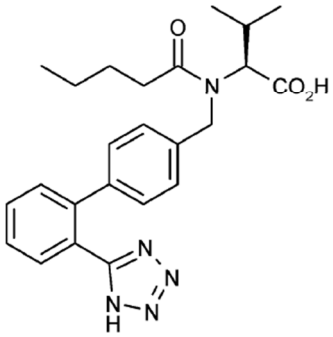

3 Valsartan

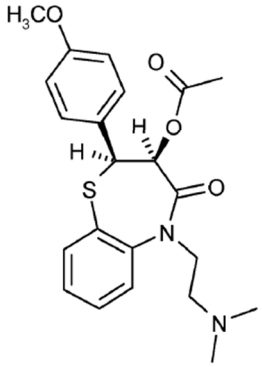

4 Diltiazem

As a consequence, the synthesis of amides has attracted considerable interest and a number of methods have been devised.

1.2 Conventional approaches for the synthesis of amides

Amide bonds are typically synthesized by acylation of amines with carboxylic acid derivatives (acid chloride, anhydride, active esters, etc.) because the unification of amine and carboxylic acid does not occur spontaneously at room temperature but take place only at high

temperatures,[3] conditions typically detrimental to the integrity of the substrates.

1.2.1 Acylation of amines with carboxylic acid derivatives

To activate the carboxylic acid moiety is necessary to convert the hydroxyl group of the acid into a good leaving group prior treatment with the amine, using coupling reagent to generate compounds such as acid chlorides, anhydrides, or active esters (**Scheme 1.1**).

Scheme 1.1

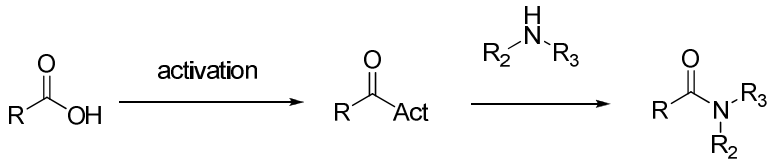

Hundreds of coupling reagents have been reported for this scope: carbodiimides have been used as activators for decades in solid-phase and solution peptide synthesis. They still hold their place, though in recent years two classes of coupling reagents became popular, the phosphonium- and the aminium-(imonium-) type reagents such as BOP, TBTU, HBTU, HATU (**Fig. 2**).

Fig. 2 Structure of the phosphonium-and the aminium-(imonium-) coupling reagents.

STRUCTURE OF COUPLING REAGENT	IUPAC NAME
BOP 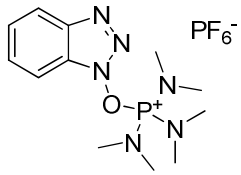	(Benzotriazol-1-yloxy)tris(dimethylamino)phosphonium hexafluorophosphate
TBTU 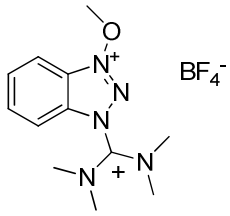	o-(benzotriazol-1-yl)-*N,N,N′,N*'-tetramethyluronium tetrafluoroborate
HBTU 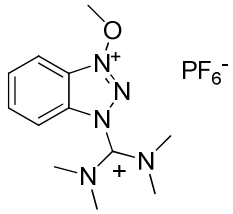	o-(benzotriazol-1-yl)-*N,N,N′,N*'-tetramethyluronium hexafluorophosphate
HATU 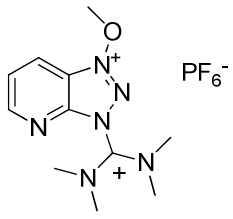	o-(7-Azabenzotriazol-1-yl)-*N,N,N′,N*′-tetramethyluronium hexafluorophosphate

These compounds have achieved high coupling rates accompanied by few undesired side reactions.[4]

Although acylation of amines with carboxylic acid derivatives is a frequent methodology used in the synthesis of current pharmaceuticals, accounting for 16% of all reactions, this strategy, besides utilizing hazardous reagents, has the innate drawback of producing a stoichiometric amount of waste product.

1.2.2 Alternative methods for amide synthesis

To circumvent the problems mentioned above, alternative methods for amide synthesis were developed (**Scheme 1.2**):

- alternative Staudinger reaction[5] by coupling of an azide group and a specifically engineered triarylphospine;
- the Beckmann[6] rearrangements, that efficiently convertes oximes into amides with very high selectivity using ruthenium or triphosphazene, 1,3,5-triazo-2,4,6-triphosphorine-2,2,4,4,6,6-chloride (TAPC) as catalysts;
- aminocarbonylation of aryl chloride[7] at atmospheric carbon oxide pressure and at moderate temperatures, employed for a wide range of aryl chlorides and amines;
- a non-conventional amide synthesis via iodonium-promoted nitroalkane–amine coupling which provides a conceptually innovative approach to amide and peptide synthesis;[8]
- direct amide synthesis from alcohols with amines or nitroarenes;[9]
- hydroamination of alkynes;[10]
- amidation of thioacids with azides;[11]
- transamidation of primary amides.[12]

Scheme 1.2 Examples of newer methodologies for amide bond formation.

Staudinger ligation

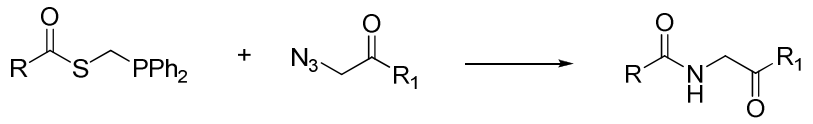

Beckmann rearrangement

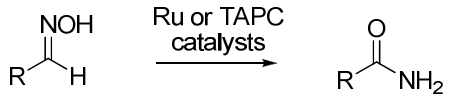

TAPC = 1,3,5-triazo-2,4,6-triphosphorine-2,2,4,4,6,6-chloride

Iodonium-promoted nitroalkane-amine coupling

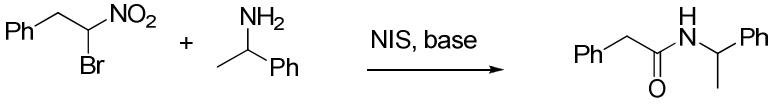

NIS = N-iodosuccinimide

Despite this great number of available synthetic pathways to obtain the amide bond, most of these are not utilized in industry due to their drawbacks such as the use of expensive transition metal catalysts, limited substrate scope, harsh reaction conditions, etc.

1.3 Formation of new bonds via C-H bond activation

The term "C-H activation" refers to reactions involving the cleavage of an unreactive C-H bond of alkanes, arenes, or alkyl chains by transition metal complexes to form products with metal-carbon bond. Many efforts have been devoted to the design and synthesis of new reagents and catalysts

that can affect C–H activation, and transform this bond into target functional groups (**Fig. 3**).

Fig.3 Representative oxidative transformations of C–H bonds.

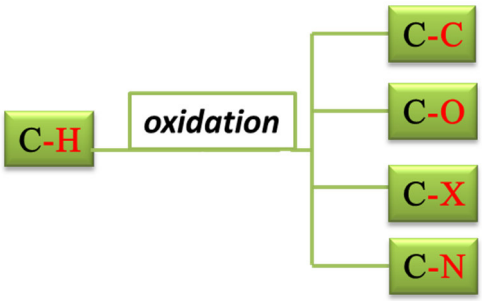

1.3.1 C-H bond activation for Carbon-Carbon and Carbon-Oxygen bond formation

The vast majority of transition-metal catalyzed C–H oxidation reactions have focused on the transformation of C–H bonds into C–C bonds,[13] because they provide key steps in building more complex molecules from simple precursors. Cross-dehydrogenative coupling, also called *CDC* reaction, is a powerful strategy for the construction of C–C bonds,[14] and a pioneering work by Li et al. in this area showed the activation of two different C-H bonds under oxidative conditions (**Scheme 1.3**). The Account describes that in the presence of simple and cheap catalysts such as copper and iron salts and oxidants [ie, hydrogen peroxide, oxygen, *tert*-butylhydroperoxide (TBHP), and 2,3-dichloro-5,6-dicyanobenzoquinone (DDQ)], to directly transform various sp^3 C-H bonds in other C-C bonds without requiring preactivation,[15] notable progress has also recently been

made in arene-arene coupling *via* the oxidative reaction of sp^2 C-H/sp^2 C-H bonds.[16]

Scheme 1.3 Examples of C-C Bond Formations.

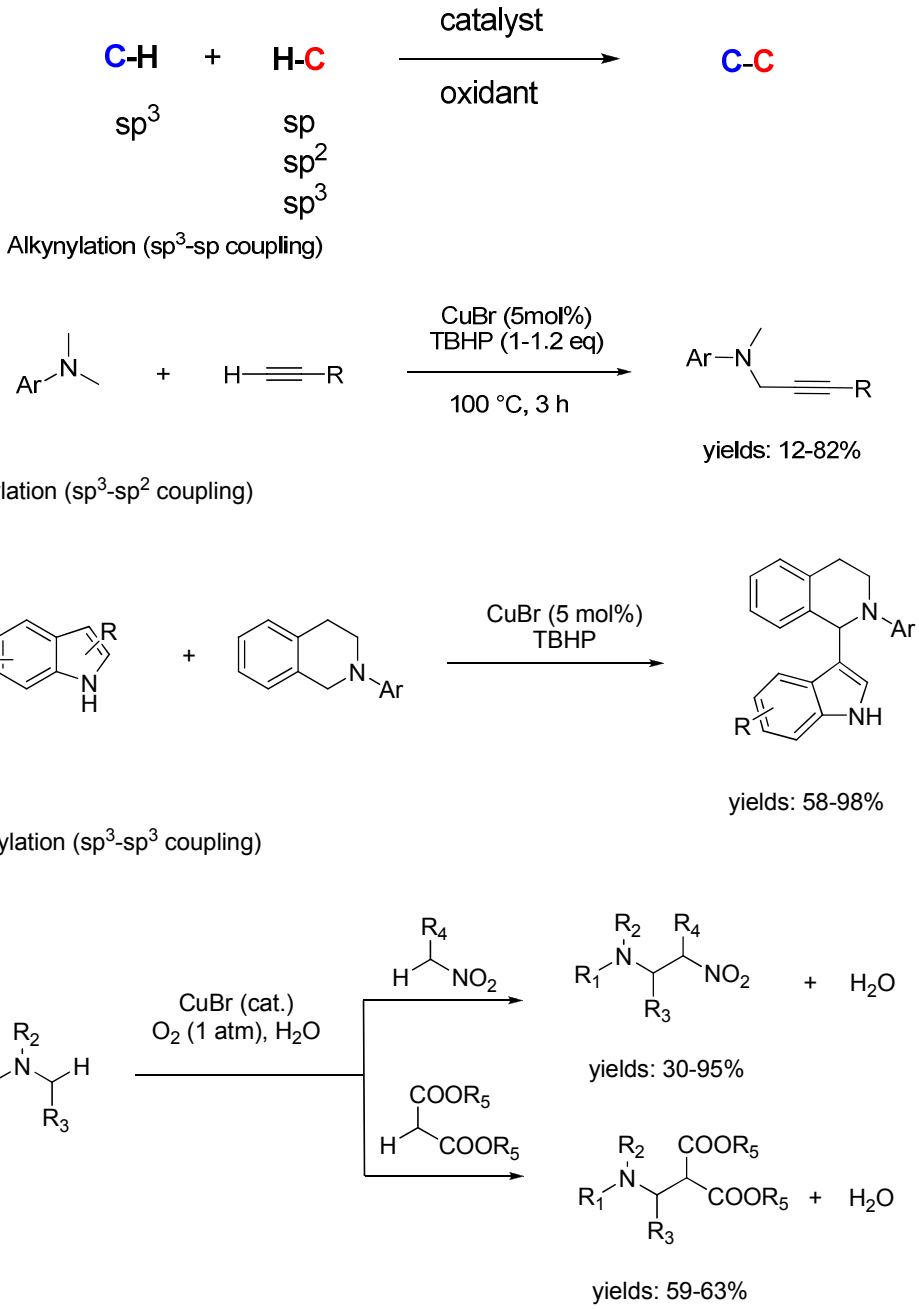

Alkane Alkylation (sp^3-sp^3 coupling)

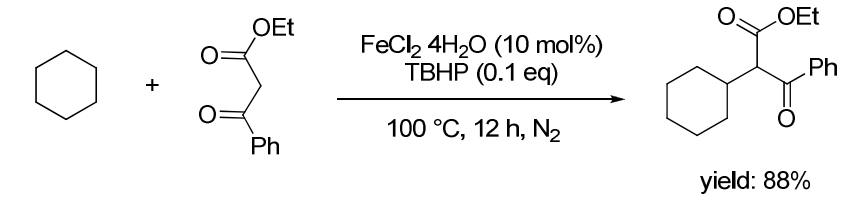

The transition-metal-catalyzed functional-group-directed C-H bond functionalization is used to achieve C-O connections too. C–O bond formation reactions are among the most important processes in chemistry because they provide key steps in building many key molecules, which are useful intermediates in organic synthesis, and are found in an impressive number of biological or natural products.

For example, in 2006 a copper-catalyzed oxidative esterification of aldehydes with β-dicarbonyl compounds was developed using *tert*-butylhydroperoxide as oxidant (**Scheme 1.4**)[17] In general, the enol esters were synthesized in good yields (up to 87%) and high stereoselectivity under the optimized reaction conditions.

Scheme 1.4

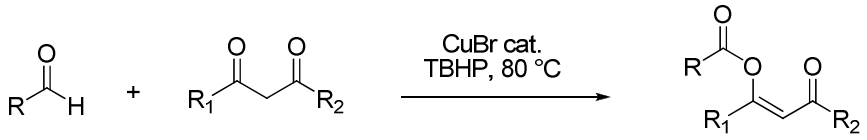

R, R_1= alkyl, aryl
R_2 = alkyl, alkoxyl

In 2010, Beller's group published the first example of iron-catalyzed selective oxidation of the sp^2 C–H bond of arenes and phenols.[18]

Under two types of three component catalytic system ($FeCl_3 \cdot 6H_2O$:H_2Pydic:amine=1:1:2.2), oxidation of 2-methyl-naphthalene and TMP (2,3,6-trimethylphenol) took place in 55% and 77% yield respectively (**Scheme 1.5**). This oxidation reaction offered an important method for the synthesis of vitamin E intermediates and vitamin K3.

Scheme 1.5

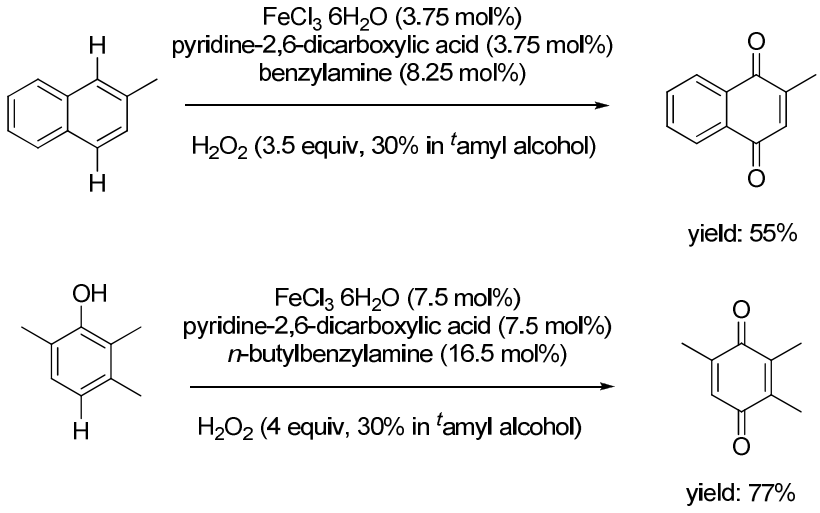

In 2011, Reddy and co-workers developed a copper-catalyzed oxidative C-O coupling reaction for the efficient synthesis of enol and phenol carbamates (**Scheme 1.6**).[19]

Scheme 1.6

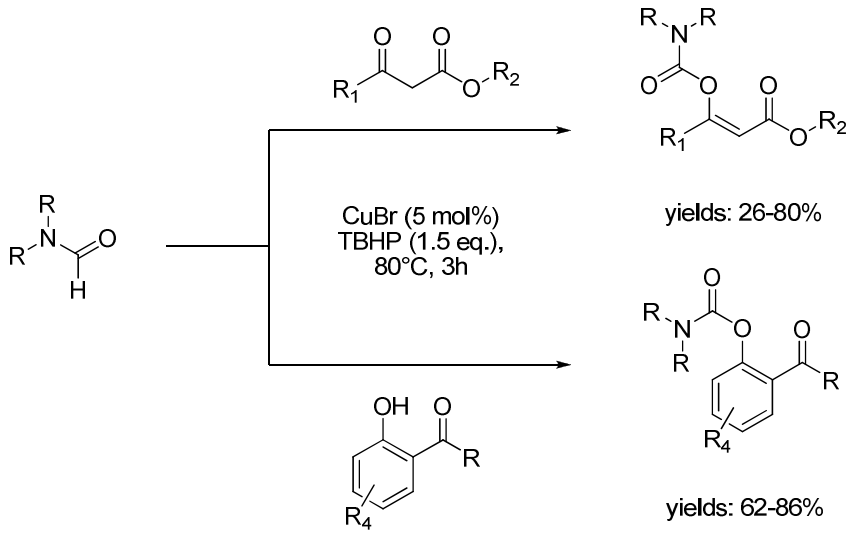

Some of the advantages of this procedure are the simple operations and the phosgene-free, thus avoiding the use of toxic and harmful reagents. Moreover, a high stereoselectivity was achieved for enol carbamates and the present strategy was also extended to oxidative esterification of carbonyl-substituted phenols.

1.3.2 C-H bond activation for Carbon-Nitrogen bond formation

The generation of new methods for direct conversion of C-H bonds into carbon-nitrogen bonds appears to be a critical but appealing challenge in organic chemistry. However, compared with widely developed and age long carbon-carbon and carbon-oxygen bond formations via C-H bond activation, the C-N bond formation from C-H's seems more problematic and was reported just in recent years.[20]

In 2008, Fu and co-workers reported the first example of amidation of benzylic sp^3 C–H bonds by using the efficient, inexpensive and air-stable $FeCl_2$/NBS as a catalyst/oxidant system.[21] Under the best reaction conditions, series of the benzylic reagents underwent amidation reaction in reasonable yields (60-80%) (**Scheme 1.7**), utilizing carboxamides and sulphonamides as amidation agents.

Scheme 1.7

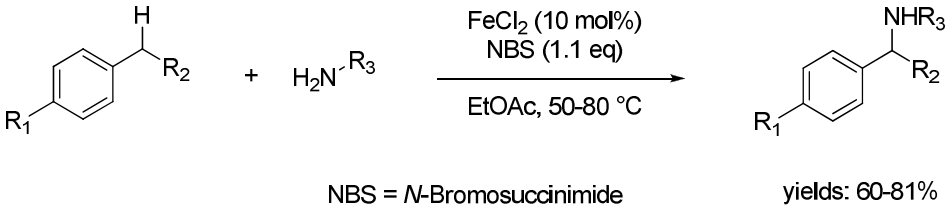

In 2011, Chang and co-workers described an intramolecular oxidative C–N bond formation for the synthesis of carbazoles (**Scheme 1.8**),[22] using diacetoxyiodobenzene as oxidant under Cu-catalyzed conditions and affording high yield of the desired product through very mild reaction conditions.

Scheme 1.8

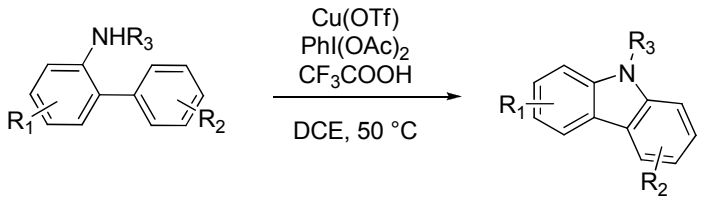

In the same year, Wu and Li described a silver and copper cocatalyzed multicomponent reaction of 2-alkynylbenzaldehyde, sulfonohydrazide, and tertiary amine, which provides a novel and efficient route for the generation of H-pyrazolo[5,1-a]isoquinolines in good yields, under mild

conditions (**Scheme 1.9**).[23] The tertiary amine was activated via the oxidation of an aliphatic C–H bond catalyzed by a dioxygen–copper system and air was used as the oxidant.

Scheme 1.9

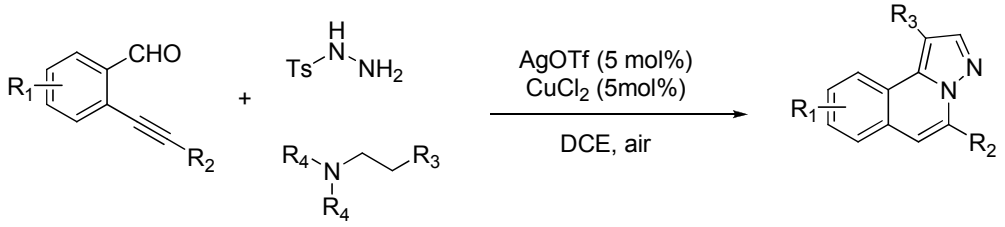

1.3.3 C-H bond activation for the Carbon-Nitrogen amide bond formation

1.3.3.1 Oxidative amidation of aldehyde with amines

Among the emerging amide formation methods, the direct oxidative amidation of aldehydes with amine (**Scheme 1.10**) is an attractive method with practicality and potential industrial applications. In fact, this method is more atom economic and utilizes very cheap and abundant starting materials. The best accepted mechanism of this method consists of the formation of a hemiaminal intermediate, which is subsequently oxidized to the amide.

Scheme 1.10 Accepted mechanism for Oxidative amidation of aldehydes with amine.

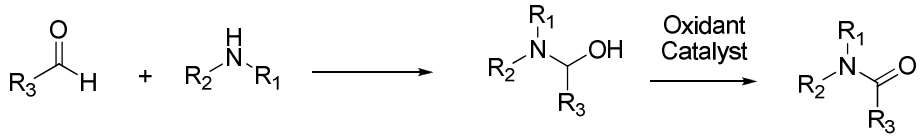

An important advantage of this approach is that C-N bond formation and oxidation are integrated into a single operation while the generation of a free carboxylic acid intermediate, which may not be compatible with other functional groups, is avoided. Although direct oxidative amination of aldehydes utilizes readily available starting materials and is considered an economically attractive alternative to routine amide formation, only a few examples have been reported until 2007. Generally, these reactions are catalyzed by metals, such as Cu,[24] Rh,[25] Ru,[26] Pd,[27] Ni,[28] and Fe.[29]

For example in 2001 Beller's groups employed ruthenium catalysts in oxidative aminations of aldehydes with secondary amines (**Scheme 1.11**).[26]

Scheme 1.11

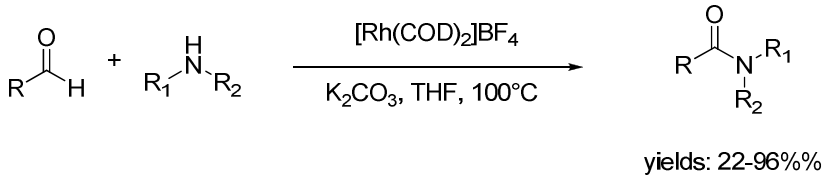

With regards to the mechanism of the rhodium-catalyzed oxidative amination of aldehydes, the authors proposed that the amino alcohol may coordinate to the rhodium(I) complex (**Scheme 1.12**). Dehydrogenation of the amino alcohol yields the corresponding amide and a rhodium(III) dihydride complex, which reduces the aldehyde to the corresponding alcohol, or the aminal to the amine.

Scheme 1.12

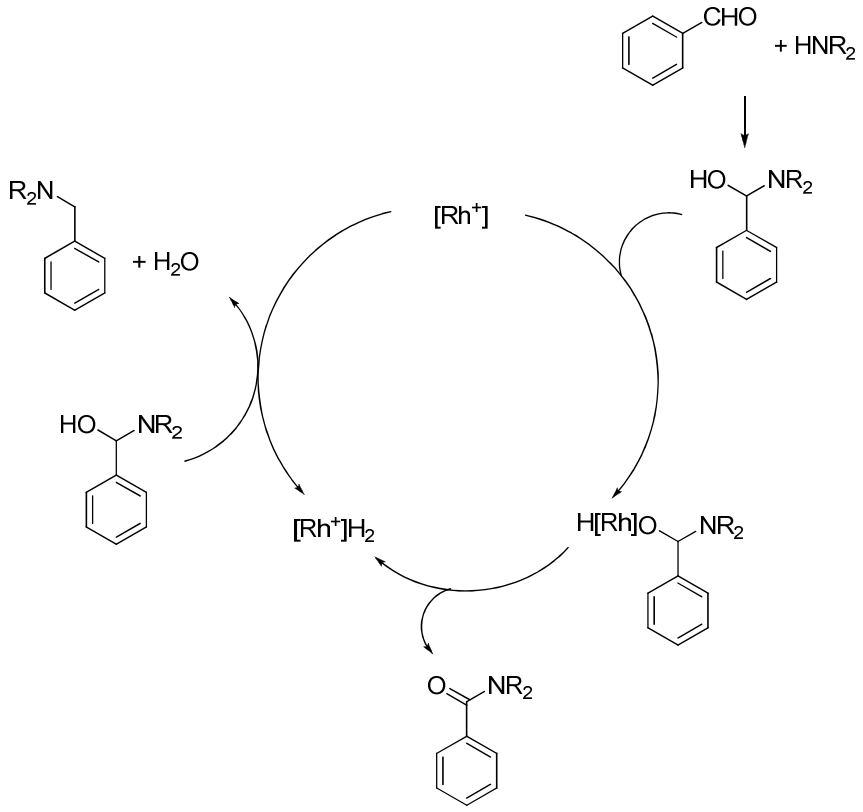

This method could be applied to different substituted aromatic and some aliphatic aldehydes, but only to secondary amines.

In 2006, Li et al. described an elegant copper-catalyzed procedure that allows oxidative amination of aldehydes in the presence of silver iodate (**Scheme 1.13**).[24]

Scheme 1.13

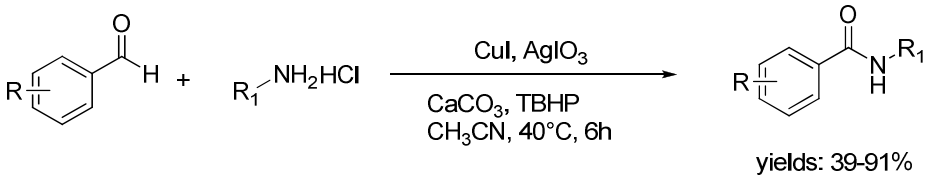

The oxidative amidation was also compatible with a variety of electron-rich and electron-poor aryl aldehydes (yields 39-91%). Interestingly, when the oxidative amidation reaction was applied to optically active amine ester, the reaction proceeded smoothly in high yield without racemization. However, when aliphatic aldehydes were utilized as a coupling partner, the desired amide was obtained with a low yield. In addition, the reaction could be applied only to amine hydrochloride salts, with the need of a base to deprotect the amine.

In 2007 Wolf et al. [30] reported the first metal-free oxidative amination of aldehydes with free amines (**Scheme 1.14**). This method affords amides in 85-99% yield with use of TBHP and in contrast to previously reported procedures, it does not require the use of an expensive transition metal catalyst, base or other additives, or an excess of either the amine or aldehyde, and it avoids harsh reaction conditions. Anyway, this method could be applied only to aromatic aldehydes and secondary amines.

Scheme 1.14

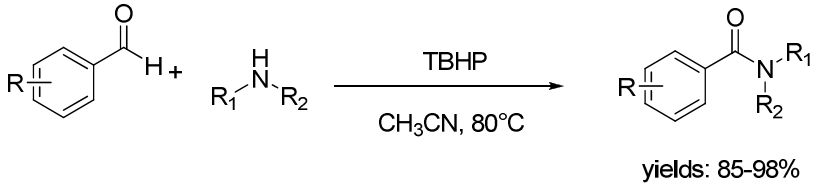

Nevertheless, most of the methods outlined above suffer from drawbacks derived from the steric attributes of the amine and the aldehyde, the formation and stability of the hemiaminal intermediate, the use of expensive transition metal catalysts, the limited substrate scope, and the utilization of coreagents. Therefore, the development of simpler, cheaper and more direct amide formation reactions remains a great goal to pursue.

1.3.3.2 C-H activation for the Carbon-Nitrogen amide bond formation via the radical pathway

In 2012, Wan[31] and Wang[32] published two interesting examples of C-N bond formation via the coupling of radicals. The Wan's paper showed a synthesis that is based upon the coupling of acyl and aminyl radicals. Undoubtedly, a radical process,[33] for example the coupling of acyl- and nitrogen-centered radicals, is a fundamentally different method for the formation of amide bonds. Previously, the same group developed a Bu_4NI-catalyzed *tert*-butyl perester synthesis,[34] in which acyl radicals, generated *in situ* from aldehydes, could be trapped by 2,2,6,6-tetramethylpiperidine 1-oxyl (TEMPO). Inspired by this success, they envisioned the coupling of a nitrogen-centered radical, instead of TEMPO, with the acyl radical to provide a method for amide synthesis. Testing the reaction on 1-naphthaldehyde, Bu_4NI as catalyst and *tert*-butyl hydroperoxide as oxidant (**Scheme 1.15**), they made a screening on a variety of amine derivatives, as *N*-chlorosuccinimide (NCS), *N*-bromosuccinimide (NBS), *N*-iodosuccinimide (NIS), Chloramine-T, hydrazine and hydroxylamine used as potential donors of nitrogen-centered radicals. It was found that DMF is an effective source of aminyl radicals.

Scheme 1.15

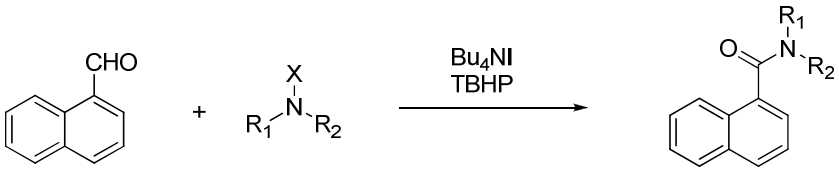

Table 1 Screening on a variety of amine derivatives as potential donors of nitrogen-centered radicals.

Entry	R^1R^2N-X	Yield (%)
1	N-Chlorosuccinimide	<5
2	N-Bromosuccinimide	<5
3	N-Iodosuccinimide	<5
4	Chloroamine-T	<5
5	NH_2NH_2	<5
6	NH_2OH	<5
7	Dimethylformamide	89

As shown in Wan's paper, the procedure is tolerant of different substrates, operationally simple, and easy to scale-up, and for these reasons this is a powerful complement to traditional approaches for the synthesis of amides. However, the methodology cannot be applied to aliphatic aldehydes and the use of formamides limits the scope of reaction only to terziary amides.

In the same year, Wang published the first efficient and direct synthesis of tertiary amides from alcohols and dimethylformamide (**Scheme 1.16**). This

transition-metal-free protocol provides a practical synthetic tool for the construction of *N*-substituted amides, especially *N,N*-dimethyl-substituted amides.

Scheme 1.16

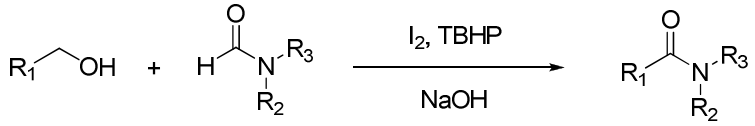

Even though this methodology suffers from some drawbacks (the procedures tolerate the use of only aromatic aldehydes or substituted benzyl alcohols and only *N,N*-disubstituted formamides), the amidation of aldehydes *via* C-H bond activation is a fundamentally different method for amide bond formation.

1.4 Synthesis of amides from aldehydes and amines via C-H bond activation

One of the aim of this PhD work was the development of an alternative and efficient one-pot procedure for the direct amidation of aldehydes with *N*-chloroamines, which can be prepared *in situ* starting from the corresponding amines, by using the *tert*-butyl hydroperoxide as an oxidant, under base-free conditions and catalyzed by an easily achievable copper salt (**Scheme 1.17**).

Scheme 1.17 Synthesis of Amides via a Cross-Coupling between aldehydes and N-chloroamines.

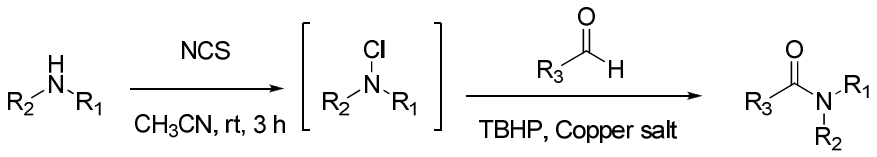

The process described here is simple, highly effective, and makes use of readily available starting materials, thus representing an attractive and suitable method for synthetic chemists.[35]

1.4.1 Optimization of the reaction conditions

Our investigation began by treating 1 equiv. of dibenzylamine **1** (**Scheme 1.18**) with 1.1 equiv. of *N*-chlorosuccinimide (NCS) in dry acetonitrile at room temperature for 3 hours. After detecting the complete conversion of the amine into the corresponding *N*-benzyl-N-chloro-1-phenylmethanamine **2**, the reaction mixture was successively treated, without further purification of the *N*-chloro-amine **2** generated *in situ*, with 5 equiv. of heptanale **3** (**Scheme 1.18**), $Cu(OAc)_2H_2O$ (0.14 mol%), and 5 equiv. of *tert*-butyl peroxybenzoate (TBPB). The resulting reaction mixture was refluxed for about 50 min, and *N,N*-dibenzyleptanamide **4a** was obtained in 38% yield (**Table 2**, entry 1).

In order to study the influence of the different parameters of the second step of the reaction, such as kind of oxidant, catalyst, stoichiometric molar

ratio of reactants and temperature, the same reaction was investigated as a model system.

Our investigation started exploring the use of different oxidants such as *tert*-butyl hydroperoxide (TBHP, 70% solution in water), hydrogen peroxide (H_2O_2) and oxone. It has been observed a significant improvement in yield, from 38% to 76% (**Table 2**, entry 2) performing the reaction with TBHP instead of TBPB, whereas no product formation was detected employing H_2O_2 and oxone (**Table 2**, entries 3 and 4).

Then, we continued our investigation by testing different CuII and CuI salts as catalyst to scan their effect on the formation product. The use of $Cu(Acac)_2$ provided the corresponding amide **4a** with a lower yield (65%, **Table 2**, entry 5) than $Cu(OAc)_2H_2O$. Less interesting results were obtained using $CuCl_2$ and CuBr, giving the amides in 36% and 47% yields, respectively (**Table 2**, entries 6 and 7). Again, no amide formation was observed in the absence of the metal catalyst (**Table 2**, entry 8) or using Bu_4NI as an organocatalyst (**Table 2**, entry 9).

Further optimization studies on the effect of reagent stoichiometry showed that the ratio of aldehyde to amine 5:1 gave better results. In fact, we observed a decrease on the yield when the same reaction is performed with 3.7 equiv. of eptanale (**Table 2**, entry 10). However, at the end of the reaction (**Table 2**, entry 2) and after purification through column chromatography, it is possible to recover 60% of unreacted aldehyde, and the formation of a aldehyde-*tert*butyl peroxyde was not detected. [36]

Moreover, we tried to reduce the number of equivalent of TBHP first trying the reaction with a ratio of TBHP to aldehyde to amine 2.5:2.5:1, but this change led a significant decrement in yield to 25% (**Table 2**, entry 11). Furthermore, we tried to utilize 3.7 equiv of TBHP, fixing the mole ratio of

aldehyde to amine 5:1, but the product yield was lower than using 5 equivalents (**Table 2**, entry 12). Again, no product formation was observed when the reaction was performed without the oxidant (**Table 2**, entry 13). Finally, we devised to change the reaction temperature, performing the experiment at room temperature, but the product was obtained with poor yield (**Table 2**, entry 14).

Scheme 1.18

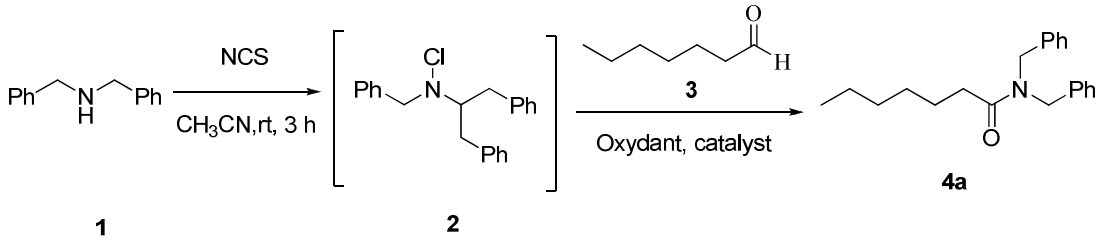

Table 2 Synthesis of Amides: Optimization study

Entry	Oxydant	Catalyst	Yield (%)
1	TBPB	$Cu(OAc)_2 \cdot H_2O$	38
2	TBHP	$Cu(OAc)_2 \cdot H_2O$	76
3	H_2O_2	$Cu(OAc)_2 \cdot H_2O$	-
4	Oxone	$Cu(OAc)_2 \cdot H_2O$	-
5	TBHP	$Cu(Acac)_2$	65
6	TBHP	$CuCl_2$	36
7	TBHP	CuBr	47

8	TBHP	-	-
9	TBHP	Bu_4NI	-
10	TBHP	$Cu(OAc)_2{\cdot}H_2O$	65[a]
11	TBHP	$Cu(OAc)_2{\cdot}H_2O$	25[b]
12	TBHP	$Cu(OAc)_2{\cdot}H_2O$	72[c]
13	TBHP	$Cu(OAc)_2{\cdot}H_2O$	26[d]
14	-	$Cu(OAc)_2{\cdot}H_2O$	-

a Reaction performed with 3.7 equiv. of heptanale. **b** Reaction performed using 2.5 equiv. of eptanale and 2.5 equiv. of TBHP. **c** Reaction performed with 3.7 equiv. of TBHP. **d** Reaction performed at room temperature.

1.4.2 Test of the methodology on different substrates

To examine the general scope of this reaction, the optimized conditions were applied of a variety of commercially available amines and aldehydes. We were pleased to note that this methodology bypassed the limitation of the classical methods of amides synthesis used till now.

In most cases, as determined by disappearance of the *N*-chloro-amine and appearance of a new spot on TLC plate, the reaction was complete in about 50 min (**Scheme 1.19**).

Scheme 1.19

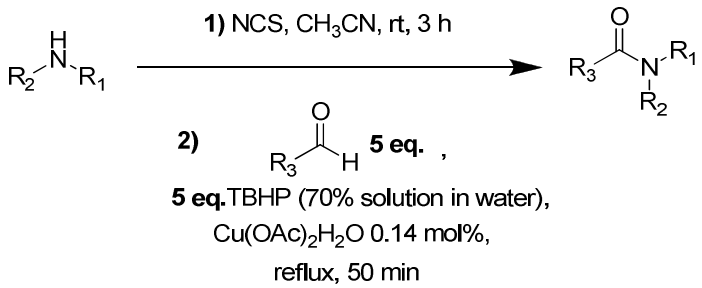

Aliphatic aldehydes provided the resultant amides in good yields (**Scheme 1.20**, 4a-d) even when they were sterically hindered as in the case of pyvalaldehyde and 3,3-dimethylbutanal (**Scheme 1.20**, 4c-d).

Scheme 1.20

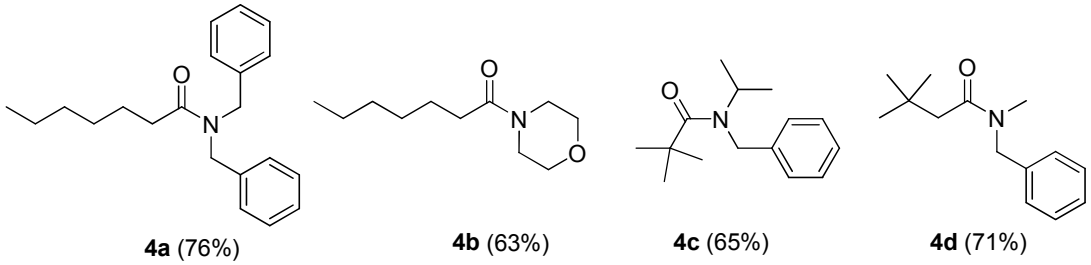

A wide variety of both electron-donating substituents such as benzylic CH and OMe and electron-withdrawing substituents (ie, NO_2 and halide substituent on the aryl moiety of aldehydes) were well tolerated, providing the desired amides in moderate to excellent yields (67-97%). These results suggested that electronic effects do not hamper the reaction progress (**Scheme 1.21**, 4e-i) and, in general, substituents at different positions on the phenyl ring do not have a significant effect on the reaction efficiency.

Scheme 1.21

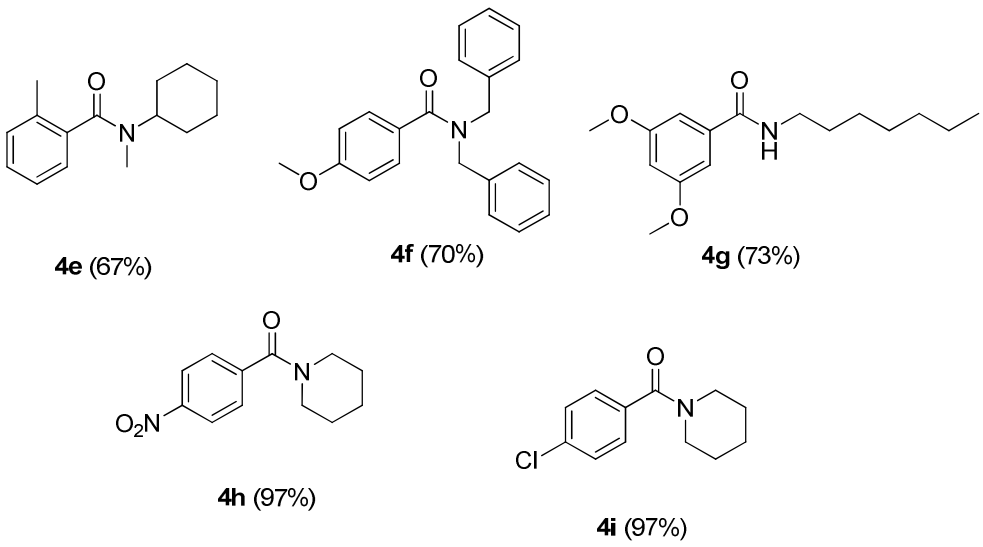

4e (67%) **4f** (70%) **4g** (73%)

4h (97%) **4i** (97%)

Aromatic aldehydes with carbonyl substituents such as carboxymethyl ester or acetyl gave good results, too (**Scheme 1.22**, 4i,j). The different functional groups of these last substrates could be very useful because they provide further opportunities for subsequent chemical manipulations to increase the molecular diversity/complexity on the amides scaffold.

Scheme 1.22

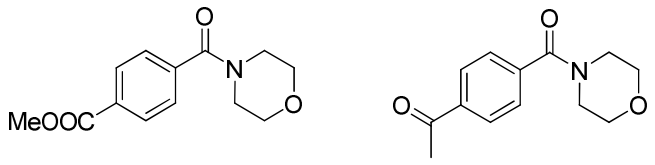

4j (62%) **4k** (85%)

This protocol has also proven to be effective with thiophene-2-carbaldehyde, affording the desired heteroaryl amide (**Scheme 1.23**, 4l) in good yield and allowing the introduction of heterocyclic rings into the amide skeleton.

Scheme 1.23

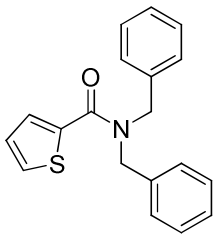

4l (73%)

In addition, we tested the methodology on a variety of amines, and the results showed an excellent tolerance. The reaction proceeded successfully with both secondary symmetric and asymmetric amines as well with acyclic and cyclic amine (**Scheme 1.24**, 4a-f, h,i, m,n.).

Scheme 1.24

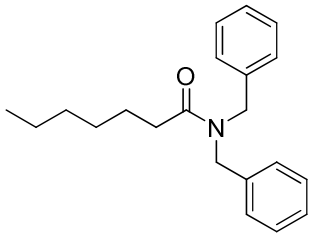

4a (76%)

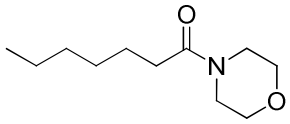

4b (63%)

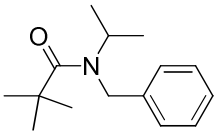

4c (65%)

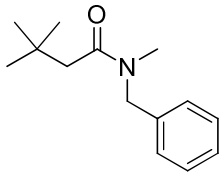

4d (71%)

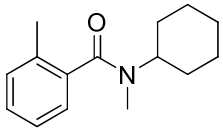

4e (67%)

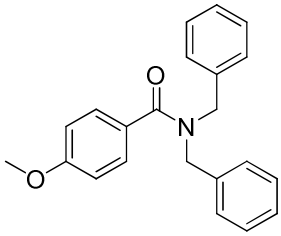

4f (70%)

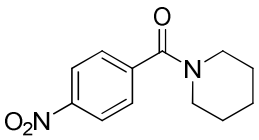

4h (97%)

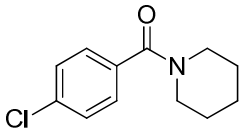

4i (97%)

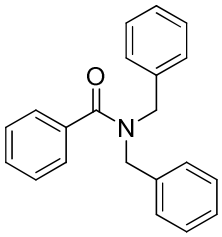

4m (75%)

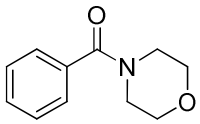

4n (65%)

Noteworthy is the cross-coupling between aldehyde and monosubstituted amine, which occurred under standard conditions allowing the preparation of the interesting *N*-monosubstituted amides that can be selectively functionalized on the NH group (**Scheme 1.25**, 4o-q) .

Scheme 1.25

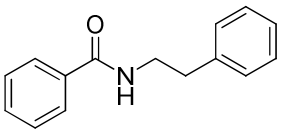

4o (96%)

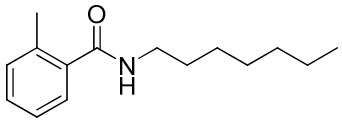

4p (96%)

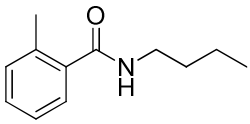

4q (64%)

1.4.2 Elucidation of reaction mechanism

Our data pertaining to the amidation of aldehydes with *N*-chloroamines can be explained by adaption of the mechanism proposed in 1962 by Kochi,[37] who used a series of redox reactions to clarify the formation of the *tert*-butyl peroxides.

We suggest that when 70% aqueous TBHP is added to a mixture of substrates and catalytic amounts of $Cu(OAc)_2$, Cu(II) react with *tert*-butylhydroperoxyde to generate *tert*-butylperoxyradical (**eqn.1**):

EQN.(1) $Cu(II) + tBOOH \longrightarrow Cu(I) + tBuOO\bullet + H^+$

The reaction is carried out in acidic medium, in which *N*-chloroamine is protonated (eqn. 2). Then, the protonate *N*-chloroamine is converted into an amino radical **A** by a redox reaction, as elucidated by Minisci[38] in 1973 (**eqn. 2**), who suggests that this key step involves the elimination of chlorine atom, rather than an electron transfer (**Scheme 1.26**):

EQN. (2) 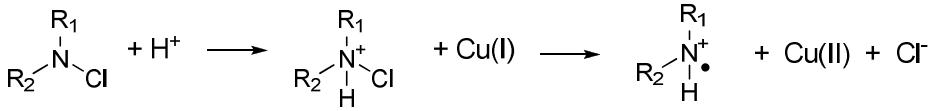

A

Scheme 1.26

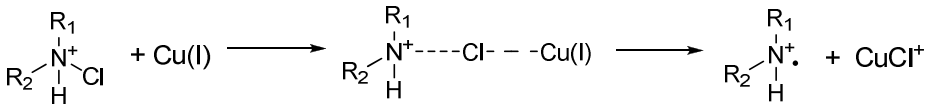

A

After the formation of amino radical, the presence of *tert*-butylperoxy radical generates an acyl radical **B** (**eqn. 3**) on the aldehyde, by abstracting the hydrogen of aldehyde, as reported in literature by Wan[31] and Li,[39] with the consequent regeneration of the *tert*-butylhydroperoxyde.

EQN.(3)

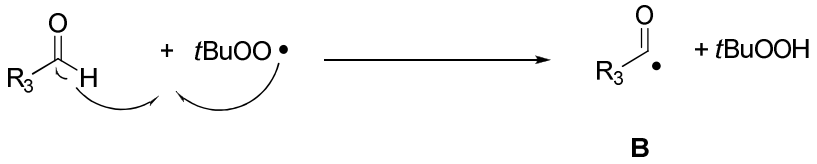

Finally, the acyl radical **B** and amino radical **A** couple to form the expected amide **C** restoring the acid environment of the reaction (**eqn. 4**).

EQN. (4)

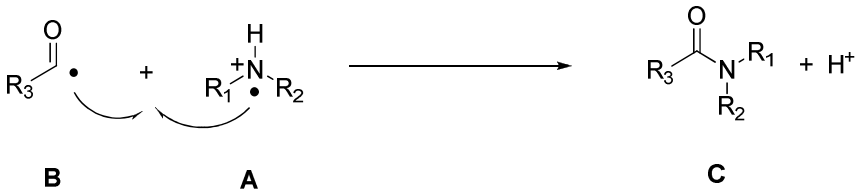

The scheme depicted below summarizes the complete catalytic cycle of the amidation of aldehyde with *N*-chloroamine with TBHP and $Cu(OAc)_2$.

Scheme 1.27 Proposed mechanism of amide formation.

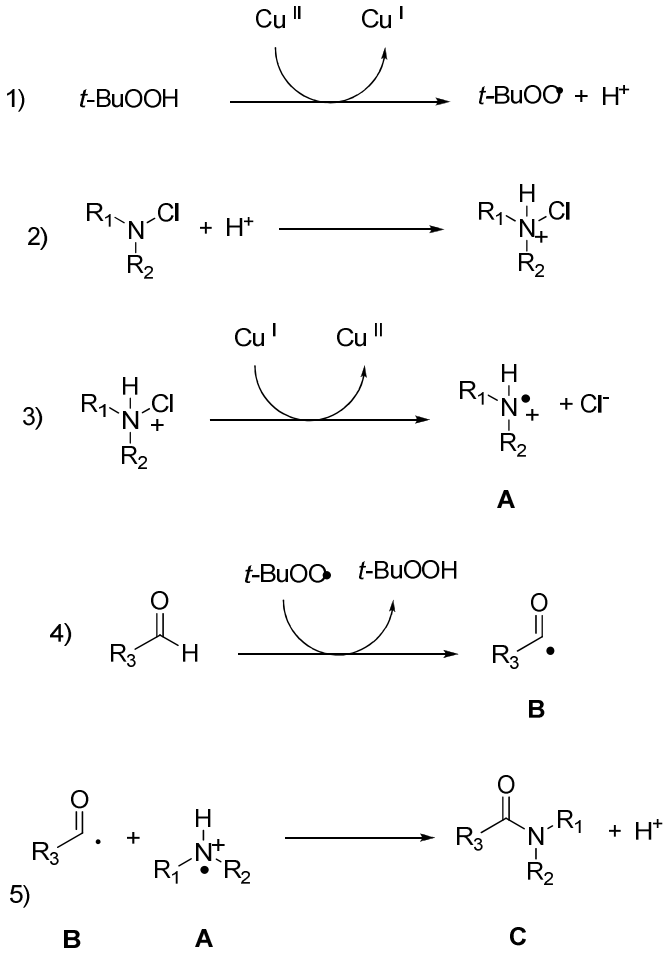

1.4.4 Trapping the acyl radical

To confirm the hypothetic catalytic cycle, we tried to trap the acyl radical, generated *in situ* from benzaldehyde under the investigated reaction conditions, with 2,2,6,6-tetramethylpiperidine 1-oxyl (TEMPO), following Wan[31] and Li[38] procedures, to isolate the TEMPO adduct (**Scheme 1.28**).

Scheme 1.28

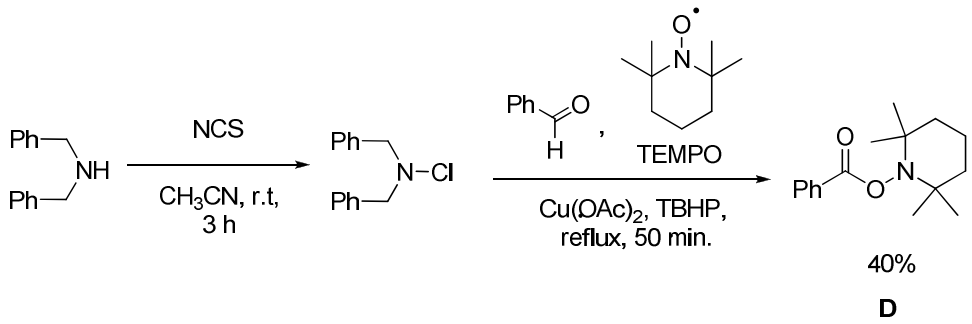

As expected, the TEMPO adduct **D** (**Scheme 1.28**) was formed (instead of the amide) in 40% yield under the optimized conditions, thus confirming the presence in the reaction medium of the acyl radical.

1.4.5 Conclusions and perspectives

In summary, we have reported a novel example of C-N bond formation *via* copper catalyzed C-H aldehyde bond activation, formed by the coupling of the acyl group with an amino radical. Our methodology was employed to prepare different amides directly from aliphatic and aromatic aldehydes and variously substituted amines. The procedure here reported appears to be simple, efficient, rapid, general in scope and uses cheap and easily available reagents.[35]

Additional studies on the mechanistic details, different catalysts, and expansion of the scope of the reaction are currently underway in our laboratory.

CHAPTER 2:

Discovery and development of novel selective Carbonic Anhydrases Inhibitors (CAIs)

2.1 Introduction on Carbonic Anhydrases (CAs)

Carbonic Anhydrases (CAs) are a family of metal enzymes present in prokaryotes and eukaryotes. These enzymes are encoded by five distinct gene families: the α-CAs, present in vertebrates, bacteria, algae and cytoplasm of green plants; the β-CAs, predominantly found in bacteria, algae and chloroplasts of mono and dicotyledons; the γ-CAs, mainly present in archaea and some bacteria; the δ-CAs, present in some marine diatoms, the ε-CAs, which occur exclusively in marine cyanobacteria that contain cso-carboxysomes.[40,41]

All these enzymes catalyze the hydration of carbon dioxide to produce bicarbonate ion and proton:

$$CO_2 + H_2O \rightleftharpoons HCO_3^- + H^+$$

In the active site of the α-, β- and δ-CAs there is a Zn^{2+} ion, which is essential for catalysis, while the active site of γ-CAs probably contain Fe^{2+} (but they are active also with Zn^{2+}or Co^{2+} ions), and the metal ion is usually represented by cadmium in the ε-CAs.[41]

2.1.1 Structure of human CAs

All human CAs (*h*CAs) belong to the α-class and up to now 16 dissimilar *h*-isozymes have been described.[42] These isoforms are identified by the use

of a roman number and differ in their catalytic activity, amino acid sequences and sites of expression (**Table 3**): *h*CA I-II-III-VII-XIII are expressed in cytoplasm; *h*CA IV, IX, XII, XIV are membrane proteins; *h*CA VA and *h*CA VB are mitochondrial isoform; *h*CA VI is secreted in saliva and milk. Again, there are non-catalytic *h*CAs, which are called carbonic anhydrases related proteins (CARPs), but their precise role is not known.

Table 3 Sites of expression of *h*CAs.

Isozyme	Subcellular localization	Catalytic activity (CO_2 hydration)
CA I	cytosol	low
CA II	cytosol	high
CA III	cytosol	very low
CA IV	membrane-bound	medium
CA VA	mitochondria	low
CA VB	mitochondria	high
CA VI	secreted into saliva and milk	low
CA VII	cytosol	high
CA VIII	cytosol	acatalytic
CA IX	transmembrane	high
CA X	cytosol	acatalytic
CA XI	cytosol	acatalytic
CA XII	transmembrane	low
CA XIII	cytosol	low
CA XIV	transmembrane	low

All *h*CA isoforms show high similarity in the primary sequence (the sequence length of CA ranges from 260 to 459 amino acid residues) and this leads to high degree of structural analogy among themselves.[43] In fact, all *h*CAs (except *h*CA VI, IX and XII) exist in monomeric forms composed of seven right handed α-helices, and a twisted β-sheet formed by 10 β-strands (two parallel and eight antiparallel).[44] The CA catalytic domains in transmembrane *h*CA IX and *h*CA XII have a similar, but dimeric structure.[39]

*h*CA II is the most abundant isozyme present in humans and is the most well studied of all *h*CA isoforms. Therefore, the description of its catalytic core has been used a suitable model for the structural comprehension of these enzymes.

The CA active site can be described as a cone-shaped cavity formed by a hydrophobic region (Val121, Val143, Leu198, Val207 and Trp209), and a hydrophilic region (Tyr7, Asn62, His64, Asn67, Thr199 and Thr200). Deep inside of the cavity is located the Zn^{2+}, which is essential for catalysis, tetrahedrally coordinated by three histidines (His94, His96 and His119) which are conserved in all isoforms (**Fig. 3**).[44] Although the core of the active site in α-CAs is highly conserved, there is variability in the polarity of its surroundings. The reason behind the CARPs being non-catalytic has been attributed to the absence of one or more histidines that coordinate the Zn^{2+} ion in the active site of a catalytic *h*CA isoforms.

Fig. 3 Structural representation of *h*CAII. Centrally coordinated zinc atom is shown in orange sphere. Aminoacid residues present in active site pocket are illustrated in stick model.[44]

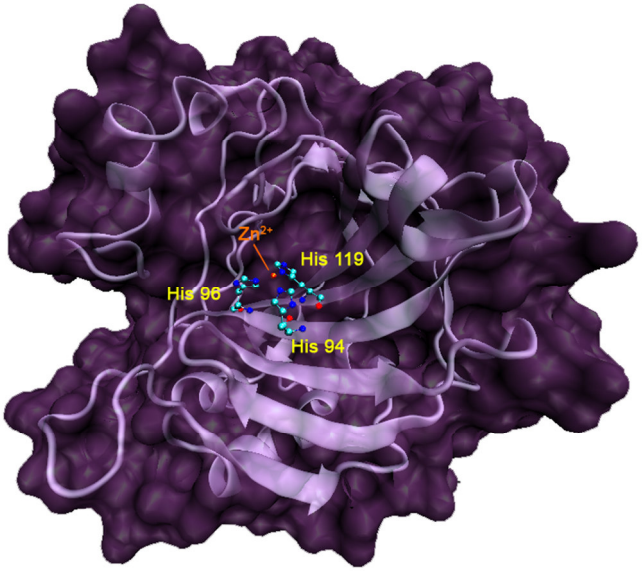

In the active site Zn^{2+} is coordinated also by a water molecule/hydroxide ion as a fourth ligand solvent generating a tetrahedral adduct. This water molecule is involved in a series of hydrogen bonds which enhance its nucleophilicity. In particular, it is bonded with the hydroxyl moiety of a conserved Thr199 and with two water molecules: one is called "deep water", which is located in the hydrophobic cavity, and the other one is located at the entrance of the active site (**Fig.4**).[39] This polyhedral structure is a conserved feature of *h*CAs, which is present among all the catalytically isoforms known.[45]

Fig.4 The active site of *h*CA II, which has been chosen as representative CA isoform. The Zn^{2+} is tetrahedrally coordinated by the three catalytic histidines and a water molecule/hydroxide ion, which is engaged in a well-defined network of hydrogen bonds. Water molecules are indicated as red spheres.[46]

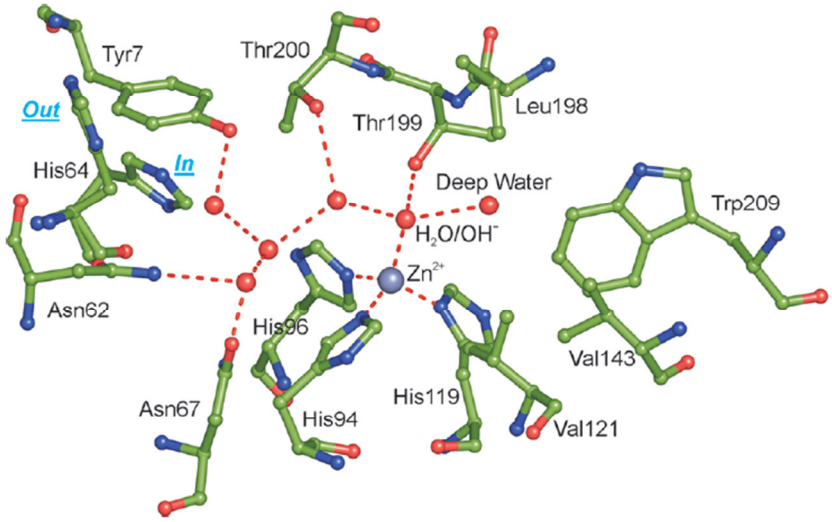

2.1.2 Catalytic mechanism of *h*CAs

The structural evidence on catalytic mechanism of *h*CAs was obtained on 2009 with two independent crystallographic studies showing the entrapment of CO_2 in the *h*CA II active site.[47]

Carbon dioxide is bound within a hydrophobic pocket in an orientation suitable to receive a nucleophilic attack on the carbon atom by the zinc bound hydroxide ion (**Scheme 2.1**). The first step of catalysis is a nucleophilic attack of the active form of the enzyme **A**, with the hydroxide bound to the zinc ion, on incoming CO_2 leading to the formation of bicarbonate coordinated to Zn^{2+} (**Scheme 2.1, C**). The binding of HCO_3^- at the metal is weak and consequently is displaced by a water molecule and liberated into solution, leading to the acid form of the enzyme, with water coordinated to Zn^{2+} (**Scheme 2.1**, **D**), which is catalytically inactive. In order

to regenerate the basic form **A**, a proton transfer reaction takes place. This process, which is the rate-limiting step, may be assisted by the active site residues (such as His 64, the proton shuttle in isozymes *h*CA I and II) or by buffers present in the medium.[40a,48]

Scheme 2.1 Catalitic mechanism of *h*CAs.

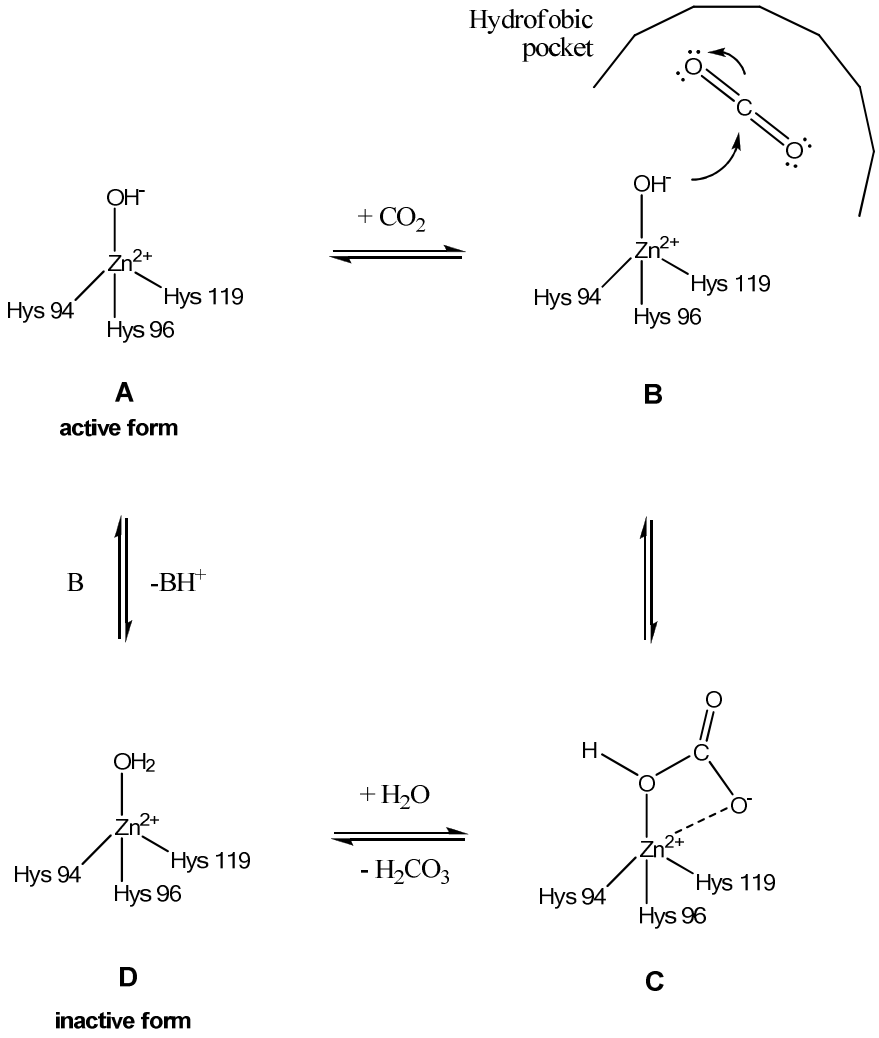

In addition to the physiological reaction, *h*CAs catalyze a variety of other reactions including the hydration of cyanate to carbamic acid, hydration of

cyanamide to urea, hydration of aldehydes to *gem*-diols, hydrolysis of carboxylic or sulfonic acid to esters.[40a] However, up to now, is not clear if these reactions play a significant role in physiological conditions.

2.1.3 Physiological functions of *h*CA isozymes[49]

In humans, the *h*CA isoforms are involved in different physiological processes. *h*CA I, II and IV play an important role in breathing the regulation of acid/base by a) transporting of CO_2/bicarbonate between tissues and sites excretion (kidneys and lungs), b) facilitating the excretion of CO_2 in capillaries and into the tissue microvascular lung, c) removing H^+ ions in renal tubules and collecting ducts, and d) reabsorbing bicarbonate ions within the brush and in the intestinal tract ascending limb of Henle in the kidneys. *h*CA II, IV and XII are involved in the enrichment in baking mood aqueous humor in the eye.[40a,48] The *h*CA II also contributes to the development of bone and osteoclast differentiation. Several isoforms are implicated in the secretion of electrolytes in different organs and tissues, making possible the formation of cerebrospinal fluid, saliva, of gastric juice, bile and pancreatic juice. Some CAs are implicated in the mechanisms olfactory and taste in gastric protection, regulation of the pH of the seminal fluid in muscle function, as well as adaptive phenomena in the processes of cellular stress. *h*CA II, *h*CA VA and *h*CA VB take part in major metabolic pathways such as gluconeogenesis, the biosynthesis of fatty acids and the synthesis of pyrimidine derivatives.[40a,49] *h*CA VI is associated with secretions from glandular tissues, so this distinctive secretory isozyme is specifically expressed in the salivary glands of mammals, and other systems having secretory activities like nasal,

lacrimal, von Ebner's and mammary glands.[50] Among the three transmembrane *h*CAs, isoforms IX and XII are expressed in the gastrointestinal mucosa. *h*CA XIV is present in the brain and retina and is believed to aid in the removal of CO_2 from the neural retina, and helps in modulation of photoreceptor function.[51]

2.1.4 Pathological implications of *h*CAs isozymes

The implication of CAs in a variety of physiological processes showed that abnormal levels or activities of these enzymes have been often associated with different human diseases. Subsequently, in recent years *h*CA isozymes have become interesting targets for the design of inhibitors or activators with biomedical applications. CA inhibitors (CAIs) have been originally used as diuretics, antiglaucoma agents, antiepileptics, and in the management of altitude sickness, antiobesity, and antitumor drugs/diagnostic tools.[40c,42] On the other hand, CA activators may have pharmacological applications in pathologies in which learning and memory are impaired, such as Alzheimer's disease or aging.[52] Some of *h*CAs (such as *h*CA I and II) are ubiquitous and may be both targets for some diseases and off-targets, and in this case their interaction should be avoided. For example, since *h*CA IX and XII can be involved in the proliferation of various hypoxic tumors, these isozymes should be inhibited by compounds which do not affect the activity of CA I, II, VA, and VB.[53] Focusing on *h*CA I, several evidences demonstrated that it is involved in different pathological processes. For example, a decrease of *h*CA I activity in erythrocytes has been correlated to some types of anaemia and chronic acidosis.[54] Interestingly, Gao *et al.* reported that the excessive retinal vascular permeability, a condition that

promotes eye diseases such as the diabetic macular edema and the proliferative diabetic retinopathy, was correlated with a high level of *h*CA I on the extracellular medium.[41,55] Moreover, high level of extracellular *h*CA I in both blood-retinal and blood-brain barrier can induce vasogenic edema.[55] Again, Chang *et al.* observed a significative increased expression of *h*CA I in the synovial membrane in patients affected by ankylosing spondylitis (SA), a condition characterized by bone formation and resorption of chronic inflammated joints.[56,57] The role of *h*CA II has been demonstrated in several diseases, such as glaucoma, edema, epilepsy and, probably, altitude sickness.[58] *h*CA III is involved in the oxidative stress, characterizing a lot of inflammatory diseases. It is not yet understood whether this feature is due to the CO_2 hydration activity of *h*CA III (which is quite low), or to other enzyme properties, such as a different enzymatic activity or the presence of Cys residues on its surface, responsible for the antioxidant effects of this protein.[59] *h*CA IV is surely a drug target for several pathologies, including glaucoma (together with *h*CA II and XII), retinitis pigmentosa and stroke.[60] The mitochondrial isoforms *h*CA VA and VB are targets suited for obtaining antiobesity agents,[61] whereas *h*CA VI is implicated in cariogenesis.[62] *h*CA IX and XII are well-established anticancer drug targets because they have been found to be overexpressed in epithelial tumors including tumours of the cervix, lungs, kidneys, prostate, breast, as well as in neuroblastoma.[42,63] In addition, these isoforms are implicated in allowing tumors to acclimate to a hypoxic microenvironment and promoting metastasis.[64] Furthermore, these isoforms can also be used for imaging of hypoxic tumors.[63a,65] Although *h*CA XII is less investigated, it is also investigated as a putative antitumor target.[63a,66]

2.1.5 Classical CAs Inhibitors (CAIs)

Two main classes of CAIs are known: a) the metal complexing anions, which add to the metal coordination sphere (**Scheme 2.2**, figure **A**) generating a trigonal-bipyramidal adduct, and b) the unsubstituted aromatic sulfonamides, which bind to the Zn^{2+} ion of the enzyme by substituting the nonprotein zinc ligand (**Scheme 2.2**, figure **B**). In the case of sulfonamides, in addition to the Zn^{2+} coordination, an extended network of hydrogen bonds ensues, involving residues Thr199 and Glu106, whereas the aromatic part of the inhibitor interacts with hydrophilic and hydrophobic residues of the cavity within the active site. For anionic inhibitors such as thiocyanate (**A**) the interactions between inhibitor and enzyme are much simpler.[67]

Scheme 2.2 Mechanisms of inhibition of carbonic anhydrase.

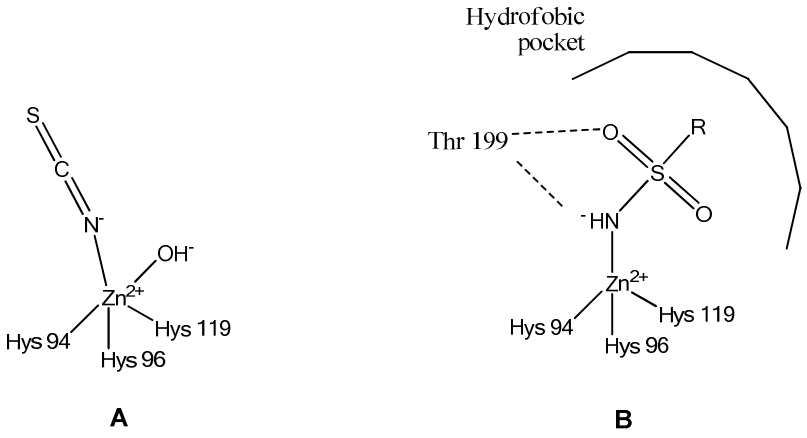

Regarding the metal complexing anions, they are aspecific for the different isozymes, and their reduced structure limits the possibility of their optimization in order to obtain selective CAIs. Conversely, sulfonamide

moieties show a stronge affinity for the Zn^{2+} ion of Cas in comparison to the firsts, and the presence of the aromatic part of these inhibitors make sulfonamides to be useful for the drug design of more potent and selective CAIs.

In the course of the last years, several structure-activity-relationships (SAR) studies combinated with X-ray crystallographic data led to identify a general binding mode of the sulfonamide CAIs, which can be schematized as a structure bearing three main moieties (**Fig. 5**):[42,68] 1) the pharmacophoric motif that binds zinc ion in the active site (ie, the Zinc Binding Function, ZBF), which is fundamental for the inhibitory activity; 2) an aromatic scaffold, which ensures the appropriate positioning of the ZBF in the active site and stabilizes the enzyme–inhibitor complex interacting with the hydrophobic/hydrophilic residues of the active site; 3) a high variable tail, almost always located in pseudo-para or meta position with respect to the ZBF, which is responsible for secondary interactions that confer better stability and high affinity to the enzyme–ligand complex.

Fig. 5 General structure of CAIs.

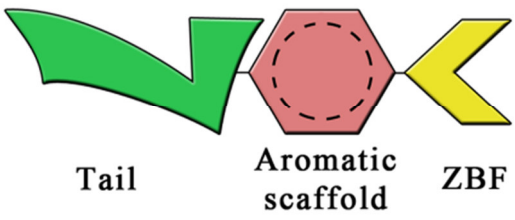

Although sulfonamide CAIs have been clinically used for decades and constitute the most investigated chemical classes of inhibitors (**Fig. 6**), they still possess many undesired side effects, mainly due to their lack of selectivity for the different CA isozymes.[40a,69]

Fig. 6 Examples of sulfonamides CAIs used in therapy (inhibition constant against *h*CA II).

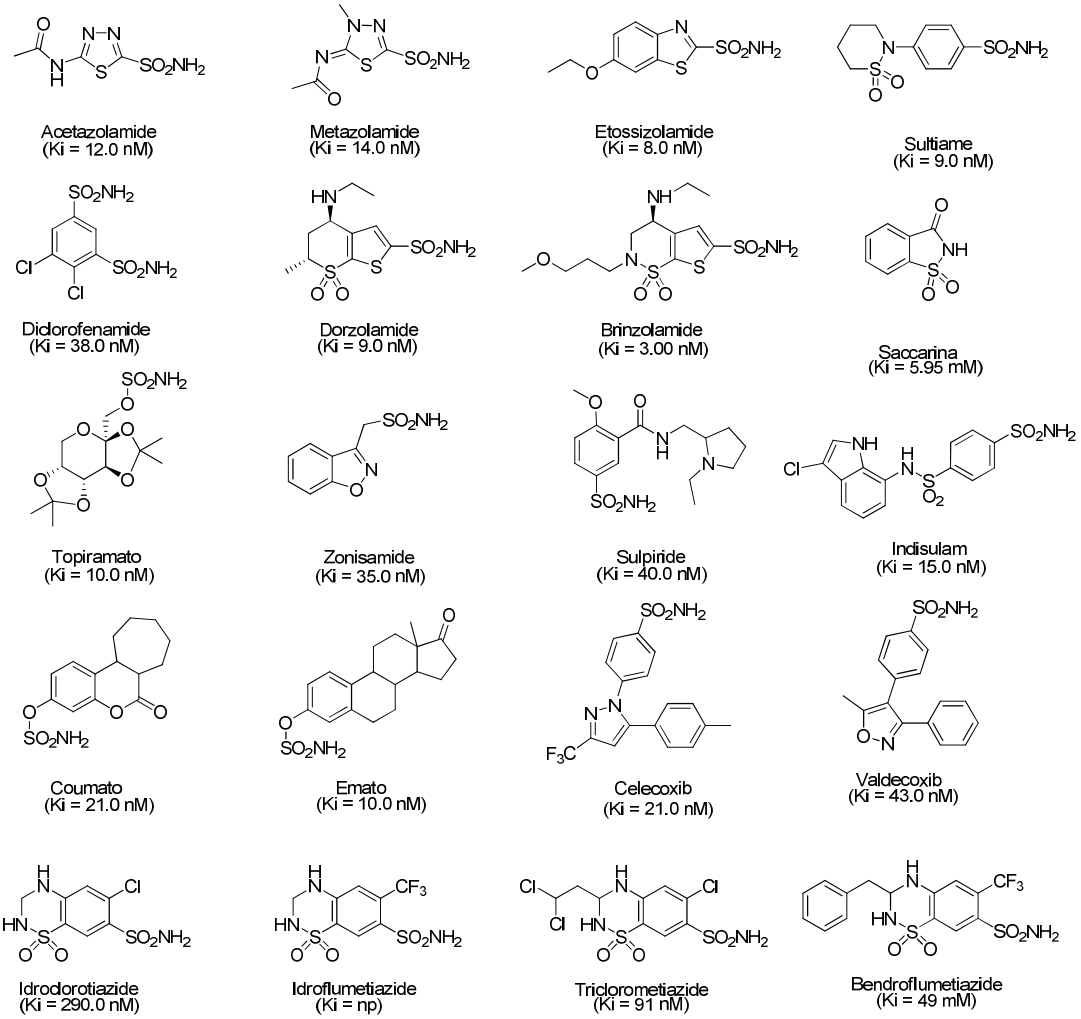

As more CAIs are entering clinical trials, due to both the toxicity and relative non-specificity of the sulphonamide-like functionality, it is important to develop diverse chemical classes of selective inhibitors.

2.2 Rational: work plan

In this scenario, the CA drug design is focused on the development of new inhibitors that combine adequate inhibitory activity and selectivity to specific isoforms, with lower toxic effects than classical CAIs.
Developing isozyme-specific CAIs should be highly beneficial in obtaining novel classes of drugs devoid of various undesired side-effects. This could be obtained by developing:

- **alternative chemical classes** of sulfonamide-CAIs;
- CAIs bearing **different zinc binding function**.

One of the first attempts to optimize pharmacological properties of sulfonamide-CAIs through the replacement of the sulfonamide pharmacophores led to the development of different sets of bioisosters (e.g., derivatives belonging to the sulfamate or sulfamide families) with often indistinguishable properties from sulfonamides. It means that this type of alternative ZBF groups showed the same behavior towards CA isozymes, without showing an interesting selectivity.
For this reason efforts are being made to find novel and original CAIs, in order to explore molecular diversities and to discover original pharmacophores.
In spite of this, to identify novel inhibitors that selectively inhibit specific isoform, and to develop hit/lead compounds able to interfere with CA 'orphan' targets, such as the *h*CA I, as well as *h*CA IX, and *h*CA XII, involved in tumour progression, we decided to focus our attention to the following strategies (**Fig.7**):

- ❖ use *click chemistry* as a powerful synthetic approach for generating inhibitors belonging to the sulfonamide class;

- ❖ structural optimization of *hits* compounds previously identified, bearing original pharmacophoric groups, alternative to sulfonamides.

Fig. 7 Adopted strategies.

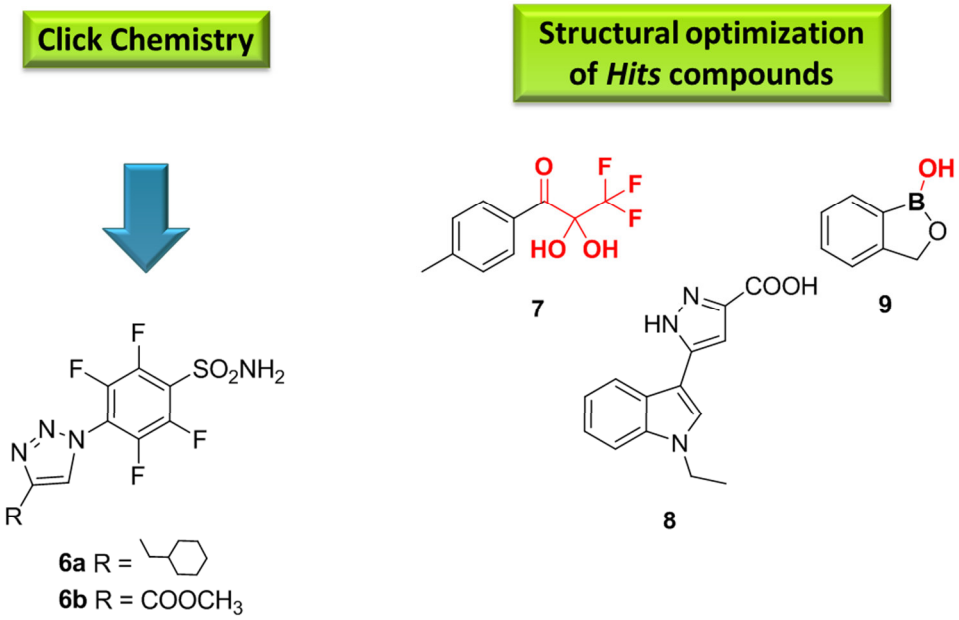

In the following subchapters of this thesis the starting points of each project and the consequent developments are described. The first subchapter reports the "click" approach used for the synthesis of the two model compounds, **6a** and **6b** (**Fig.7**), and the investigation of the binding modes within the enzyme active site obtained by their cocrystallization with *h*CA II.

The second subchapter details the identification of the *hit* compound **7** (**Fig.7**), an original structure bearing a trifluorodihydroxypropanone moiety, and the strategy adopted for its biological optimization.
The third subchapter describes the discovery and development of the *lead compound* **8** (**Fig.7**), which presents a pyrazole-carboxylic acid motif, and its pharmacobiological optimization.
Finally, the last subchapter discusses on the synthetic approach used for the structural expansion of the hit compound **9** (**Fig**.**7**), identified as representative model carrying a benzoxaborole scaffold.

2.3 Click Chemistry as powerful tool for generating CAIs

"Click chemistry" has extensively been used to obtain inhibitors of the metallo-enzyme carbonic anhydrase belonging to the sulfonamide class.[70] Recently, "thiol-ene click chemistry" has been successfully employed to obtain CA inhibitors of the sulfonamide type, which again had excellent inhibitory activity against the tumor-associated isoforms *h*CA IX and XII.[71]

Among click techniques, the copper-catalyzed azide-alkyne cycloaddictions (CuAAC) have acquired a prominent role due to their modularity, the short reaction times, and increased yields. By exploiting the high reactivity of aromatic/heterocyclic sulfonamides incorporating azide/alkyne moieties which were reacted with alkynes/azides, a large number of compounds possessing a variety of chemotypes, difficultly available by other procedures, were synthesized and the obtained compounds were assayed as inhibitors of many mammalian CA isoforms of the 16 presently known. For example, sulfonamides incorporating glycosyl moieties (both protected

and deprotected at the OH groups of the sugar) of type **C**, **E** and **F**,[70] as well as a heterocyclic or aromatic groups (**Scheme 2.3)**, have been obtained, many of which showed excellent inhibitory activity against physiologically/ pathologically relevant isoforms such as *h*CA I, II, IX and XII.[72]

Scheme 2.3 Sulfonamides obtained *via* click-chemistry.

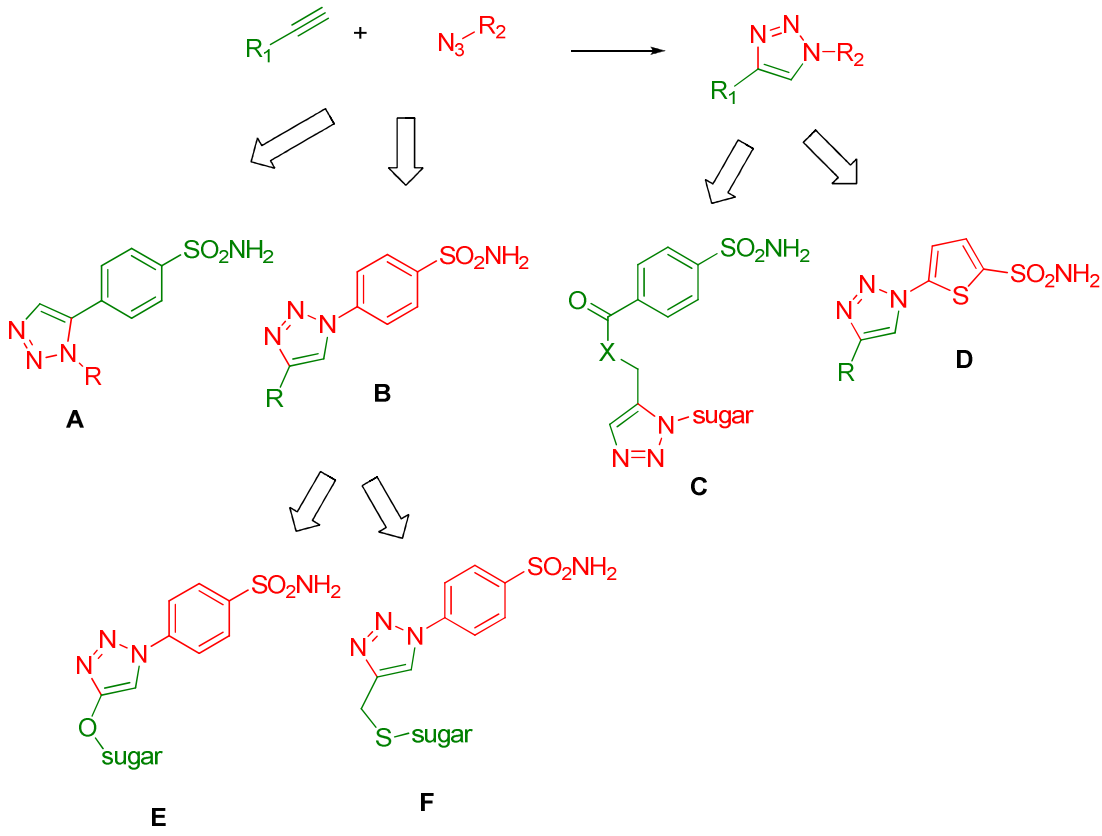

Thus, click chemistry is a powerful tool for generating both chemical diversity as well as novel applications for targeting tumours, based on inhibitors of various CA isoforms with medicinal chemistry applications.

As far as the features to be considered in drug design and discovery process are concerned, fluorine atom has demonstrated several properties that make it extremely attractive, particularly in the biological optimization

process. These characteristics include (a) the small atomic size and the length of the C–F bond, which make fluorine a putative substitute of the hydrogen, without affecting significantly on the molecular geometry; (b) the high electronegativity that induces substantial changes of the physicochemical properties of the molecules (i.e., change in the lipophilicity, decrease of the pKa, and ability to act as H-bond acceptor). Indeed, fluorine atoms are able to alter, often drastically, the binding mode, the affinity, and the selectivity of the molecule for the respective target. For example, perfluorination of benzenes dramatically increases the acidity of substituents.

In this context, the Sechi's group used the click-tailing approach for the synthesis of two homologous series of 4-(R-1H-1,2,3-triazol-1- yl)-benzenesulfonamides **I** and 2,3,5,6-tetrafluoro-4-(5-R-1H-1,2,3-triazol-1-il)benzenesulfonamide **II** incorporating a large variety of different moieties (**Fig**. **8**).[73]

Fig. 8

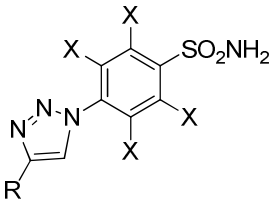

I: X=H
II: X=F

The new compounds were medium potency inhibitors of the cytosolic CA isoforms I and II and low nanomolar/subnanomolar inhibitors of the tumor associated *h*CA IX and XII isoforms.

In order to understand the factors governing inhibitory potency, two representative compounds (**6a** and **6b**, **Fig. 9**) have been selected among the series and were synthetized by using the click approach. In particular compound **6a** was 10.9 times more effective as *h*CA II inhibitor compared to the congener **6b** (K_Is= 41.3 nM and 450 nM, for **6a** and **6b**, respectively). Also, these two compounds resulted the most and the less potent *h*CA IX inhibitors of the fluorinated compounds of the series (K_Is= 1.5 nM and 115 nM, for **6a** and **6b**, respectively).

Then, two X-ray crystal structures of these compounds in adduct with *h*CA II have been solved in collaboration with Prof. McKenna of University of Florida.

Fig.9 Selected compounds.

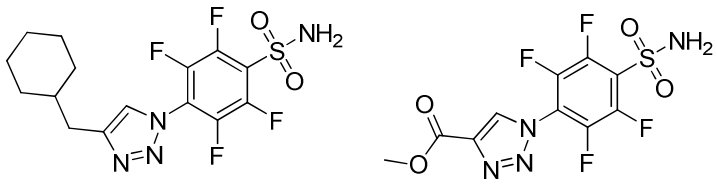

6a **6b**

2.3.1 Chemistry

The preparation of the perfluorinated key intermediate **12** started from pentafluorobenzenesulfonyl chloride **10**, which was converted to the corresponding sulfonamide **11** by reaction with concentrated aqueous ammonia. Since the 4-fluoro atom is the most reactive one for nucleophilic substitution reactions, it has been replaced by the azido moiety, as depicted in scheme below:

Scheme 2.4

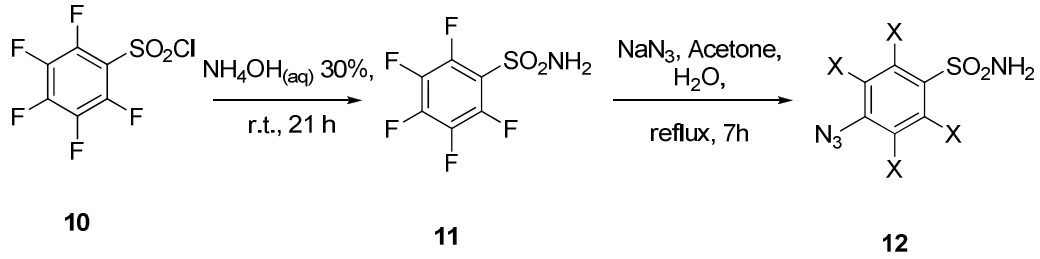

10 **11** **12**

.

The synthesis of the selected compounds **6a,b** was achieved by reacting the azides **12** (incorporating the sulfamoyl zinc-binding group ZBG) with alkynes **13a,b** in the presence of nanosized metallic copper as catalyst (**Scheme 2.5**).

Scheme 2.5

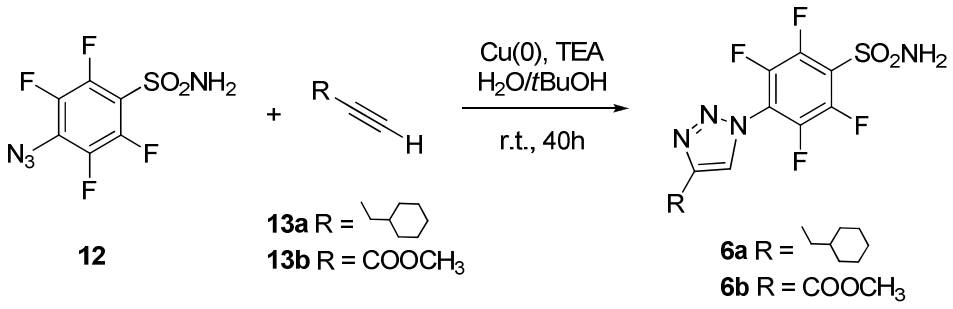

12

13a R =

13b R = $COOCH_3$

6a R =

6b R = $COOCH_3$

2.3.2 X-ray crystallography

The crystal structures of *h*CA II in complex with sulfonamides **6a** and **6b** have been determined (**Fig. 10**) to 1.5 Å resolution. The structures were solved using protocols as previously described (see Table S1 and details in Experimental Section).

Fig. 10 (A) Surface representation of hCA II in complex with **6a** (green) and **6b** (pink) extending out of the active site. (B) Zoomed active site details. Figure was made using PyMOL.

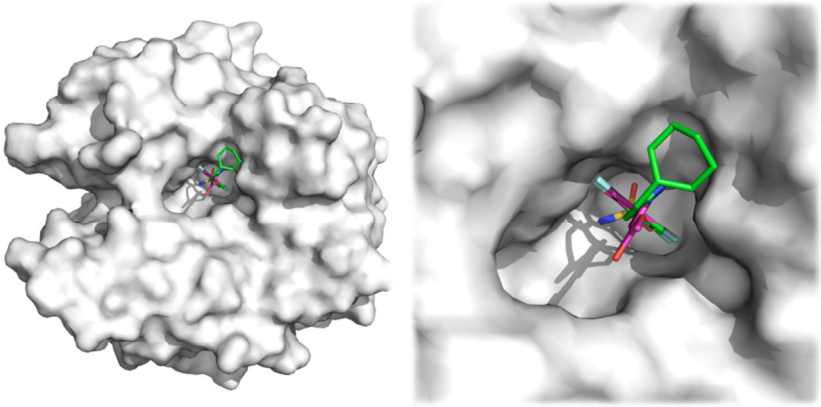

The hydrophobic nonplanar compounds were found buried deep into the active site, displacing the catalytic zinc-bound solvent, such that the nitrogen of the sulfonamide group binds directly to the zinc atom of CA II (distance ≈ 2.0 Å). Hence, the overall Zn coordination can be described as a distorted tetrahedron. The O atom of the site displaces the catalytic zinc-bound solvent, such that the nitrogen of the sulfonamide group binds directly to the zinc atom of *h*CA II (distance ≈ 2.0 Å). Hence, the overall Zn coordination can be described as a distorted tetrahedron. The O atom of the sulfonamide group lied within hydrogen bonding distance (2.9 Å) from the backbone N atom of Thr 199. The tetrafluorophenyl moiety of the inhibitors was stabilized by the surrounding hydrophobic residues (Val121, Leu141, and Leu198) and also exhibited van der Waals interactions with the side chains of Asn62, His64, Gln92, His94, Phe131, and Pro202. However, as the compounds extend out of the active site (**Fig. 10A**), their tail groups became less ordered, with weaker density seen for the tails in the difference map (Fo−Fc) for both compounds. Hence, different

orientations were modeled, and the one that best satisfied the observed data was selected as the final refined structure. The nonpolar, puckered cyclohexyl ring in **6a** was found in the hydrophobic pocket lined by residues Phe131, Val135, Pro202, and Leu204 (**Fig. 10A**). Again, the tail of **6b** was observed to be orientated toward the bulk solvent, not being involved in any hydrophobic or polar interactions with the surface of the protein. Compounds **6a** and **6b** bury a total surface area of 394.3 $Å^2$ (75.0% of its total area) and 328.5 $Å^2$ (67.1% of its total area) with the protein interface and have average B-factors of 18.3 and 19.7 $Å^2$, respectively.[74]

2.3.3 Conclusions

The copper-catalyzed azide-alkyne cycloaddictions (CuAAC) has been successfully employed to obtain CA inhibitors of the sulfonamide type.

The X-ray crystal structure of two such sulfonamides in adduct with *h*CA II provided insights to understand the factors governing inhibitory activities.

Overall, the interactions between the model compounds **6a** and **6b** with *h*CA II are consistent with those seen with the classical, clinically used sulfonamide CAIs.[75] Although **6b** was 10.9 times less effective as a *h*CA II inhibitor compared to the cyclohexylmethyl substituted congener **6a** (K_I **6a** =41.3 nM and K_I **6b** =450 nM), both compounds accommodate similarly within the enzymatic active site. Thus, structural modifications in the aromatic tail dramatically influence the inhibition potenty, without affecting the interaction within the amino acid binding pocket within the catalytic site.

2.4 Development of a novel class of CAIs containing a trifluorohydroxy propanone pharmacophore

In 2011 the Sechi's group in collaboration with Dr. Supuran of the University of Florence, and Dr. Andrea Brancale of the Cardiff University, indentified novel CAIs carrying an original pharmacophore through a combinated ligand- and pharmacophore-based virtual screening approaches.[76]

The key points of the experimental strategy were the following:

- the construction of a suitable pharmacophore model, using a four-point pharmacophore, which consisted by the classical ZBF as metal ligator, two H-bond acceptor functions, and an aromatic hydrophobic region (**Fig. 11**);

Fig. 11 Pharmacophore model represented into the active site. Schematic view and distance geometries of the pharmacophore functions (rectangular insert).

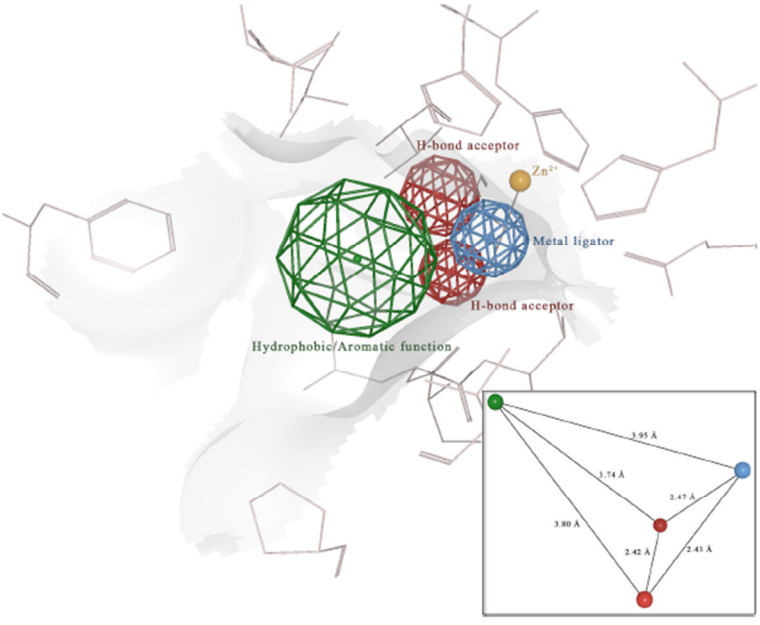

- the virtual screening of free database of commercially available compounds by means of docking procedures;
- the study of the poses on *h*CA II enzyme model of the most interesting selected compounds.

Among these, one compound bearing a trifluoro-dihydroxy-propanone moiety (**Fig. 12**, compound **7**) showed anti-CA II activity in the low micromolar concentration range (Ki CA II = 9 μM, **Table 4**), as predicted by the docking studies. Interestingly, compound **7** (commercially available) resulted approximately 45-fold more active in inhibiting the human CA II isoform with respect to CA I (K_i *h*CA II = 9 μM vs K_i *h*CA I = 410 μM), thus demonstrating similar specificity toward *h*CA II isoform as compared to reference compound acetazolamide (K_i ratios = 45 and 75, for **7** and AZA, respectively).

Fig. 12

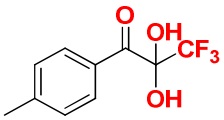

7

Table 4 Inhibition of *h*CA isoforms I and II by compound **7** in comparison with acetazolamide (AAZ; 5-acetamido-1,3,4-thiadiazole-2-sulfonamide) as standard, by a stopped-flow CO_2 hydrase assay.

Compound	**K_i (μM)***	
	*h*CA I	*h*CA II
7	410	9.0
AAZ	0.90	0.012

* Errors in the range of ± 5-10% of the reported value from 3 different assays.

It has also been hypothesized that **7** could be involved in complexation with the Zn^{2+} ion, through the deprotonated dihydroxy system. This putative binding mode has been supported by docking studies, which evidenced an accommodation within the CA active site already demonstrated by sulfonamide-containing compounds.

Presumably, the electron-withdrawing character of the trifluoro-group present on the pharmacophore fragment might contribute in enhancing the acidity of germinal diol, thus favouring its metal chelating properties.

Fig. 13 Proposed binding mode of compound **7**

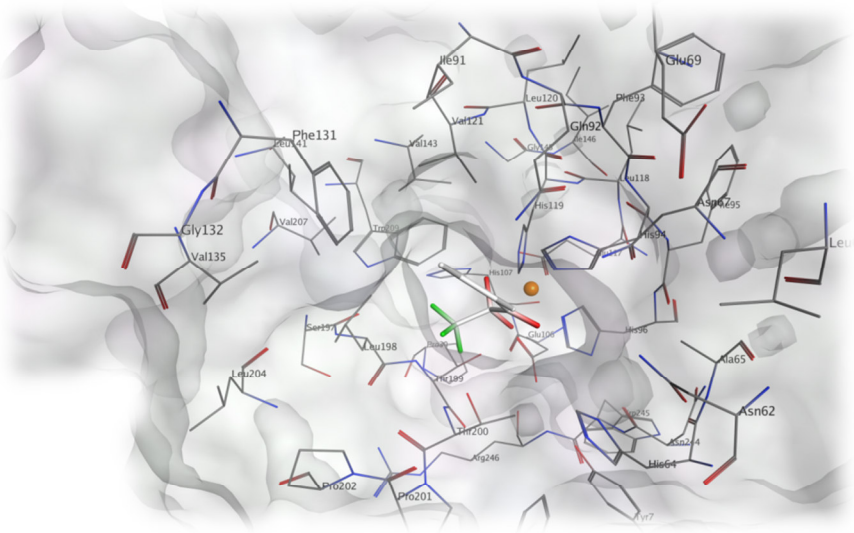

Since the inhibition values of compound **7** fall into the average hit potency values for all VS studies (range from 4 to 19 µM),[77] these fulfill the criteria for a useful *hit*, which must exceed a specific potency threshold against the target (e.g., <10 µM inhibition).[78]

Due to the chemical originality of this new pharmacophore, compound **7** has been proposed as an important bioisosteric alternative to the sulfonamido-based functionalities, thus leading to the development of a new class of CAIs.

2.4.1 Objectives

Like a sulfonamide-based CA inhibitor, compound **7** presents three main components schematized by an aromatic scaffold, in which is located the ZBF (the trifluoro dihydroxy propanone moiety), and a tail constituted by a methyl group as a substituent in *para* position (**Fig. 14**).

Fig. 14 Schematic structure of *hit* compound **7**.

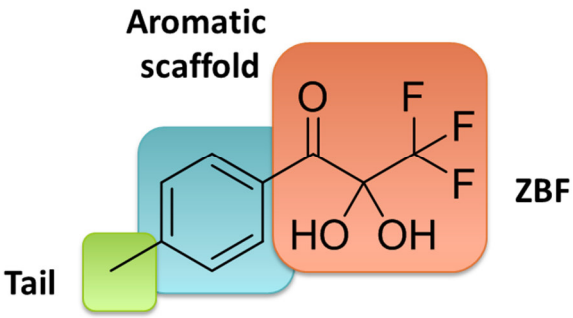

To improve the inhibition profile of the *hit* compound **7,** a series of its derivatives has been designed and synthesized, in order to evaluate the potency towards CA II, as well as that toward other human CA isozymes. Meanwhile, selected derivatives will be crystallised into the target proteins to elucidate their accommodation within the enzyme active site.

In particular, the nature of the tail on the aromatic scaffold of the *hit* compound **7** has been modified by sequential chemical change by a) increasing or decreasing the length of the carbon chain, b) modifying the steric bulk of alkyl substituents (also considering the molecular simplification by synthetizing the analogue without methyl group in *para* position), c) insertion of electron donating group as substituent on aromatic scaffold, d) planning a structure extension (**Fig. 15**):

Fig. 15

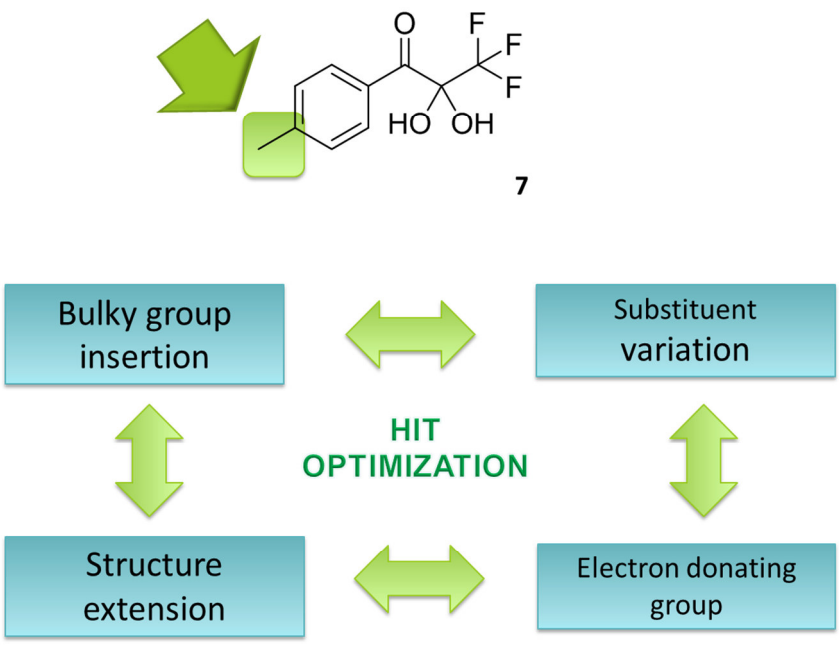

A set of the designed compounds belonging to the series **III** is reported in **Figure 16**:

Fig. 16

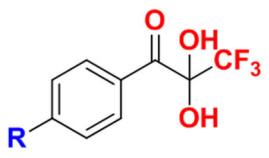

III

	R
III a	H
III b	iPr
III c	OCH_3
III d	*n*-Bu
III e	Ph

2.4.2 Chemistry

A suitable synthetic route for the preparation of the compound **7** and its derivatives has been planned by a multistep synthesis, through a logical approach for disconnecting a complex target molecule via retrosynthetic analysis.

From the literature analysis of the trifluoro dihydroxy propanone moiety of the model compound **8**, it emerged that water adds rapidly to the carbonyl function of aldehydes and ketones to give geminal diols. The hydration reaction is catalyzed by acids and bases, with a reversible mechanism, and the diol can eliminate water to regenerate the aldehyde or ketone. Anyway, the presence of an electron-withdrawing group as substituent in the starting material **14** (as CF_3 in our case) favors the hydrate form **15** (**Scheme 2.6**).

Scheme 2.6

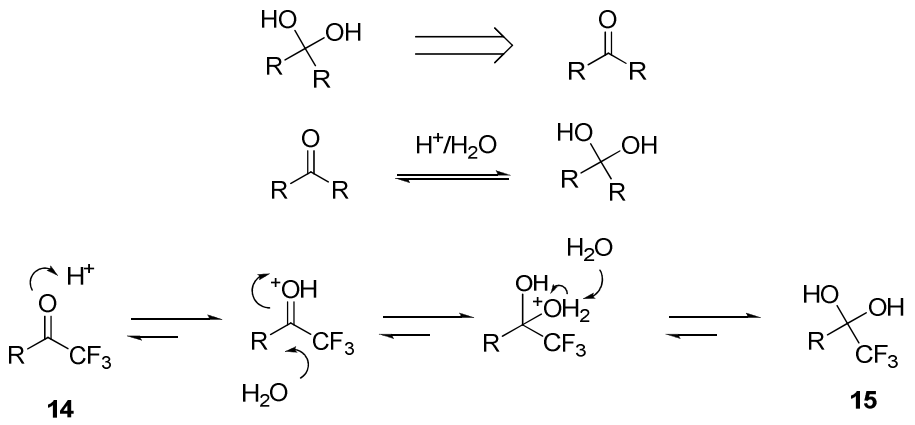

Moreover, the insertion of the trifluoroacetyl group on the starting material **14** could be made using the trifluoroacetyc anhydride agent by well-known procedures[79] (**Scheme 2.7**):

Scheme 2.7

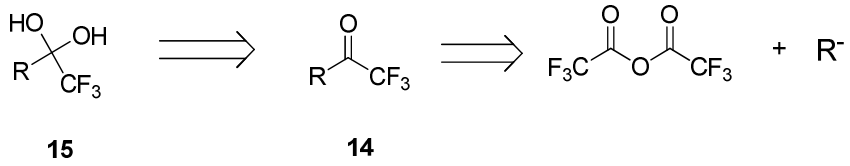

A method for obtaining the compound **7** and some its derivatives was developed in 1988 by Kamitori[80] through a synthetic approach based on the abovementioned observations. The work described the multistep synthesis of trifluorodihydroxy propanone **7,** as depicted the **Scheme 2.8**:

Scheme 2.8

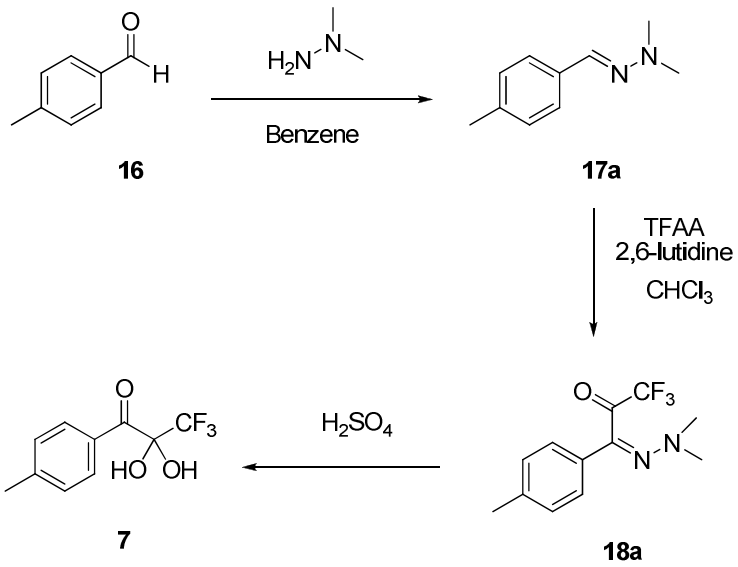

In the first step, the reaction between *p*-tolualdehyde and *N-N'*-dimethyl hydrazine in benzene at room temperature occurs, with the consequent formation of the *p*-tolualdehyde *N,N'*-dimethylhydrazone (**Scheme 2.8**, intermediate **17a**).

Hydrazone is a nitrogen analogue of enamines, and some hydrazones are known to behave as 1,3-dipolar compounds in which the azomethine carbon is a center of nucleophilic attack.[81] However, there are few reports of simple electrophilic substitution at the azomethine carbon,[82] but none involving acylation of this carbon. The Kamitori's paper reports on the electrophilic acylation of aldehyde hydrazones using 2,6-lutidine as base to deprotonate hydrazone (**Scheme 2.9**).

Scheme 2.9

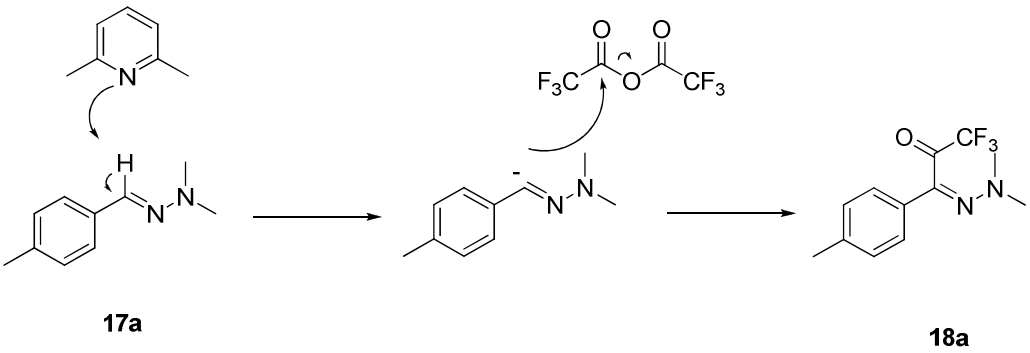

17a **18a**

The work also reports that the acid hydrolysis of the intermediate **18a** with 5N H_2SO_4 at 25°C should lead to the formation of the 1,2-diketones. Otherwise, microanalytical data suggested **7** to be monohydrates in which the carbonyl group far from aromatic ring should be hydrated (**Scheme 2.10**).

Scheme 2.10

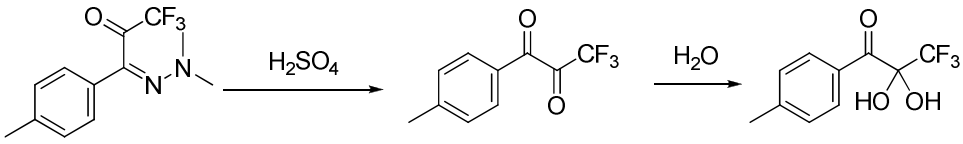

18a **7**

This available synthetic method, used for the preparation of compound **7** has been also tested with variously substituted aromatic aldehydes to give the designed trifluorodyhydroxy propanone derivatives reported in the serie **III**.

To obtain the formation of hydrazones (**17b-f**), benzene has been replaced with dichloromethane as solvent when performing the reaction with solid biphenyl 4-carboxaldehyde, and without using solvent when conducting

the reaction with liquid aldehydes miscible with *N,N'*-dimethyl hydrazine (as for benzaldehyde, and 4-isopropyl/methoxy/butyl benzaldehyde).

Scheme 2.11

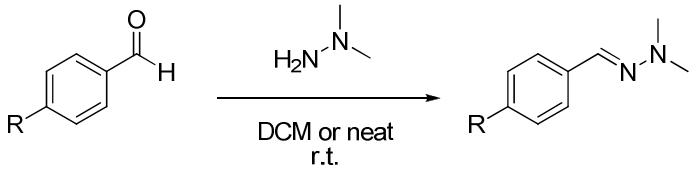

16b R = H
16c R = iPr
16d R = OMe
16e R = Bu
16f R = Ph

17b R = H
17c R = iPr
17d R = OMe
17e R = Bu
17f R = Ph

Regarding the acetylation step, the reaction has been carried out in dichloromethane instead of chloroform, as described in Kamitori's procedures. The optimized parameters to achieve the desired intermediates are shown in **Table 5**.

Table 5

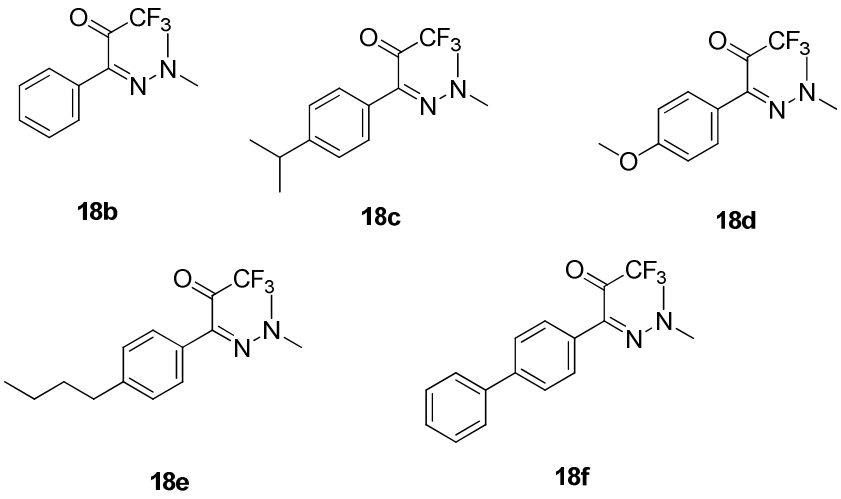

18b **18c** **18d**

18e **18f**

Intermediate	TFAA (equiv.)	2,6-lutidine (equiv.)	Yield (%)
18b	2	2	63
18c	4	3	30
18d	10	3	35
18e	6	3	65
18f	7	4	89

Concerning the acid hydrolysis of trifluoroacetylated hydrazones with 5N H_2SO_4, the procedure works well at room temperature in almost all examples (yielding derivatives of series **III** in the range of 59-82%, **Fig.17**), with the exception if **IIIe**, which needs of heating at 60°C for 24 hours (**Fig.17**, 85% yield).

Fig. 17

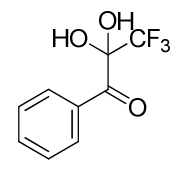

IIIa, 60%

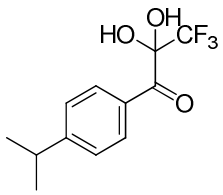

IIIb, 82%

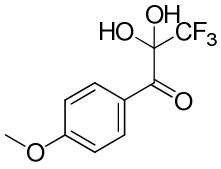

IIIc, 59%

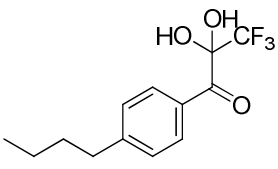

IIId, 74%

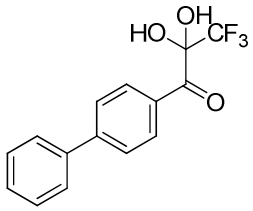

IIIe, 85%

2.4.3 Biological assays

The connection between carbonic anhydrase and cancer is known from approximately fifteen years, since two tumor-associated transmembrane carbonic anhydrase isozymes (*h*CA IX and *h*CA XII) have been identified, cloned and sequenced. These isoforms, in fact, are expressed in a wide variety of malignancies and appear to be tightly regulated by microenvironmental hypoxia.[83] *h*CA IX expression is linked to poor prognosis in a number of human tumors, and it is an established marker of aggressive malignant phenotype and involved in the mechanism of progression.[84] Inhibition of CA IX with sulfonamide- and/or coumarin-based inhibitors was recently shown to lead to a potent retardation for the growth of both primary tumors and metastases.[85]

In contrast to *h*CA IX, *h*CA XII is expressed in a variety of normal human tissues including kidney, colon, prostate, pancreas, ovary, testis, lung, and brain, but its expression appears up-regulated in tumors compared to the corresponding normal tissues.[86] *h*CA IX and *h*CA XII are thus emerged as suitable targets for both diagnostic and therapeutic intervention, particularly on the management of hypoxic tumors normally non-responsive to classical chemio- and radiotherapy.[85]

In this context, *hit* compound **7** and its derivatives were tested for their ability to inhibit the catalytic activities of tumor associated *h*CA IX and XII isoforms, in addition to the the cytosolic CA isoforms I and II. Such enzymatic activities were measured by a stopped-flow technique (**Table 6,** see details in Experimental Section).

Table 6 Inhibition of hCA isoforms I, II, IX and XII with compounds of the series **III**, and acetazolamide (AAZ; 5-acetamido-1,3,4-thiadiazole-2-sulfonamide), used as standard, by a stopped-flow CO_2 hydrase assay.

Compound		**K_I (μM)***			
		*h*CA I	*h*CA II	*h*CA IX	*h*CA XII
7	4-Me-C_6H_4	410	9.0	0.84	9.05
IIIa	Ph	54.3	63.5	4.51	6.86
IIIb	4-iPr-C_6H_4	86.0	>100	0.80	5.87
IIIc	4-MeO-C_6H_4	520	3.2	0.83	24.3
IIId	4-nBu-C_6H_4	17.3	4.7	0.78	19.7
IIIe	4-Ph-C_6H_4	65.7	2.5	5.60	7.21
AAZ	-	0.25	0.012	0.025	0.006

* Errors in the range of ± 5-10 % of the reported value from 3 different assays.

Surprisingly, the *hit* compound **7** showed an interesting inhibitory activity in submicromolar/high nanomolar range against *h*CA IX (Ki 0.84 μM), also demonstrating overlapping activity toward CA II and CA XII (K_is ~9 μM of **7** in both isozymes). As summarized in **Table 6**, with the exception of **IIIa** and **IIIe**, all compounds selectively inhibited *h*CA IX, with K_i values ranging from 0.78 to 0.83 μM, independently from the nature of substituent in the aromatic scaffold. Preliminary SAR indicate that the tail tolerates derivatization with various aliphatic moieties, while complete removal of the substituents (in **IIIa**) or insertion of bulkier group (in **IIIe**) appeared detrimental.

2.4.4 Molecular Modelling

A preliminary molecular modelling study was conducted in collaboration with Roberto Dallocchio and Alessandro Dessì (ICB-CNR, Sez. Sassari), in order to simulate the binding mode of compounds belonging to this new class inhibitors within the active site of *h*CA IX. Interactions between *h*CA IX and the *hit* compound **7**, as well as *h*CA IX with all members of series **III** (**III a-e)** have been predicted by docking experiments using AutoDock 4.2.5, and the coordinates for *h*CA IX-mimic protein (PDB code: 3IAI) were used for computational docking.

Figures 18 and **19** show that all derivatives are deeply buried into the catalytic pocket of *h*CA IX, where the first oxygen of the diol group makes an H-bond with Thr199, while the second oxygen interacts with the zinc ion, thus corroborating the hypothesis that the trifluoromethyl-dihydroxy propanone group could be a suitable bioisostere of the sulfonamide group.

Fig. 18 AutoDock predicted binding modes for ligands (*hit* compound **7** and series **III**) in *h*CA IX protein. Ligands are in sticks, overall protein (blue) comprising binding pocket (violet) is represented as surface, and zinc ion is depicted as orange sphere.

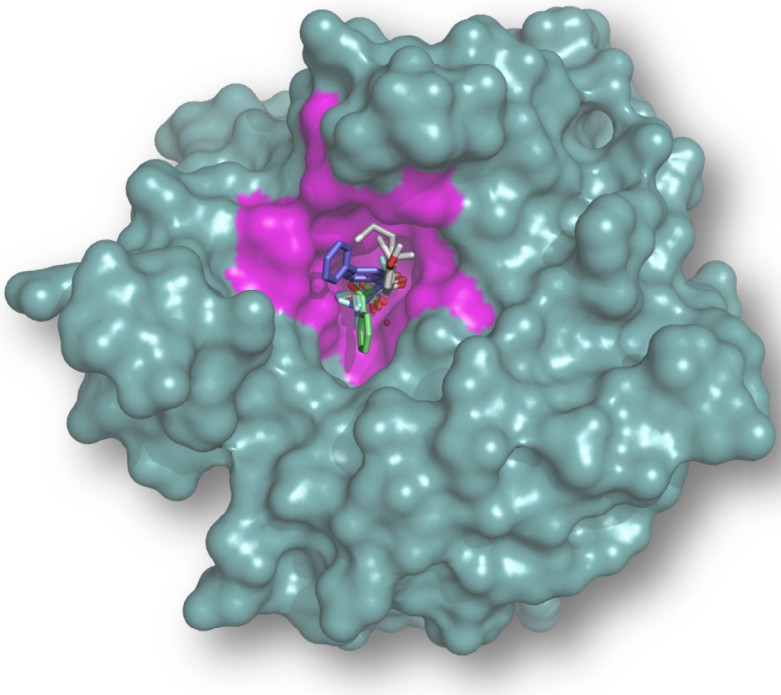

Fig. 19 Zoomed view of docked ligands into the binding pocket.

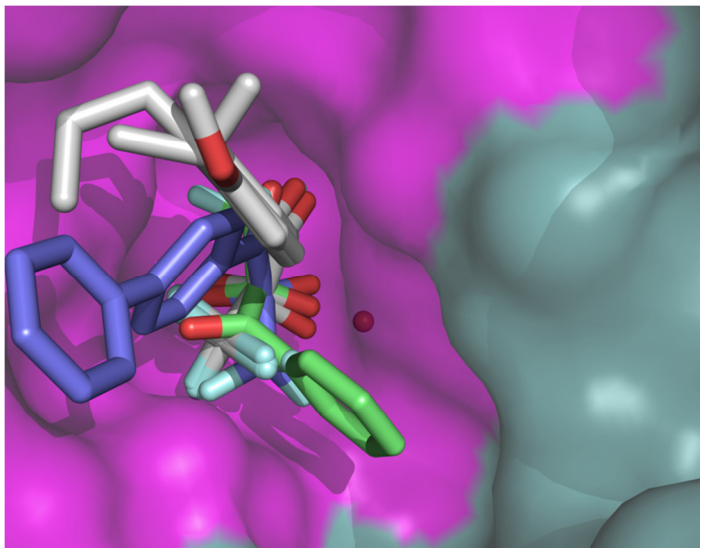

The main differences in terms of binding modes are referred to **IIIa** and **IIIe,** the less active derivatives toward *h*CA IX.

In particular, the aromatic ring of **IIIa** is rotated of 180° with respect to those of the others ligands (**Fig. 19**, green sticks). This mobility is probably due to the absence of a tail on the aromatic scaffold, necessary to establish interactions within the aminoacid pocket, and this orientation may have a negative effect on the activity of this compound.

Concerning the compound **IIIe**, its structural rigidity and molecular expansion introduced by the biphenyl group can also affect the achievement of a favorable position in the catalytic site (**Fig. 19**, blue sticks), thus leading to a decreasing in the activity.

2.4.5 Conclusions and perspectives

In this subchapter is reported the synthesis, biological evaluation and preliminary molecular modeling study of a novel class of CAIs bearing a trifluorodihydroxypropanone moiety (series **III**). With the exception of **IIIa** and **IIIe**, all compounds selectively inhibited *h*CA IX, with K_i values ranging from 0.78 to 0.83 μM, independently of the nature of substituent on the aromatic scaffold.

Some representative compounds have been selected to be crystallized with the target protein to obtain useful information to direct further structural and biological optimization.

These results show that this new class of CAIs possess strong inhibitory effects against *h*CA IX and may be used as a platform for the development of potential anticancer agents.

2.5 Synthesis of a series of substituted heteroaryl-pyrazole carboxylic acid derivatives as CAIs

Since the discovery of CAIs with peculiar selectivity for each CA isozyme is of paramount importance, in 2012 Sechi's group,[87] in collaboration with Dr. Supuran of the University of Florence, made a major effort in identifying novel and original CAIs, endowed with selectivity against relatively unexplored CA targets such as *h*CA I.

The outline of the experimental strategy was the following:

- throughput screening on in-house chemical library of about 150 compounds, built by choosing aromatic/heteroaromatic backbones carrying carboxylic/carboxylate functionalities as bioisosteric alternative to the sulfonamido-based functionalities;
- intensive inhibition study against the main cytosolic/transmembrane carbonic anhydrase isoforms *h*CA I, II, IX and XII, and identification of putative *hit* compounds.

In particular, the 5-(1-ethyl-1*H*-indol-3-yl)-1*H*-pyrazole-3-carboxylic acid **8** (**Fig. 20**) proved to be the most potent and selective compound tested toward *h*CA I isoform (K_I = 0.042 μM), with a very high *h*CA I versus *h*CA II selectivity (K_I = 1829 μM for *h*CA II, SI, selectivity index > 40,000), without it significantly affects the catalytic activities of the other isozymes. Due to its selectivity index between CAs, compound **8** shows a potential therapeutic window.

Fig. 20

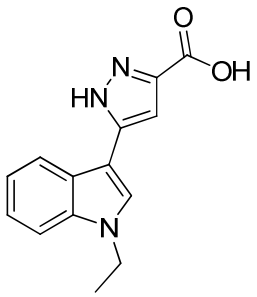

8

This compound represents the first prototype of CAIs targeting the *h*CA I isoform, carrying an original pharmacophore, able to selectively interfere with such isozyme in nanomolar concentration range. Interestingly, computational simulations suggested that compound **8** can meet desirable ADME criteria and favorable pharmacokinetic properties for further development (**Table 7**).

Table 7 Physicochemical properties of compound **8.**

Compound	MW	HBA	HBD	Rbond	cLogP[a]	miLogP[b]	TPSA[c]
8	255.3	4	2	3	3.65	2.397	70.916

Abbreviations: MW, molecular weight; HBA, number of hydrogen bond acceptors; HBD, number of hydrogen bond donors; Rbond, number of rotatable bonds; cLogP, log octanol–water partition coefficient; miLogP, logP prediction based on group contributions; TPSA, topological polar surface area.
a Parameters calculated by ChemDraw Ultra 2005.
b Parameters calculated by miLogP 2.2 method implemented in Molinspiration Cheminformatics 2012 software.
c Parameters calculated by Molinspiration Cheminformatics 2012.

Concerning the CA inhibition mechanism, the heteroaryl-pyrazole carboxylic acids could interact with the Zn^{2+} involving their carboxylate

functionalities, similarly to sulfonamides and related inhibitors, as revealed by X-ray in co-crystals of *h*CA II with other carboxylates.[88]

For the mentioned reasons, compound **8** can represent a novel promising lead compound for the development of potent and selective *h*CA I inhibitors.

The synthetic approach for the preparation of **8** started with the alkylation reaction of 3-acetyl indole **19** (**Scheme 2.12**) with bromoethane and KOH in anhydrous DMSO at room temperature, to afford the *N*-ethyl-3-acetyl indole **20a**. This intermediate undergoes Claisen condensation with diethyl oxalate in the presence of freshly prepared sodium methoxide to provide compound **21a**, which, as in the case of the analogous β-diketo acids, was found to exist predominantly in the keto-enol form.[89]
The next step resulted on the cyclization of the diketoester **21a** to pyrazol ring **22** using hydrazine monohydrate in isopropyl alcohol and glacial acetic acid, as previously reported.[90] Then, compound **8** was obtained by alkaline hydrolysis with 20% NaOH of heteroaryl-pyrazole ester **22**.

Scheme 2.12 reports the synthetic route for the preparation of **8**.

Scheme 2.12

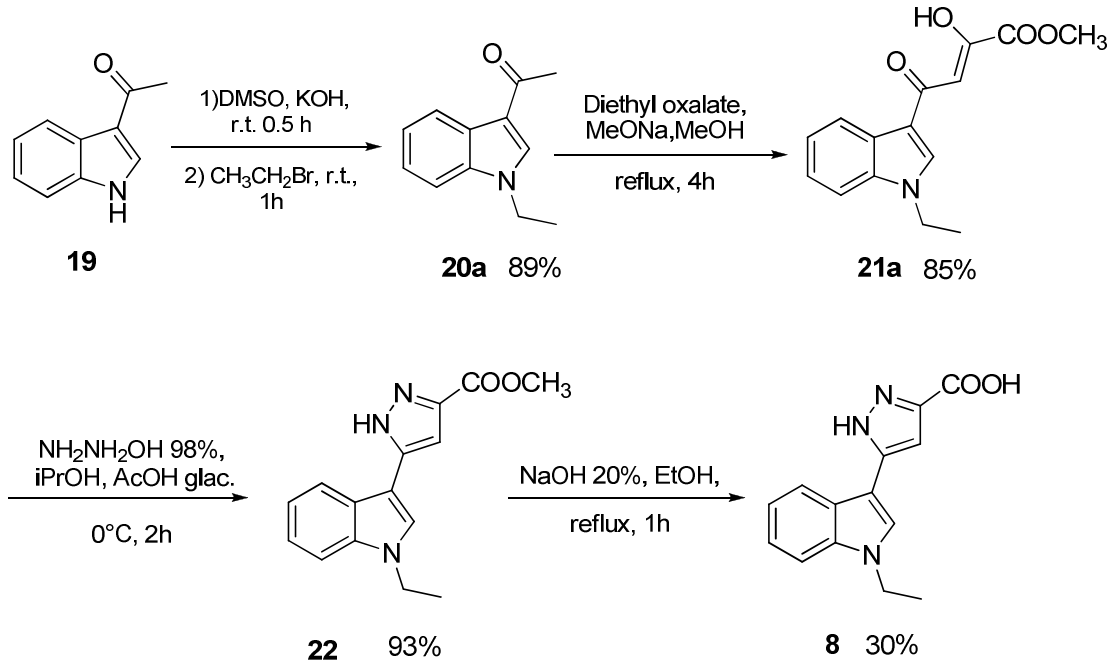

19 **20a** 89% **21a** 85%

22 93% **8** 30%

2.5.1 Objectives

According with the rational of the project, this specific topic was focused on the structural optimization of the lead compound **8**, in order to generate a new series of 3-(1*H*-indol-3-yl)pyrazole-5-carboxylic acids, with improved inhibition profile.

In particular, pharmacomodulation of **8** should be addressed:

- ❖ to improve affinity towards *h*CA I, and to define the pharmacophoric motif endowed with the activity;
- ❖ to test the activity of these heteroaryl-pyrazole carboxylic acid derivatives toward a panel of isozymes (*h*CA I, *h*CA II, *h* CA IX, and *h*CA II);
- ❖ to obtain solved co-crystal structures with few representative derivatives with the target proteins (i.e., *h*CA II and *h*CA IX mimic

enzymes), to acquire useful details about the binding modes of these compounds within the CA catalytic site.

In this direction, major modifications of **8** have been made by varying the substituents in the nitrogen atoms both on the indole and pyrazole rings, as well as by esterification of the carboxylic functionality (**Fig. 21**).

Fig. 21

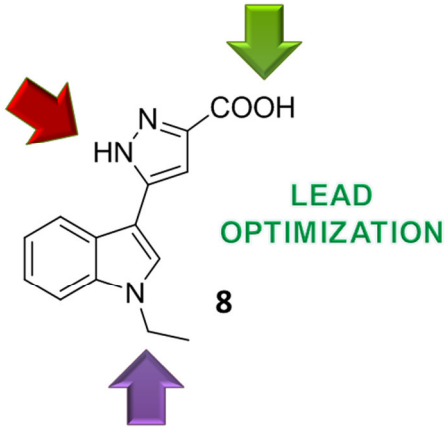

A set of the designed compounds (series **IV)** is depicted in **Fig. 22**.

Fig.22 a) General chemotype of title compounds. b) Designed compounds of the series **IV**.

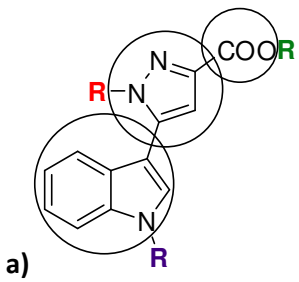

b)

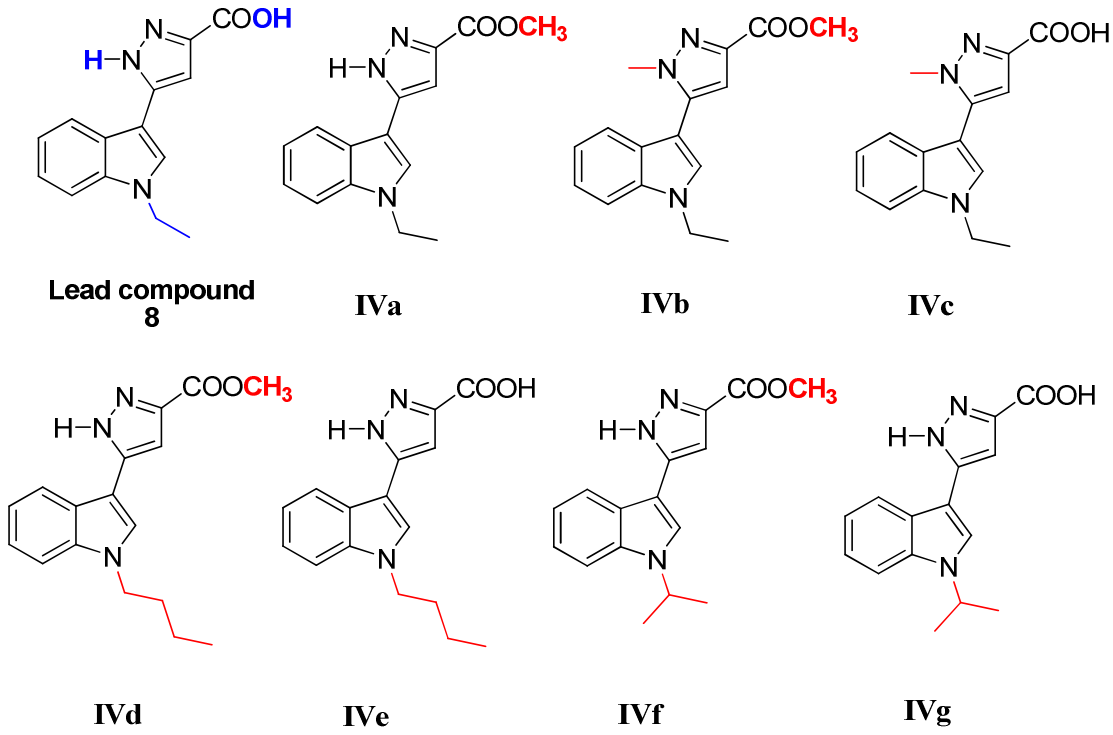

Lead compound 8 **IVa** **IVb** **IVc**

IVd **IVe** **IVf** **IVg**

2.5.2 Chemistry

Compounds **IVa**, **IVd-g** of series **IV** were synthesized by using the above mentioned synthetic procedure, starting from the 3-acetyl indole **19**.

The first step was the alkylation reaction of **19** with the appropriate alkyl bromide to obtain the *N*-alkyl-3-acetyl-indole derivatives **20a-c** (**Scheme 2.13**).

Scheme 2.13

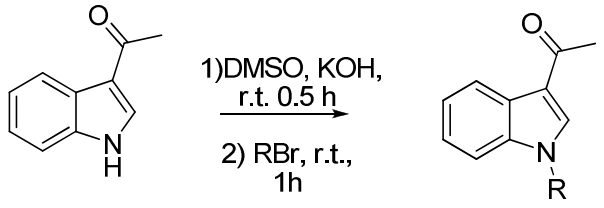

19

20a R = Et 89%
20b R = Bu 91%
20c R = iPr 50%

These intermediates were then reacted with diethyl oxalate in the presence of sodium methoxide in MeOH, to provide the analogous β-diketo esters **21a-c (Scheme 2.14)**, which were found to exist in the keto-enol form. In fact, ^{1}H-NMR experiments showed a singlet centered at about 6.87 ppm (6.87 for compounds **21a,b**, 6.89 for **21c**) attributable to the enolic CH of the hydroxy-keto motif.[89]

Scheme 2.14

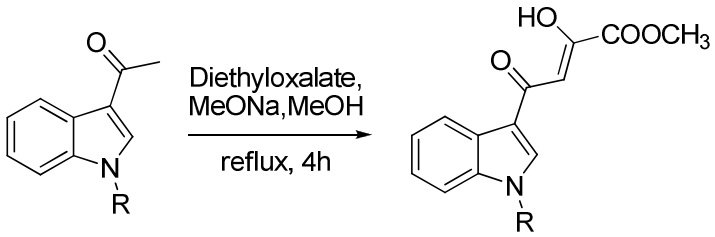

20a R = Et
20b R = Bu
20c R = iPr

21a R = Et 85%
21b R = Bu 54%
21c R = iPr 93%

The β-diketoesters **21a-c** were treated with hydrazine monohydrate to generate the pyrazole derivatives **IVa**, **IVd** and **IVf** in appreciable yields (46-93%, **Scheme 2.15**).

Scheme 2.15

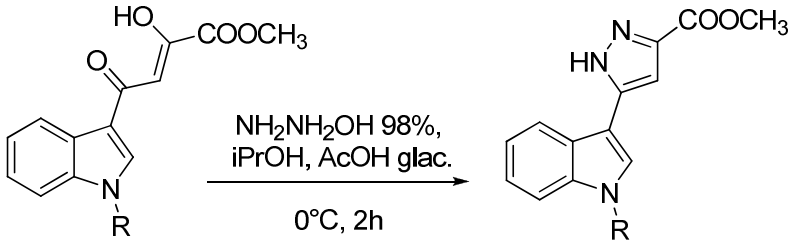

21a R = Et
21b R = Bu
21c R = iPr

IVa R = Et 93%
IVd R = Bu 46%
IVf R = iPr 66%

Then, the acids **IVe** and **IVg** were obtained by alkaline hydrolysis of the esters **IVd** and **IVf** (**Scheme 2.16**).

Scheme 2.16

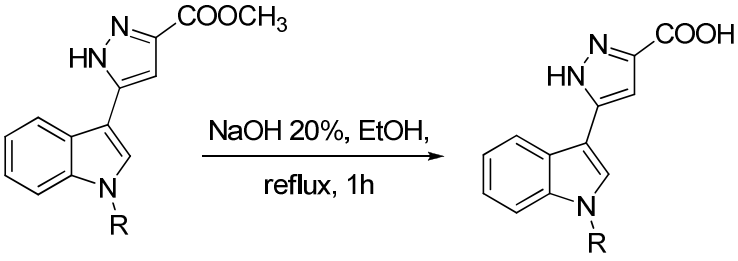

IVd R = Bu
IVf R = iPr

IVe R = Bu 86%
IVg R = iPr 64%

Compounds **IVb** and **IVc**, containing a *N*-CH_3 on the pyrazole ring, were synthesized starting from **IVa**, following the synthetic route reported in the **Scheme 2.17**. Briefly, the intermediate **IVa** was converted to **IVb** by alkylation of the pirazole nitrogen with CH_3I in the presence of NaH (**Scheme 2.17**).[90] Compound **IVc** was then obtained from **IVb** by alkaline hydrolysis with 20% NaOH in ethanol at reflux (**Scheme 2.17**).

Scheme 2.17

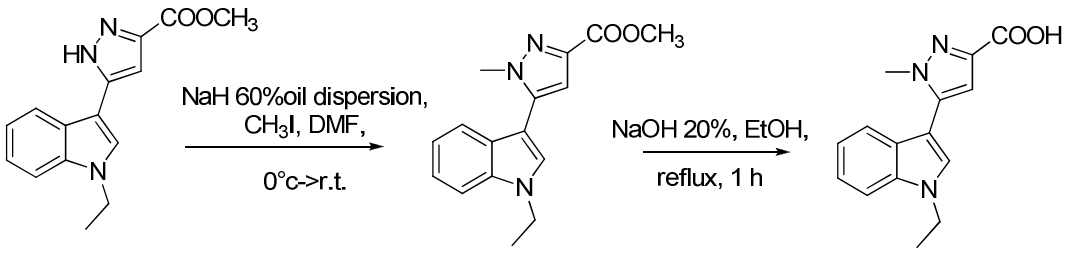

IVa

IVb 39%

IVc 64%

2.5.3 Biological assays

As previously explained, considering the abnormally high expression of *h*CA IX and *h*CA XII in different hypoxic tumors and their demonstrated role in the tumor acidification processes and oncogenesis, these isoforms constitute potential targets for anticancer therapy. Thus, agents that can inhibit *h*CA IX and *h*CA XII activity may have therapeutic value and offer opportunities for the prevention and/or treatment of a variety of cancers.

For these reasons these heteroaryl-pyrazole carboxylic acid derivatives (series **IV)** were tested for their ability to inhibit IX and XII α-isoforms, in addition to *h*CA I and II.

Catalytic activities were measured by a stopped-flow technique, as previously described (**Table 8,** see details in Experimental Section).

Table 8. Inhibition of *h*CA isoforms I, II, IX and XII with carboxylic acids and esters of series **IV**, and acetazolamide (AAZ; 5-acetamido-1,3,4-thiadiazole-2-sulfonamide)), methazolamide (MZA; *N*-[5-(aminosulphonil)-3-methyl-1,3,4-thiadiazol-2(3*H*)-ilydene]acetamide), dichlorophenamide (DCP; 4,5-diclhorobenzene-1,3-disulphonamide) as standard by a stopped-flow CO_2 hydrase assay.

Compound	K_I (μM)*			
	***h*CA I**	***h*CA II**	***h*CA IX**	***h*CA XII**
8	0.042	1820	7.79	7.78
IVa	4.31	6.95	0.47	0.57
IVb	0.62	0.41	3.02	0.31
IVc	6.61	0.78	2.91	0.44
IVd	5.93	0.53	7.90	0.35
IVe	5.33	4.70	4.51	0.34
IVf	6.45	0.76	7.36	0.21

IVg	4.83	0.70	18.9	0.28
AAZ	0.25	0.012	0.025	0.006
MZA	0.78	0.014	0.027	0.034
DCP	1.2	0.038	0.050	0.050

* Errors in the range of ± 5-10 % of the reported value from 3 different assays.

Although structural modifications of the lead compound **8** reduced the potency and selectivity against *h*CA I isoform (work is in progress to clarify the behavior), this new class of compounds showed an interesting selectivity toward *h*CA XII, with K_i values ranging from 0.21 to 0.57 μM (**Table 8**). This biological profile appeared to be independent from the nature of substituents on indole and pyrazole ring. Furthermore, no relevant differences could be observed between acids and esters (**Table 8**).

Among the tested compounds, compound **IVf** (K_I = 0.21 μM) proved to be the most active compound in inhibiting the *h*CA XII isoform.

2.5.4 Molecular Modelling

A preliminary molecular modelling study on this new class of CAIs was conducted to better understand binding geometries and the interactions of these compounds within the catalytic site. Graphical representations of top-ranking binding modes obtained for these ligands are depicted in Figure **23**.

Results of docking experiments within the active site of *h*CA XII (PDB code: IJD0) share a common binding pattern for all ligands, thus confirming that

the carboxylate group is involved in metal binding with the metal cofactor (**Fig. 23**).[88]

It should be also noted that no relevant differences in binding modes could be observed between acids and esters, being they able to chelate the Zn ion in the same way.

Fig. 23. Superimposition of the best binding pose of compounds **IVa-g**. Ligands are depicted as yellow sticks with the exception of **IVd** (shown in cyan). The target structure was represenated by molecular surface and cartoons (rendered in light-gray), and Zn^{2+} is depicted as orange sphere. Figure was prepared using MacPyMol.

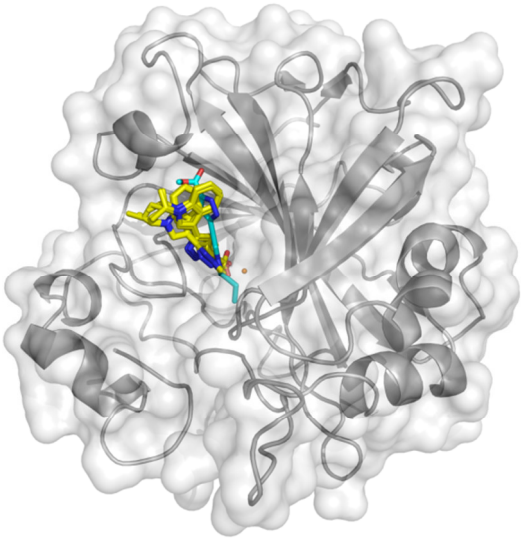

On the other hand, not satisfactory docking results were obtained for **IVd,** since the docking program failed in generating a consistent binding mode for this ligand. This behavior could be explained by considering that this ligand well accommodates into the binding pocket, but in opposite orientation with respect to those of the other compounds.

In this context, the carboxylate group does not readily engage in a correct bridging mode for metal ion coordination, and this may have a negative effect on the activity of this compound.

Thus, with the exception of **IVd**, for all ligands the two coplanar oxygen atoms of the carboxylate functionality are involved in metal chelation of the divalent ions (**Fig. 24**).

Fig. 24. Comparison of the best docking pose for compounds **8** and **IVa-g**. Colors code of **Fig. 23** was preserved together with the side chains of relevant residues (shown as white sticks). Figure was prepared using MacPyMol.

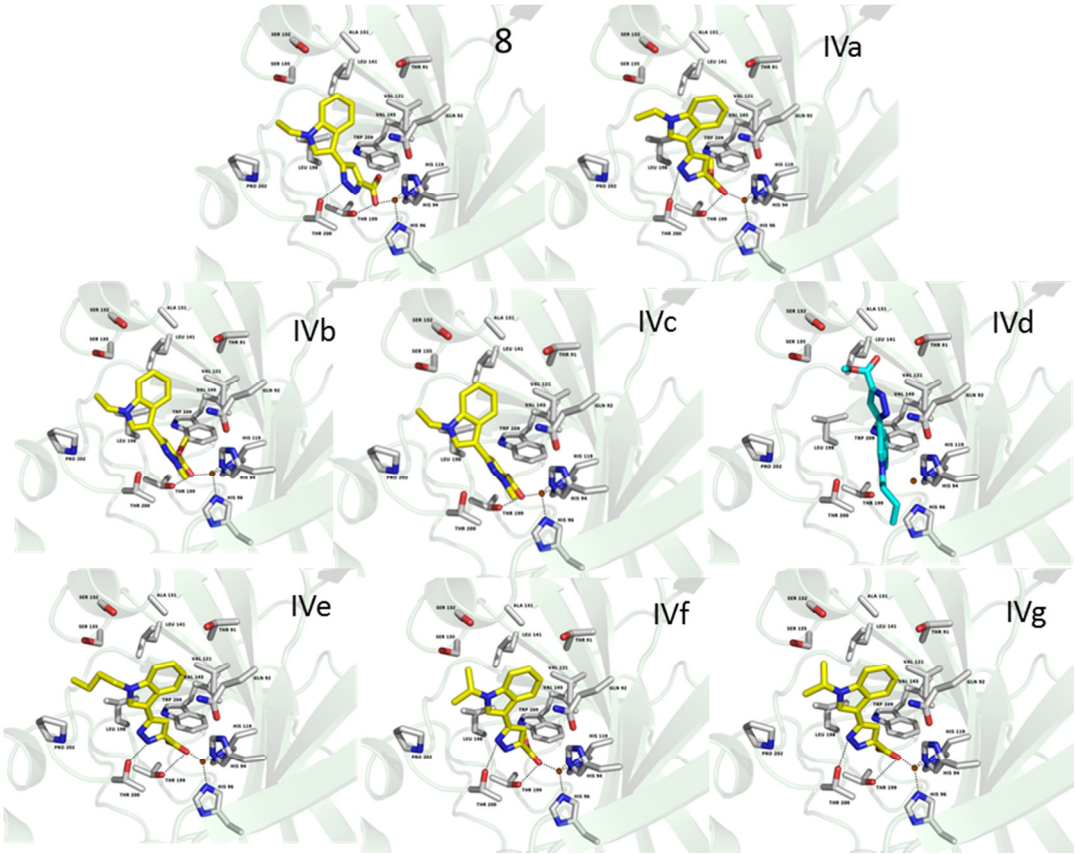

2.5.5 Conclusions and perspectives

According with the rational of the project, this subchapter was focused on the structural optimization of the lead compound **8**, in order to generate a new series of compounds bearing a 3-(1*H*-indol-3-yl)pyrazole-5-carboxylic acid scaffold (series **IV**).

All tested compounds selectively inhibited *h*CA XII, with K_i values ranging from 0.21 to 0.57 μM, independently from the nature of substituents on indole or pyrazole ring. Among the tested compounds, **IVf** (K_i = 0.21 μM) resulted the most potent *h*CA XII inhibitor, which could provide structural determinants for the development of novel anticancer agents.

2.6 Preliminary evaluation of antiproliferative activity for representative compounds of series III and IV

The putative effect of inhibition of CA activity (particularly of *h*CA IX and/or XII) demonstrated by compounds of the series **III** and **IV** on the viability of three human cancer cell lines (hormone-independent prostate cells, PC-3; human embryonic kidney, HEK 293 cells; human neuroblastoma cells, SH-SY5Y) was evaluated by MTS colorimetric assay, in collaboration with Dr. Ciro Iaccarino, University of Sassari.

First, HEK 293 cells were treated for 24 hours with compounds **7**, **IIIa**, **IIId**, **8**, **IVf**, **IVg**, and **IVa**, at diverse inhibitor concentrations (**Fig.25**). At the end of 24 hours of exposure, no significative antiproliferative effect has been detected at the 1 μM, 10 μM, 30 μM, and 100 μM concentration exposure, with the exception of **IIId** and **IVf**, which exhibited cell growth inhibition of

about 50% and 70 % (for **IIId** and **IVf**, respectively) after treatment with 100 µM concentration.

Fig 25. Antiproliferative activity of some representative compounds of series **III** and **IV** on human renal HEK 293 cells at various concentration assessed by percentage of cell viability after 24 hours.

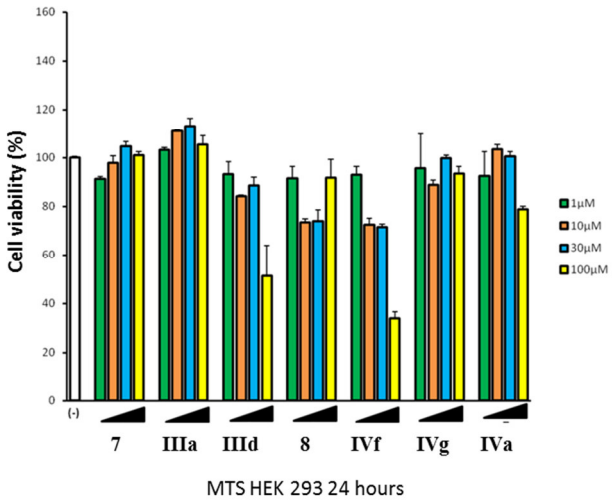

Similar results are found when the same compounds were tested in PC-3 cells (**Fig.26**). In fact, with the exception of **IVf**, none of the trifluoromethyl-dihydroxy propanone derivatives demonstrated significative cytotoxicity. It could be speculated that this cell line is more susceptible to inhibition of *h*CA XII than *h*CA IX. However, differences in physicochemical properties for these compounds should also be considered.

Fig 26. Antiproliferative activity of some representative compounds of series **III** and **IV** on humane prostate PC-3 cells at various concentration assessed by percentage of cell viability after 24 hours.

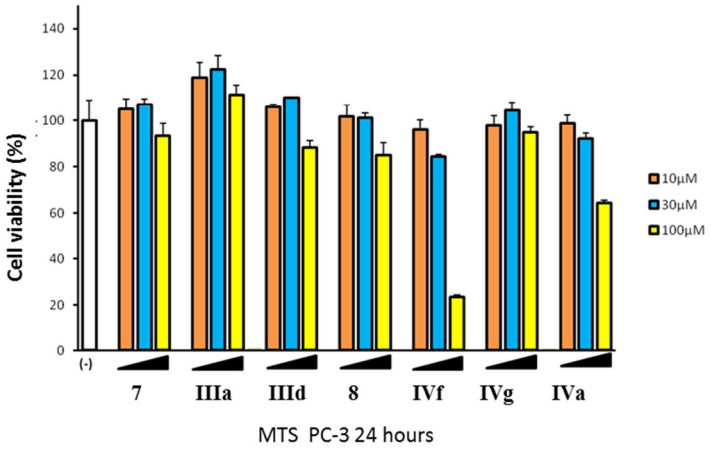

In the third experiments (**Fig.27**), treatment of the same compounds on SH-SY5Y cell lines, after 48 hours exposure, displayed an overlapping behavior, with appreciable cytotoxicity effect for **IVf** and **IIId** at μ100 M concentration.

Fig 27. Antiproliferative activity of some representative compounds of series **III** and **IV** on human neuronal SH-SY5Y cells at various concentration, assessed by percentage of cell viability after 48 hours.

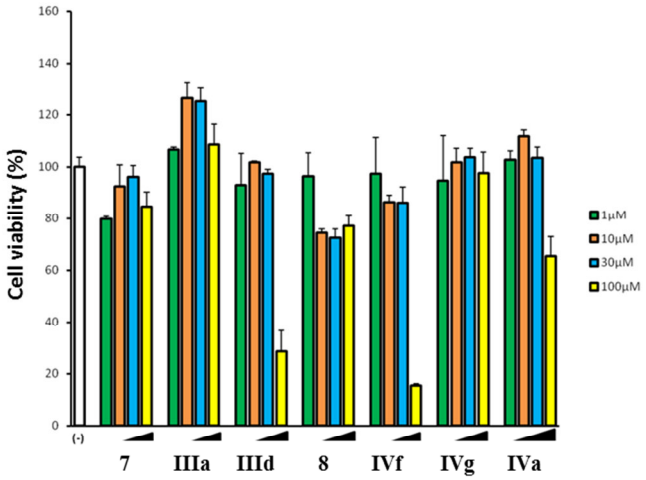

Because *h*CA IX and *h*CA XII were predicted to be involved in tumor processes related to the hypoxic phenomena, compound **IVf** was further investigated for its antiproliferative potency in neuroblastoma cells at different concentrations of inhibitor (1-100 µM) both in normal and in simulated hypoxic condition (**Figure 28**). This experimental model has been planned by adding cobalt(II) chloride, a known chemical inducer of hypoxia-inducible factors in several cell lines.[91] Interestingly, from the analysis of the results, it emerged that the addition of $CoCl_2$ significantly increased the susceptibility of the cells to the treatment with **IVf,** showing a reduction of cell viability of about 25%. Of course, the implication of CA XII on the growth inhibition mechanism should be better investigated.

Fig 28. Antiproliferative activity of **IVf** on human neuronal SH-SY5Y cells (measured by percentage of cell viability after 48 hours) at various concentration was assessed in normal (cyan) and in simulated hypoxic (green) conditions, after 2 hours of exposure to MTS).

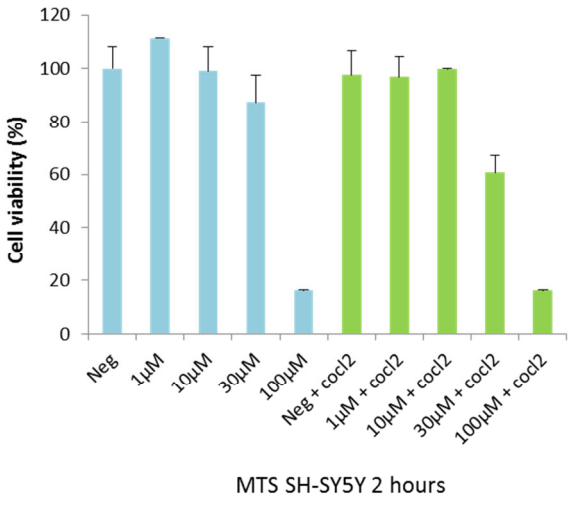

In summary, preliminary cytotoxicity evaluation on three different cancer cell lines was performed *in vitro* using MTS colorimetric assay. Among the tested compounds, **IVf** displayed the best cell growth inhibitory toward all

cell lines. Moreover, an improved antiproliferactive effect was observed for **IVf** when tested in simulated hypoxia conditions, as expected by considering the putative involvement of *h*CA XII inhibition.

2.7 Synthesis of potential CAIs carrying a benzoxaborole scaffold

2.7.1 Introduction

Unsubstituted benzoxaborole **9** (**Fig. 29**), generally named as 1,3-dihydro-1-hydroxy-2,1-benzoxaborole, consists of a benzene ring fused with an oxaborole heterocycle:

Fig. 29 Benzoxaborole structure.

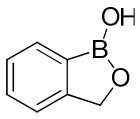

9

In the past fifty five years, the applications of benzoxaboroles covered various fields, exemplified by organic synthesis, glycopeptides recognition and supramolecular chemistry.[92] Compared with corresponding arylboronic acids or other compounds, benzoxaboroles show exceptional properties.

All boronic acids, with their empty p-orbitals, are Lewis acids where the neutral form adopts a trigonal planar geometry while the conjugate base is tetrahedral with the negative charge formally localized on the boron atom itself. This addition of water with the accompanying loss of a proton is responsible for their acid/base properties.

Scheme 2.18 pKa of benzoxaborole compared to that of phenylboronic acid.

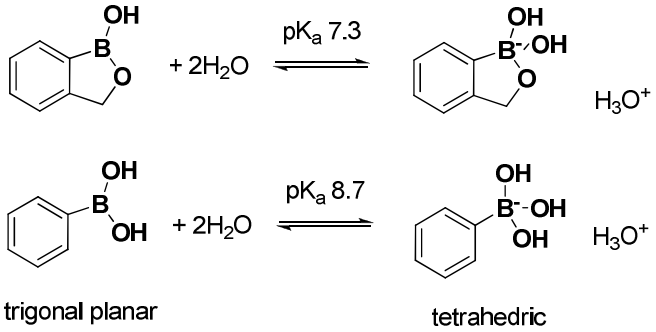

Consequently, benzoxaboroles have better solubility in water at physiological pH compared with phenylboronic acids. A good solubility in physiological pH required for clinical drug candidates is one of the drug-like properties.[93]

The stability of the benzoxaborole core allows modifications under various reaction conditions. For instance, benzoxaborole ring could be nitrated with fuming nitric acid to obtain 6-nitrobenzoxaborole, which can subsequently be reduced to 6-aminobenzoxaborole under hydrogen in the presence of catalysts (**Scheme 2.19**, **a**).[94] Moreover, it can be oxidized with CrO_3 without any damage of the scaffold (**Scheme 2.19**, **b**).[86] Again, this heterocyle can be heated to reflux for 6 hours under 6 mol/L NaOH (**Scheme 2.19**, **c**).[95] Furthermore, it can tolerate concentrated hydrochloric acid or reduction with lithium aluminum hydride (**Scheme 2.19**, **d**).[96]

Scheme 2.19

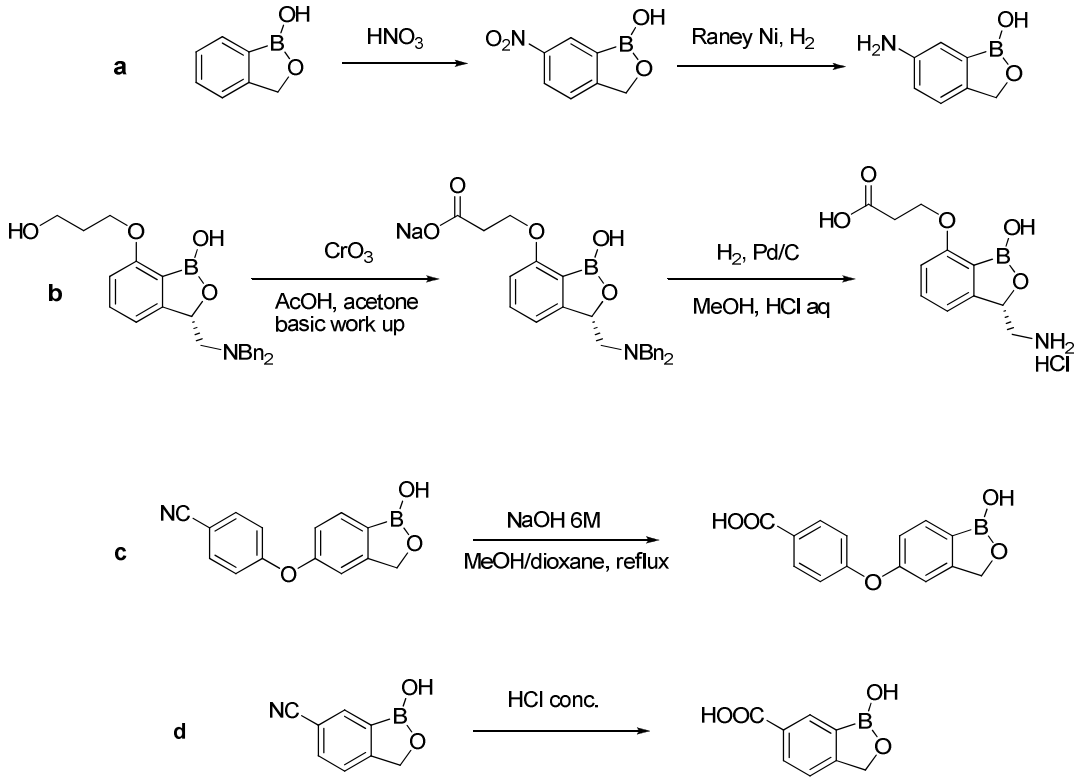

Part of the reason arises from the benzoxaboroles unique chemical properties, especially in comparison to their acyclic boronic acid counterparts. Furthermore, the low bio-toxicity combined with the high target specificity associated with benzoxaboroles make them very attractive as therapeutic agents.[93a]

2.7.2 Benzoxaborole scaffold in drug design

Many of the applications of benzoxaboroles in molecular recognition involve the development of improved carbohydrate sensors. Benzoxaboroxoles, in fact, are known to bind 1,2-diol motifs in

carbohydrates in an aqueous environment. In 2010 Hall's group[97] applied his discovery of efficient saccharide binding by benzoxaboroles to the construction of a peptidyl bis-benzoxaborole library that would be used as a synthetic receptor. The receptor was targeted against a disaccahride unit (Gal-b-1,3-GalNAc) that is found on the surface of many tumor cells, the Thomsen-Friedenreich (TF) antigen. The best candidate (**Fig. 30**) exhibited high selectively for TF-antigen with a Kd 0.9 mM, similar to the values reported with some naturally-occuring lectins.

Fig. 30

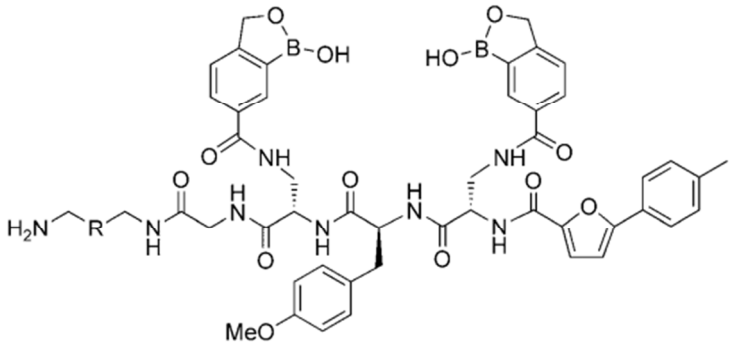

Material scientists have also begun to take advantage of the high affinity of benzoxaboroles for sugars and other diols under neutral aqueous conditions. In 2012 Liu and co-workers[98] have reported a method to append benzoxaboroles to the surface of a monolithic capillary column for the chromatographic separation of various diols. 6-carboxy-benzoxaborole was used to functionalize methylene bisacrylamide/glycidyl methacrylate polymer capillary monoliths via amide bond formation (**Fig. 31**). The columns prepared provided efficient chromatographic separation of a variety of nucleosides as well as efficient retention of model glycoproteins

at neutral pH. These columns may also be useful in the selective enrichment of nucleosides and glycosylated proteins.

Fig. 31 Benzoxaborole incorporated for affinity chromatography on monolithic capillary.

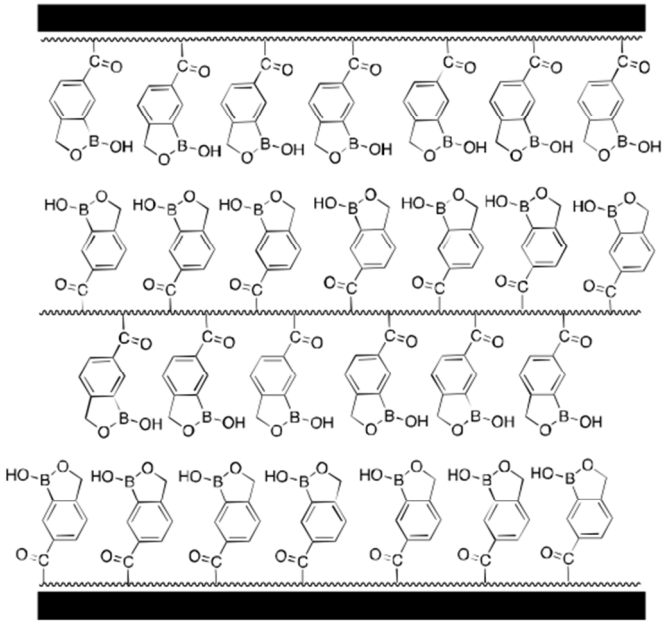

As far as the medicinal chemistry field is concerned, benzoxaboroles have emerged as a novel class of small molecule therapeutic agents, with a rapidly growing number of literature examples reporting their diverse potential applications, many of which are actively being explored by pharmaceutics. Small modifications to the benzoxaborole structure can lead to potent therapeutic candidates for various human diseases, including fungal, bacterial, and viral infections, inflammation, cancer, and even for drug delivery.[99]

Benzoxaboroles also offer new opportunities for treating other important and often neglected diseases. SAR screening has shown that many benzoxaboroles are potent inhibitors of *T. brucei* LeuRS, making them

promising new antitrypanosomal agents.[100] Guided by the knowledge of the *T.vbrucei* LeuRS active site structure, a series of 6-substituted benzoxaboroles were designed and found to exhibit low μM IC_{50} values for *T. brucei* LeuRS. Among them, *SCYX-7158* (**Fig. 32**) exhibited desirable drug-suitability traits in pre-clinical studies, and it is currently in Phase I clinical trial.[101]

Fig. 32

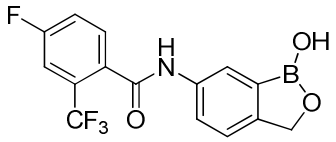

SCYX-7158

Malaria is a mosquito-borne infectious disease of humans and other animals caused by parasitic protozoans of the *Plasmodium* type.

Several benzoxaboroles with 7-carboxyethyl substituents have been reported to have very potent antimalarial properties with IC_{50} values in the nM concentration range.[102] It is demonstrated that the boron atom is absolutely essential for the antimalarial effect, and replacing boron with carbon leads to the loss of inhibition. In particular AN3661 (**Fig. 33**, IC_{50} 44 nM) is being currently developed as a new treatment for malaria.[101]

Fig. 33

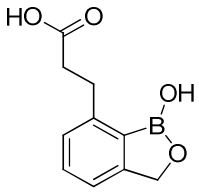

AN3661

Again, a series of phenoxy-substituted benzoxaboroles was found to exhibit good phosphodiesterase 4 (PDE4) inhibition. PDE4 is responsible for catalyzing the breakdown of 3',5'-adenosine cyclic monophosphate (cAMP) and it is ubiquitously expressed in inflammatory cells. Inhibition of PDE4 function has been shown to suppress the activity of human inflammatory cells, making PDE4 an attractive target for fighting various inflammatory diseases, such as asthma, chronic obstructive pulmonary disease, inflammatory bowel disease, and psoriasis.[93a] AN2728 (**Fig. 34**) is among the most effective compounds identified for this purpose. It has passed Phase II clinical trials for topical treatment of psoriasis and atopic dermatitis.[101]

Fig. 34

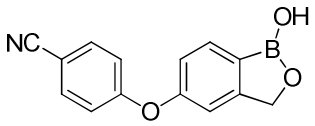

AN2728

To summarize, benzoxaboroles have been proven to be a unique class of compounds with very distinct chemical reactivity from acyclic aryl boronic acids. The diverse utility of benzoxaboroles has only been recognized recently, and they have already been utilized for detecting biomolecules and for treating various health issues. The most exciting aspect of benzoxaboroles' therapeutic potential is that they are very safe and thus provide a novel therapeutic pharmacophore for use against diseases where resistance is emerging to existing approaches.

2.7.3 Benzoxaborole as potential CAI

In this context the attention has been focused on benzoxaborole scaffold as an alternative chemotype to develop a new class of CAIs.

In particular, benzoxaborole **9** (**Fig. 29**) was recently tested on some α-CA isozymes and demonstrated interesting inhibition potency against *h*CA I and *h*CA II (K_i =648 nm against *h*CA I, K_i =642 nm against *h*CA II). No inhibition was observed against the isozymes *h*CA IX and *h*CA XII. Preliminary X-ray crystallographic data of the benzoxaborole/*h*CA II adduct seems to predict a binding mode in the active site where the B-OH hydroxyl group bind to the zinc ion in a tetrahedral geometry.[103]

These preliminary results showed the benzoxaborole moiety as an original pharmacophoric group in the CAIs drug discovey. This compound represents a novel promising lead structure suitable of chemical modification and consequent biological optimization. In this scenario, part of the project was addressed to synthesize a library of benzoxaborole derivatives, substituted on the C-6 aryl position, in order to improve the biopharmaceutical profile of the starting model compound (**Fig. 35**).

Fig. 35 Benzoxaborole functionalization.

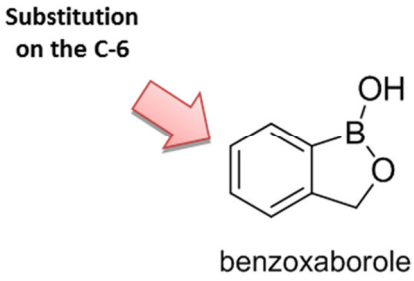

2.7.3.1 Design of synthetic plan for benzoxaborole derivatives

A good strategy to synthesize benzoxaboroles derivatives is to start from the 6-amino benzoxaborole (6-aminobenzo[c][1,2]oxaborol-1(3H)-ol) **24**. Compound **23** was synthesized according to literature,[94,104] starting with the nitration of the commercially available 1,3-dihydro-1-hydroxy-2,1-benzoxaborole (**9**) in position 6 with fuming nitric acid (important to use nitric acid with a concentration of 90% for this reaction) at –45 °C and followed by hydrogenation over palladium on carbon in acetic acid–tetrahydrofuran at room temperature under atmospheric pressure (**Scheme 2.18**).

Scheme 2.18 Synthetic approach.

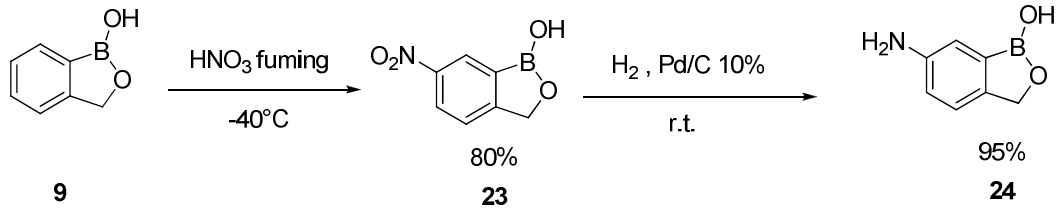

6-Amino benzoxaborole **24** was obtained as a foamy orange solid and characterized by ^{1}H and ^{13}C NMR in d^{6}-DMSO, and ESI-MS. In particular, a broad singlet at δ = 9.05, a singlet at 4.90, and a singlet at 4.81 were assigned to the NH_2, BOH, $BOCH_2$ and protons, respectively.

The amino group in the 6 position could be well suited to derivatize the benzoxaborole structure by reacting **24** with a series of isocyanates and isothiocyanates to obtain two different sets of *N,N'*-disubstituted ureas and thioureas (**Fig.36**).

Fig.36

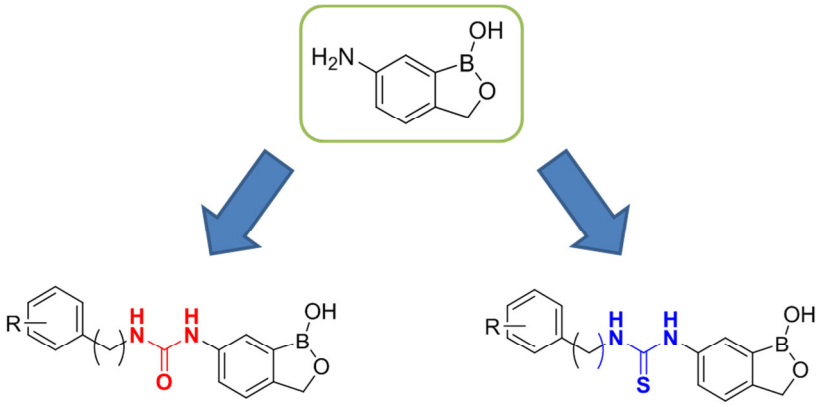

2.7.3.2 Synthesis of a series of *N,N'*-disubstituted ureas

The investigation began by treating 6-amino benzoxaborole **24** (1 equiv.) with phenyl isocyanate (**25a**, 1 equiv.) in acetone at room temperature. When 6-amino benzoxaborole was consumed, petroleum ether was added to the mixture, and a precipitate was filtered. The crude solid was washed with methanol to afford the desired product **26a** as a solid with a yield of 42% (**Scheme 2.19**).

Scheme 2.19

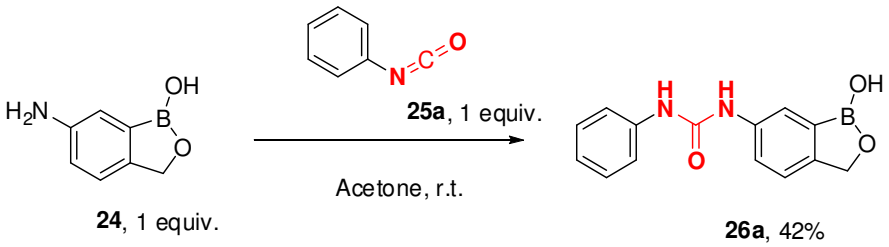

After that, the methodology has been tested with an array of commercially available aromatic isocyanates **25b-j**, and the method provided the desired ureas in moderate yields (**Scheme 2.20**, **26b-j** 23-46%).

Scheme 2.20 Series of *N,N'*-disubstituted ureas.

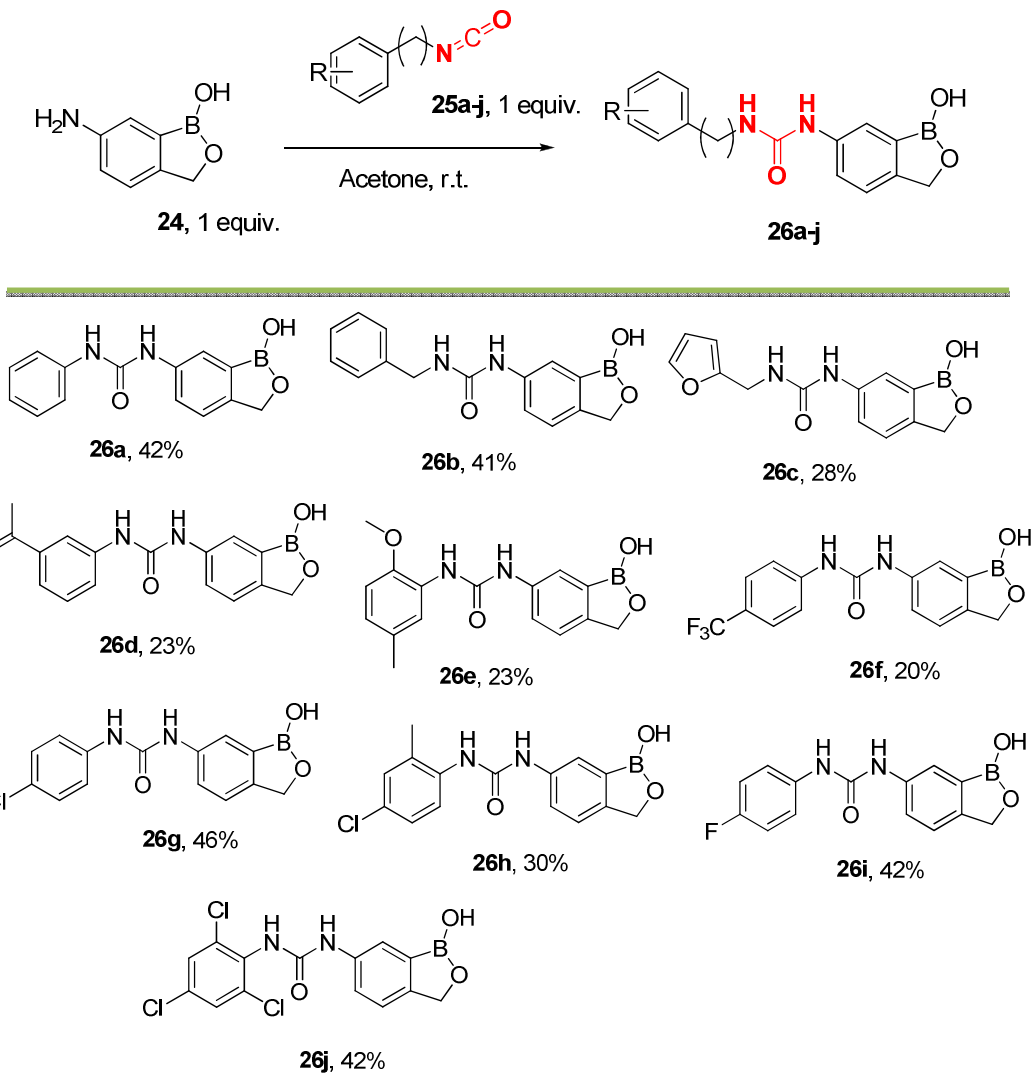

2.7.3.3 Synthesis of a series of *N,N'*-disubstituted thioureas

On the base of these encouraging results, the method has been tested on various commercially available aromatic isothiocyanate to obtain a series of *N,N'*-disubstituted thioureas. The procedure started by treating 6-amino benzoxaborole **24** (1 equiv.) with 4-methoxy phenyl isothiocyanate **27a** in acetone at room temperature (**Table 9**, entry 1). After 1 hour the formation of the new product **28a** was not observed. Moreover, no

product formation was observed when performing the reaction overnight (**Table 9**, entry 2). For this reason the mixture reaction was refluxed, and after about 2 hours the reaction was completed, leading to the expected product with a 15% yield (**Table 9**, entry 3). In order to find the optimum reaction, the reaction was carried out by increasing the equivalents of 4–methoxy phenyl isothiocyanate. Better result were observed using 1.2 equiv. of isothiocyanate (**Table 9**, entry 4-5).

Table 9 Synthesis of *N,N'*-disubstituted thioureas: optimization of the reaction conditions.

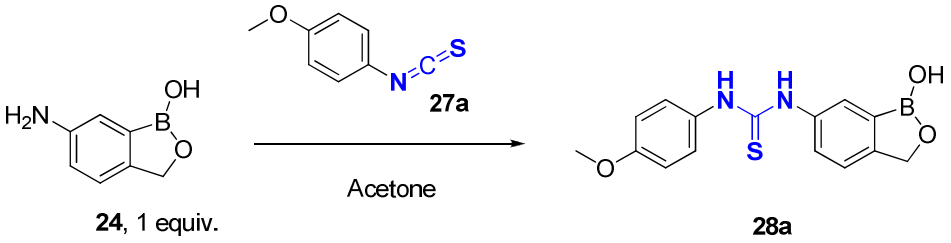

24, 1 equiv. **28a**

Entry	*Compound 27a (equiv)*	*Temp. (°C)*	*Time (hours)*	*Yield on 7 (%)*
1	*1*	*r.t*	*1*	-
2	*1*	*r.t*	*24*	-
3	*1*	*50*	*2,5*	*15*
4	*1.2*	*50*	*2,5*	*25*
5	*1.3*	*50*	*2,5*	*25*

In the following table are shown both the different derivatives synthetized (using the optimized parameters and the different isothiocyanates **27a-j)** and the relatives yields (**Table 10**, **28a-j**):

Table 10 Series of *N,N'*-disubstituted thioureas.

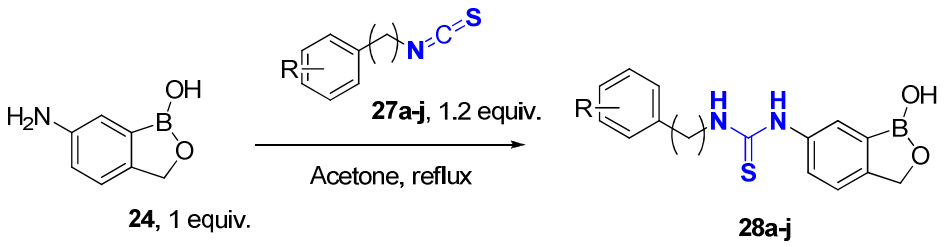

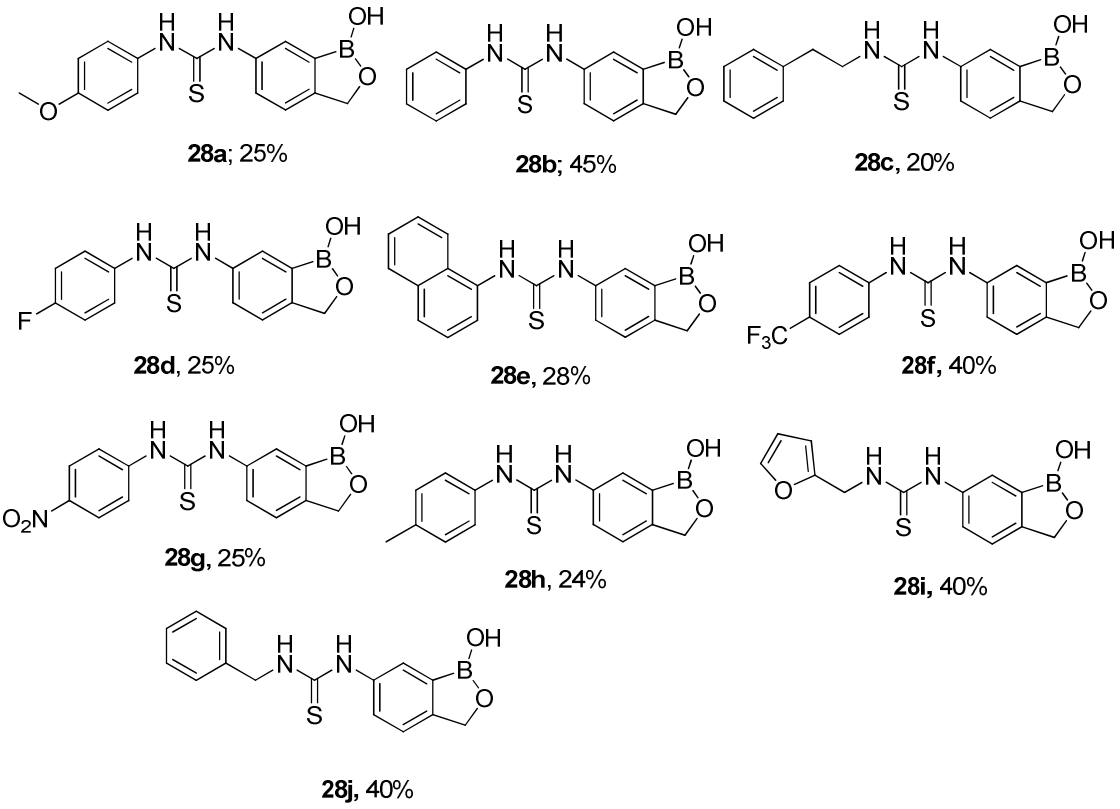

2.7.3.4 Characterization of the compounds

All the synthesized compounds were characterized by ^{1}H and ^{13}C NMR in d^{6}-DMSO, and ESI-MS. In general, *N,N'*-disubstituted ureas showed the characteristic proton signal at about 4.90 ppm and carbon signal at about 69 ppm assigned as the $BOCH_2$, and carbon signal at 140 ppm assigned as

NHCONH (not always observed). *N,N'*-disubstituted thioureas shared a similar pattern, with the signals at about 4.96 ppm and at about 69 ppm, for proton and carbon, respectively, assigned as the $BOCH_2$, as well as the carbon signal centered at 184 ppm, assigned as NHCSNH (difficult to be detected). All the ESI-MS data showed the $[M+1]^+$ ion.

2.7.3.5 Enzyme assays

N,N'-disubstituted thioureas **28a-j** have been tested for the inhibition of two transmembrane cancer-associated isoforms, *h*CA IX and XII (**Table 11**). Data for the inhibition of the dominant human isoforms *h*CA I and II with these compounds are also included in **Table 11**, for comparison reasons.

Table 11. Inhibition of *h*CA isoforms I, II, IX and XII with benzoxaborole **9** and *N,N'*-disubstituted thioureas **28a-j**, and acetazolamide (AAZ; 5-acetamido-1,3,4-thiadiazole-2-sulfonamide), methazolamide (MZA; *N*-[5-(aminosulphonil)-3-methyl-1,3,4-thiadiazol-2(3*H*)-ilydene]acetamide), dichlorophenamide (DCP; 4,5-diclhorobenzene-1,3-disulphonamide) as standard by a stopped-flow CO_2 hydrase assay.

Compound	K_I (nM)			
	*h*CA I	*h*CA II	*h*CA IX	*h*CA XII
9	648	642	-	-
28a	514	1250	490	79.4
28b	548	1148	436	76.1
28c	639	1547	42.0	67.7
28d	355	1500	336	88.7
28e	532	1625	94.0	66.9

28f	417	1838	92.9	71.2
28g	385	>10000	84.1	48.6
28h	318	1253	77.2	611
28i	258	2230	912	90.7
28j	380	1305	610	42.4
AAZ	250	12	25	5.7
MZA	780	14	27.0	3.4
DCP	1200	38	50.0	50.0

* Errors in the range of ± 5-10 % of the reported value from 3 different assays.

In general, almost all the *N,N'*-disubstituted thioureas showed an interesting inhibitory profile in nanomolar/micromolar concentration range. In particular, with the exception of **28c** and **28h**, all compounds demonstrated a certain selectivity against *h*CAXII. Moreover, some compounds of the series (ie, **28c-h**) also displayed inhibition constants in the range of 42.0-94.0 nM toward *h*CA IX.

From the structural point of view, it emerges that the derivatization of benzoxaborole **9** *via* the formation of thioureas **28a-j** represents a key feature for the selectivity towards isoforms CA IX and XII. It should be remarked that these derivatives share a selective profile towards the transmembrane isoforms *h*CA IX and *h*CA XII rather than to the cytosolic isoforms *h*CA I and *h*CA II.

It is worth nothing that the compounds **28g** and **28j** proved to be the most potent and selective compounds tested toward *h*CA XII isoform (K_Is = 42.4 nM and 42.4 nM, for **28g** and **28j**, respectively), being comparable with

that clinically used sulfonamide DCP (**Table 11**). Moreover, these compounds exhibited a selectivity ratios CA XII/CA II of ~205 and ~30.7, for **28g** and **28j**, respectively, whereas the selectivity for the clinical used standard drugs (AAZ, MZA and DCP) resulted in the range of 0.36-4.11, calculated for the same isozymes.

Furthermore, compound **28c** showed inhibitory activity against the transmembrane cancer-associated isoform *h*CA IX (K_I= 42.0 nM), with selectivity ratios CA IX/CA II of 36.8, whereas the inhibition potency against the other enzymes resulted 67.7 nM (for CA XII), 639 nM (for CA I), and 1547 nM (for CA II). **28c** demonstrated a significant selectivity compared to that of the clinical used standard drugs (AAZ, MZA and DCP), which resulted in the range of 0.33-0.76 (**Table 11**).

2.7.3.6 Work in progress

All *N,N'*-disubstituted ureas are currently under investigation for their inhibition profile against an extended panel of CAs.

Moreover, selected *N,N'*-disubstituted ureas and *N,N'*-disubstituted thioureas will be crystallized with the target protein with the hope that detailed knowledge of the binding of the compounds to the active site can be used to direct further structural and biological optimization.

2.8 General conclusions

Enzyme inhibition is one important issue for drug design and pharmacological applications. In this context, to identify novel CAIs that selectively inhibit specific isoforms, and to develop hit/lead compounds able to interfere with CA 'orphan' targets, such as the *h*CA I, as well as isoforms involved in hypoxic tumors (ie, *h*CA IX and *h*CA XII), *tiolene-click chemistry* has been successfully employed as a powerful synthetic approach for generating inhibitors belonging to the sulphonamide class. Moreover, pharmacomodulation of previously identified *hits* compounds bearing original pharmacophoric groups, as well as novel chemical scaffold, have been performed in order to improve and to better investigate their biopharmaceutical profile. Some of the synthesized derivatives showed interesting inhibitory activity against the tumor-associated CAs, *h*CA IX and *h*CA XII, providing new chemical platforms for the development of novel anticancer agent.

We hope that these findings can contribute on the development of novel and effective CAIs suitable of clinical use.

EXPERIMENTAL SECTION

General Experimental Procedures.

Anhydrous solvents and all reagents were purchased from Sigma-Aldrich, Merck or Carlo Erba and used without further purification. All reactions involving air- or moisture-sensitive compounds were performed under a nitrogen atmosphere using oven-dried glassware and syringes to transfer solutions. Melting points (m.p.) were determined using an Electrothermal melting point or a Köfler apparatus and are uncorrected. Analytical thin-layer chromatography (TLC) was carried out on Merck silica gel F-254 plates. Flash chromatography purifications were performed on Merck Silica gel 60 (230-400 mesh ASTM) as the stationary phase and column chromatography was performed on silica gel (pore size 60 Å, 40-63 μm particle size). NMR spectra were recorded at 27 °C on Bruker Avance III nanobay 400 MHz (400 MHz for 1H and 101 MHz for ^{13}C, 376 MHz for ^{19}F) or Varian NMR spectrometer VXR-300MHz (at 300 MHz for ^{1}H and 75.4 MHz for ^{13}C) by using $SiMe_4$ as internal standard; the assignment of exchangeable protons (O*H* and N*H*) was confirmed by the addition of D_2O. Elemental analyses were performed by using a Perkin-Elmer Elemental Analyzer 2400-CHN. LC-MS were recorded with a Absciex 4000 QTRAP LC-MSMS system. High-resolution mass spectra (HMRS) were obtained from an ESI-MS spectrometer (SYNAPT G- of Waters).

EXPERIMENTAL SECTION: CHAPTER I

General procedure for the synthesis of amides:

Appropriate amine (0.5 mmol, 1 equiv.) was added to a solution of *N*-chlorosuccinimide (0.55 mmol, 1.1 equiv.) in acetonitrile (7 mL) under nitrogen atmosphere and the solution was stirred at room temperature for about 3 hours. Then, the appropriate aldehyde (2.5 mmol, 5 equiv.), TBHP (2.5 mmol, 5 equiv., 0.34 mL of a 70 wt% in water) and $Cu(OAc)_2H_2O$ (14 mol%) were added under nitrogen atmosphere. The reaction mixture was refluxed for about 50 min. The progress of reaction was monitored by TLC until disappearance of *N*-chloroamine. Then the reaction mixture was quenched with 40 mL of a saturated solution of Na_2SO_3 (for removal of excess TBHP) and extracted with diethyl ether. The organic layer was dried over anhydrous Na_2SO_4 and the solvent was evaporated under reduced pressure. The crude product was purified by silica gel column chromatography to provide the pure amide.

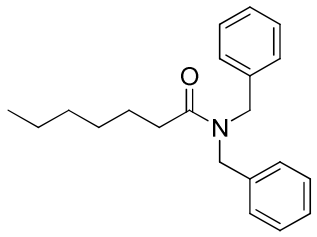

4a

N,N-Dibenzylheptanamide[105]

Coloress oil.

Yield: 76 %.

R*f* : 0.47 (ethyl acetate : petroleum ether = 92:8).

^{1}H NMR 300 MHz ($CDCl_3$): δ 7.40-7.15 (overlapping,10H, ArH), 4.60 (s, 2H, CH_2), 4.44 (s, 2H, CH_2), 2.42 (t, *J* = 7.53 Hz, 2H, CH_2), 1.77-1.67 (overlapping, 2H, CH_2), 1.38-1.27 (overlapping, 6H), 0.87 (t, *J* = 7.23 Hz, 3H, CH_3).

^{13}C NMR 75 MHz ($CDCl_3$): δ 173.7, 137.5, 136.7, 128.9, 128.5, 128.2, 127.5, 127.2, 126.3, 49.8, 48.0, 33.2, 31.5, 29.0, 25.3, 22.4, 14.0.

IR (film): ν˜=2928 (m),1644 (s), 1494 (w), 1453 (m), 1265 (m), 1206 (w), 1078, (w) 736 (s), 699 (m).

Elemental analysis: $C_{21}H_{27}NO$. Calculated C 81.51 H 8.79, N 4.53 Found: C 81.45, H 8.83, N 4.48.

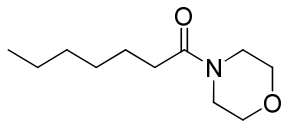

4b

1-Morpholinoheptan-1-one[106]

Pale yellow oil.

Yield: 63 %.

R*f* : 0.40 (ethyl acetate : petroleum ether = 1:1).

^{1}H NMR 300 MHz ($CDCl_3$): δ 3.69-3.47 (overlapping, 6H, ArH), 3.47 (t, J = 5.11 Hz, 2H), 2.32 (t, J = 7.89 Hz, 2H), 1.64-1.57 (m, 2H, CH_2), 1.33-1.27 (overlapping, 6H), 0.89 (t, *J* = 7.01 Hz, 3H).

^{13}C NMR 75 MHz ($CDCl_3$): δ 171.9, 66.9, 66.6, 46.0, 41.9, 33.1, 31.5, 29.1, 25.2, 22.4, 13.9.

IR (film): ν˜=2928 (m), 2858 (m), 2637 (m), 1637 (s), 1457 (m), 1435 (m), 1266 (s), 1115 (s), 1069 (w), 1039 (w), 910 (m), 850 (w), 736 (s), 702 (w), 665 (w).

Elemental analysis: $C_{11}H_{21}NO_2$. Calculated C 66.20, H 10.62, N 7.03 Found: C 66.23, H 10.69, N 6.98.

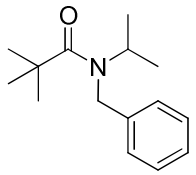

4c

***N*-benzyl-N-isopropyl-2,2-dimethylpropanamide**

Pale yellow oil.

Yield: 65 %.

R*f* : 0.33 (ethyl acetate : petroleum ether = 16:84).

^{1}H NMR 300 MHz ($CDCl_3$): δ 7.41-7.21 (overlapping, 5H, ArH), 5.43 (s, 1H, CH), 4.67 (s, 1H, CH), 4.10-3.99 (m, 1H, CH), 1.24-11 (overlapping, 15H, CH_3).

^{13}C NMR 75 MHz ($CDCl_3$): δ 177.8, 129.4, 128.6, 127.2, 126.4, 41.3.

IR (film): ν˜=3051 (m), 2998 (w), 2938 (s), 2857 (s), 1633 (s), 1442 (s), 1369 (w), 1351 (s), 1277 (s), 1237 (m), 1174 (m), 1127 (m), 110 (s), 1088 (s), 1026 (m), 1001 (s), 954 (m), 885 (s), 838 (s), 734 (s), 701 (m), 662 (w), 626 (w).

Elemental analysis: $C_{15}H_{23}NO$. Calculated C 77.21, H 9.93, N 6.00 Found: C 77.23, H 9.88, N 6.04.

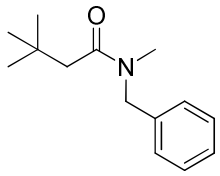

4d

***N*-benzyl-*N*,3,3-trimethylbutanamide**

Pale yellow oil.

Yield: 71 %.

R*f* : 0.40 (ethyl acetate : petroleum ether = 9:1).

^{1}H NMR 300 MHz ($CDCl_3$): δ 7.39-7.14 (overlapping, 5H, ArH), 4.59 (d, *J* = 11.43 Hz, 2H, CH_2), 2.94 (s, 3H, CH_3), 2.32 (s, 2H, CH_2), 1.09 (s, 5H, CH_3), 1.07 (s, 4H, CH_3).

^{13}C NMR 75 MHz ($CDCl_3$): δ 172.4, 172.0, 137.8, 136.9,128.9, 128.5, 128.1, 127.5, 127.2, 126.3, 54.0, 50.7, 44.9, 44.7, 35.9, 33.8, 31.6, 31.4, 30.04, 30.00.

IR (film): ν˜=3063 (w), 3029 (w), 2953 (s), 2866 (m), 1645 (s), 1477 (m), 1453 (m), 1387 (m), 1363 (m), 1254 (w), 1233 (w), 1192 (w), 1106 (s), 1028 (w), 1001 (w), 953 (w), 735 (w).

Elemental analysis: $C_{14}H_{21}NO$. Calculated C 76.67, H 9.65, N 6.39 Found: C 76.73, H 9.61, N 6.43.

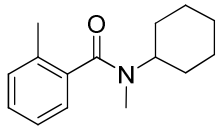

4e

_N_-cyclohexyl-_N_,2-dimethylbenzamide

White solid.

M.p. 49-51 °C.

Yield: 67 %.

R*f* : 0.37 (diethyl ether : petroleum ether = 8:2).

^{1}H NMR 300 MHz ($CDCl_3$): δ 7.24-7.12 (overlapping, 4H), 2.99 (s, 3H), 2.64 (s, 3H, CH_3), 1.78-0.99 (overlapping, 10H, CH_2).

^{13}C NMR 75 MHz ($CDCl_3$): δ 171.3, 171.0, 137.7, 137.2, 133.9, 133.5, 130.3, 130.2, 128.4, 125.9, 125.7, 125.5, 125.1, 58.1, 52.0, 31.2, 30.6, 29.8, 26.8, 25.6, 25.1, 19.0, 18.6.

IR (film): ν̃= 2928 (s), 2855 (m), 1632 (s), 1492 (w), 1449 (m), 1403 (m), 1403 (m), 1367 (w), 1322 (m), 1258 (w), 1186 (w), 1137 (w), 1113 (w), 1061 (m), 1040 (w), 997 (w), 894 (w), 770 (m), 728 (m), 656 (w), 640 (w), 617 (w).

Elemental analysis: $C_{15}H_{21}NO$. Calculated C 77.88, H 9.15, N 6.05. Found C 77.89, H 9.11, N 6.09.

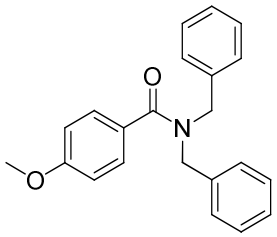

4f

_N_,_N_-dibenzyl-4-methoxybenzamide[107]

White solid.

M.p. 120-122 °C.

Yield: 70 %.

R*f* : 0.29 (diethyl ether : petroleum ether = 8:2).

^{1}H NMR 300 MHz ($CDCl_3$): δ 7.48 (d, J = 8.50 Hz, 2H, ArH), 7.38-7.20 (overlapping, 10H), 6.88 (d, J = 8.81 Hz, 2H, ArH), 4.67 (br s, 2H, CH_2), 4.48 (br s, 2H, CH_2), 3.80 (s, 3H, CH_3).

^{13}C NMR 75 MHz ($CDCl_3$): δ 172.1, 160.7, 136.9, 128.7, 128.5, 128.2, 127.5, 127.0, 113.8, 55.0, 50.9, 47.1.

IR (film): ν̃= 3062 (w), 2923 (s), 2852 (m), 1631 (s), 1513 (m), 1494 (m), 1452 (s), 1421 (s), 1363 (w), 1301 (m), 1249 (s), 1174 (m), 1143 (w), 1078 (m), 1031 (m), 993 (m), 923 (w), 840 (s), 734 (s), 700 (s).

Elemental analysis: $C_{22}H_{21}NO_2$. Calculated C 79.73, H, 6.39, N, 4.23. Found: C 79.67, H 6.35, N 4.19.

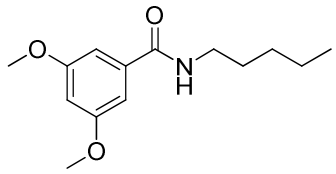

4g

3,5-dimethoxy- *N*-pentylbenzamide[108]

Pale yellow oil.

Yield: 73 %.

R*f* : 0.30 (ethyl acetate : petroleum ether = 2:8).

^{1}H NMR 300 MHz ($CDCl_3$): δ 6.87 (d, J = 2.29 Hz, 2H, ArH), 6.56 (t, J = 2.28 Hz, 1H, ArH), 6.13 (br s, 1H, NH), 3.81 (s, 6H, CH_3), 3.45-3.39 (m, 2H, CH_2), 1.62-1.55 (m, 2H, CH_2), 1.37-1.32 (m, 4H, CH_2), 0.90 (t, J = 7.25 Hz, 3H, CH_3).

^{13}C NMR 75 MHz ($CDCl_3$): δ 167.5, 161.1, 137.4, 105.0, 103.5, 55.7, 40.3, 29.5, 29.3, 22.6, 14.2.

IR (film): ν̃= 2957 (m), 2930 (m), 2857 (m), 1639 (m), 1593 (s), 1541 (m), 1457 (m), 1426 (m), 1348 (m), 1266 (w), 1206 (s), 1157 (s), 1065 (m), 926 (w), 842 (w), 738 (m), 702 (w).

Elemental analysis: $C_{14}H_{21}NO_3$. C, 66.91, H, 8.42, N, 5.57. Found: C, 66.87, H, 8.39, N, 5.62.

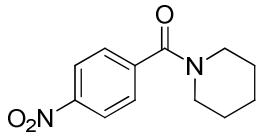

4h

_N_-(4-Nitrobenzoyl)piperidine[109]

White solid.

M.p. 119-120 °C.[110]

Yield: 95 %.

R*f* : 0.32 (ethyl acetate : petroleum ether = 4:6).

^{1}H NMR 300 MHz ($CDCl_3$): δ 8.26 (d, *J* = 8.63 Hz, 2H, ArH), 7.54 (d, *J* = 7.53 Hz, 2H, ArH), 3.72 (s, 2H, CH_2), 3.28 (s, 2H, CH_2), 1.70 (s, 4H, CH_2), 1.52 (s, 2H, CH_2).

^{13}C NMR 75 MHz ($CDCl_3$): δ 168.1, 148.2, 142.7, 127.8, 123.8, 48.6, 43.2, 26.5, 25.5, 24.4.

IR (film): ν̃= 3055 (w), 2924 (m), 2857 (m), 1633 (s), 1600 (m), 1523 (s), 1444 (s), 1351 (s), 1276 (s), 1106 (m), 1001 (m), 888 (w), 862 (m), 850 (m), 826 (w), 736 (s).

Elemental analysis: $C_{12}H_{14}N_2O_3$. Calculated C 61.53, H 6.02, N 11.96. Found: C 61.48, H 6.07, N 11.89.

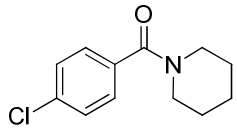

4i

***N*-(4-Chlorobenzoyl)piperidine**[101]

Pale yellow oil.

Yield: 97 %.

R*f* : 0.32 (ethyl acetate : petroleum ether = 1:9).

^{1}H NMR 300 MHz ($CDCl_3$): δ 7.39-7.32 (overlapping, 4H, ArH), 3.68 (s, 2H, CH_2), 3.33 (s, 2H, CH_2), 1.67-1.53 (overlapping, 6H, CH_2).

^{13}C NMR 75 MHz ($CDCl_3$): δ 169.0, 135.2, 134.7, 128.5, 128.2, 48.6, 43.2, 29.5, 25.6, 24.4.

IR (film): ν̃= 2936 (s), 2855 (s), 1630 (s), 1439 (s), 1276 (s), 1088 (m), 1016 (m), 1001 (m), 885 (m), 838 (m).

Elemental analysis: $C_{12}H_{14}ClNO$. Calculated C 64.43, H 6.31, N 6.26. Found C 64.39, H, 6.35, N, 6.29.

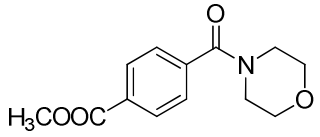

4j

Methyl 4-(morpholine-4-carbonyl)benzoate[111]

White solid.

M.p. 73-75 °C.

Yield: 82 %.

R*f* : 0.36 (ethyl acetate : petroleum ether = 7:3).

^{1}H NMR 300 MHz ($CDCl_3$): δ 8.09 (d, *J* = 8.14 Hz, 2H, ArH), 7.48 (d, *J* = 8.15 Hz, 2H, ArH), 3.94 (s, 3H, CH_3), 3.79-3.93 (ovelapping, 8H, CH_2).

^{13}C NMR 75 MHz ($CDCl_3$): δ 169.3, 166.1, 139.5, 131.3, 129.8, 127.0, 66.7, 52.2, 42.4.

IR (film): ν˜= 2955 (w), 2856 (w), 1720 (s), 1633 (s), 1507 (w), 1433 (s), 1362 (w), 1278 (s), 1180 (m), 1156 (w), 1114 (s), 1067 (m), 1014 (m), 962 (w), 895 (m), 895 (w), 865 (w), 842 (w), 824 (w), 785 (m), 726 (m).

Elemental analysis: $C_{13}H_{15}NO_4$. C 62.64, H 6.07, N 5.62. Found: C 62.61, H6.11, N 5.58.

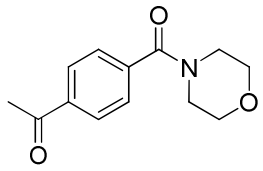

4k

1-(4-(Morpholine-4-carbonyl)phenyl)ethanone[112]

White solid.

M.p. 96-98 °C.

Yield: 82 %.

R*f* : 0.38 (ethyl acetate : petroleum ether = 8:2).

^{1}H NMR 300 MHz ($CDCl_3$): δ 8.01 (d, *J* = 8.52 Hz, 2H, ArH), 7.50 (d, *J* = 8.51 Hz, 2H, ArH), 3.79-3.41 (overlapping, 8H, CH_2), 2.63 (s, 3H, CH_3).

^{13}C NMR 75 MHz ($CDCl_3$): δ 197.4, 169.5, 139.9, 138.2, 128.8, 127.5, 67.0, 29.9, 26.9.

IR (film): ν̃= 2922 (m), 2854 (m), 1716 (m), 1685 (s), 1532 (s), 1507 (w), 1458 (m), 1432 (m), 1402 (w), 1360 (m), 1300 (m), 1262 (s), 1157 (w), 1114 (s), 1068 (w), 1024 (m), 1011 (m), 959 (w), 913 (m), 838 (m), 732 (s), 647 (w).

Elemental analysis: $C_{13}H_{15}NO_3$. C, 66.94, H, 6.48, N, 6.00. Found: C, 66.91, H, 6.43, N, 6.04.

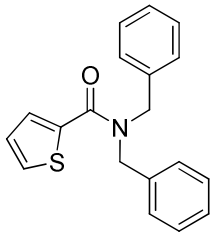

4l

N,N -Dibenzylthiophene-2-carboxamide[113]

White solid.

M.p. 48-50 °C.

Yield: 73%.

R*f* : 0.30 (ethyl acetate : petroleum ether = 1:9).

^{1}H NMR 300 MHz ($CDCl_3$): δ 7.45 (d, *J* = 5.04 Hz, 1H, ArH), 7.38-7.26 (overlapping, 11H, ArH), 6.95 (t, *J* = 3.70 Hz, 1H, ArH), 4.72 (s, 4H, CH_2).

^{13}C NMR 75 MHz ($CDCl_3$): δ 165.0, 137.7, 136.6, 129.3, 128.8, 128.6, 127.6, 126.9, 50.

IR (film): ν̃= 3029 (m), 2921 (m), 1616 (s), 1521 (m). 1494 (m), 1452 (m), 1428 (s), 1363 (m), 1253 (s), 1203 (w), 1076 (w), 1027 (w), 975 (m), 910 (w), 854 (m), 734 (s), 698 (s).

Elemental analysis: $C_{19}H_{17}NOS$. C, 74.23, H, 5.57, N, 4.56. Found: C, 74.26, H, 5.54, N, 4.59.

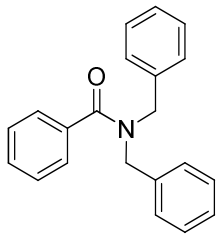

4m

***N*,*N*-Dibenzylbenzamide**[97]

White solid.

M.p. 114-115 °C.

Yield: 75 %.

R*f* : 0.24 (diethyl ether : petroleum ether = 92:8).

^{1}H NMR 300 MHz ($CDCl_3$): δ 7.51-7.48 (overlapping, 2H, ArH), 7.37-7.28 (overlapping, 11H, ArH), 7.14-7.12 (s, 2H, ArH), 4.70 (s, 2H, CH_2), 4.40 (s, 2H, CH_2).

^{13}C NMR 75 MHz ($CDCl_3$): δ 172.2, 136.2, 129.5, 128.7, 128.4, 127.5, 126.9, 126.6, 51.4, 46.8.

IR (film): ν̃= 3061 (m), 3029 (m), 2923 (m), 1634 (s), 1577 (w), 1495 (s), 1451 (s), 1421 (s), 1363 (m), 1307 (m), 1264 (s) 1204, (w) 1142 (m), 1077 (m), 1028 (m), 992 (m), 931 (w), 894 (w), 786 (w), 733 (s), 699 (s), 649 (w).

Elemental analysis: $C_{21}H_{19}NO$. Calculated C 83.69, H 6.35, N 4.65. Found: C 83.67, H 6.39, N 4.72.

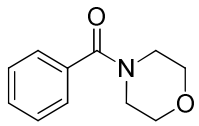

4n

Morpholino(phenyl)methanone[99]

White solid.

M.p. 40-50 °C.

Yield: 65 %.

R*f* : 0.37 (diethyl ether : petroleum ether = 8:2).

^{1}H NMR 300 MHz ($CDCl_3$): δ 7.41-7.34 (overlapping, 5H, ArH), 3.79-3.42 (overlapping, 8H, CH_2).

^{13}C NMR 75 MHz ($CDCl_3$): δ 170.3, 135.3, 129.8, 128.5, 127.0, 66.8, 42.3.

IR (film): ν˜=3058 (m), 2973 (m), 2923 (m), 2857 8m), 1613 (s), 1496 (m), 1432 (s), 1365 (w), 1301 (m), 1278 (s), 1259 (s), 1365 (w), 1301 (m), 1278 (s), 1259 (s), 1157 (w), 1114 (s), 1068 (m), 1018 (s), 933 (m), 890 (m), 842 (m), 788 (m), 734 (s) 646 (w).

Elemental analysis: $C_{11}H_{13}NO_2$. Calculated C 69.09, H 6.85, N 7.32 Found: C 69.01, H 6.88, N 7.36.

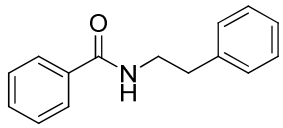

4o

N-Phenethylbenzamide[114]

White solid.

M.p. 114-115 °C.

Yield: 96 %.

R*f* : 0.43 (ethyl acetate : petroleum ether = 3:7).

^{1}H NMR 300 MHz ($CDCl_3$): δ 7.68 (d, J = 6.85 Hz, 2H, ArH), 7.49-7.30 (overlapping, 5H, ArH), 7.26-7.22 (overlapping, 3H), 6.20 (br s, 1H, NH), 3.71 (q, J = 5.96 Hz, 2H, CH_2), 2.93 (t, J = 6.88 Hz, 2H, CH_2).

^{13}C NMR 75 MHz ($CDCl_3$): δ 167.4, 138.9, 134.7, 131.3, 128.8, 128.7, 128.5, 126.8, 126.6, 41.1, 35.7.

IR (film): ν˜= 3343 (s), 3054 (m), 1640 (s), 1545 (m), 1486 (w), 1455 (w), 1265 (s), 1193 (w),

739 (s), 699 (m), 665 (m).

Elemental analysis: $C_{15}H_{15}NO$. C, 79.97, H, 6.71, N, 6.22. Found: C, 79.91, H, 6.63, N, 6.25.

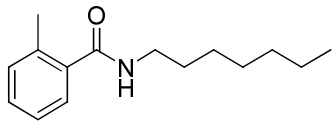

4p

***N*-heptyl-2-methylbenzamide**

Pale yellow solid.

Yield: 96 %.

R*f* : 0.30 (ethyl acetate : petroleum ether = 1:9).

^{1}H NMR 300 MHz ($CDCl_3$): δ 7.31-7.13 (overlapping, 4H, ArH), 5.94 (bs, 1H, NH), 3.38 (q, *J* = 6.88 Hz, 2H, CH_2), 2.41 (s, 3H, CH_3), 1.62-1.52 (m, 2H, CH_2), 1.34-1.29 (overlapping, 8H, CH_2), 0.91-0.86 (m, 3H, CH_3).

^{13}C NMR 75 MHz ($CDCl_3$): δ 170.0, 136.8, 135.8, 130.8, 129.5, 126.5, 125.5, 39.7, 31.7, 29.6, 28.9, 26.8, 22.5, 19.6, 13.9.

IR (film): ν̃= 2958 (w), 2927 (m), 2856 (m), 1639 (s), 1540 (m), 1485 (w), 1456 (w), 1377 (w), 1309 (w), 1265 (m), 1159 (w), 1108 (w), 1063 (w), 940 (w), 738 (s).

Elemental analysis: $C_{13}H_{23}NO$. C, 77.21, H, 9.93, N, 6.00. Found: C, 77.25, H, 9.89, N, 5.94.

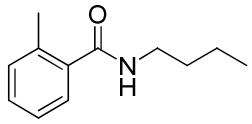

4q

***N*-butyl-2-methylbenzamide**[115]

Pale yellow oil.

Yield: 64 %.

R*f* : 0.35 (ethyl acetate : petroleum ether = 2:8).

^{1}H NMR 300 MHz ($CDCl_3$): δ 7.31-7.14 (overlapping, 4H, ArH), 5.92 (bs, 1H, NH), 3.39 (q, *J* = 7.01 Hz, 2H, CH_2), 2.4 (s, 3H, CH_3), 1.59-1.54 (m, 2H, CH_2), 1.41-1.38 (m, 2H, CH_2), 0.95 (t, *J* = 7.27 Hz, 3H, CH_3).

^{13}C NMR 75 MHz ($CDCl_3$): δ 170.3, 137.0, 136.0, 131.1, 129.8, 126.8, 125.8, 39.7, 31.9, 20.3, 19.9, 13.9.

IR (film): ν˜= 3052 (m), 2960(s), 2930 (s), 2873 (m), 1643 (s), 1601 (w), 1537 (s), 1485 (m), 1456 (m), 1379 (w), 1307 (m), 1265 (s), 1158 (w), 1109 (w), 1007 (w), 856 (w), 739 (s), 703 (m), 658 (w).

Elemental analysis: $C_{12}H_{17}NO$. C, 75.35, H, 8.96, N, 7.32. Found: C, 75.31, H, 8.92, N, 7.38.

Trapping of the acyl radical:[31,39]

Dibenzylamine (0.5 mmol, 1 equiv.) was added to a solution of *N*-chlorosuccinimide (0.55 mmol, 1.1 equiv.) in acetonitrile (7 mL) under nitrogen atmosphere and the solution was stirred at room temperature for

about 3 hours. Then benzaldehyde (2.5 mmol, 5 equiv.), 2,2,6,6-tetramethylpiperidine 1-oxyl (TEMPO, 2.5 mmol, 2.5 equiv), TBHP (2.5 mmol, 5 equiv., 0.34 mL of a 70 wt% in water) and $Cu(OAc)_2H_2O$ (14 mol%) were added under nitrogen atmosphere. The reaction mixture was refluxed for about 50 min. The reaction mixture was refluxed for about 50 min. Then the reaction mixture was quenched with 40 mL of a saturated solution of Na_2SO_3 (for removal of excess TBHP) and extracted with diethyl ether. The organic layer was dried over anhydrous Na_2SO_4 and the solvent was evaporated under reduced pressure. The crude product was purified by silica gel column chromatography to provide the TEMPO adduct.

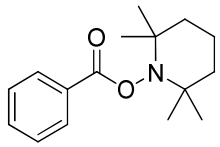

2,2,6,6-tetramethylpiperidin-1-yl benzoate[39]

Colorless oil.

Yield: 40 %.

R*f* : 0.30 (ethyl acetate : petroleum ether = 1:6).

^{1}H NMR 300 MHz ($CDCl_3$): δ 8.08 (d, *J* = 7.11 Hz, 2H, ArH), 7.57 (t, *J* = 7.93 Hz, 1H, ArH), 7.46 (t, *J* = 7.32 Hz, 2H, CH_2) 1.78-1.60 (overlapping, 6H, CH_2), 1.28 (s, 6H, CH_3), 1.12 (s, 6H, CH_3).

^{13}C NMR 75 MHz ($CDCl_3$): δ 166.3, 132.8, 129.5, 128.4, 60.4, 39.1, 31.9, 20.8, 16.9.

IR (film): ν̃= 3062 (m), 2975 (m), 2938 (m), 1745 (s), 1601 (w), 1451 (m), 1379 (m), 1364 (m), 1348 (w), 1313 (w), 1257 (s), 1238 (m), 1176 (m), 1082 (s), 1063 (s), 994 (m), 953 (m), 911 (m), 875 (w), 737 (s), 706 (s), 650 (w).

Elemental analysis: $C_{16}H_{23}NO_2$. C, 73.53, H, 8.87, N, 5.36. Found: C, 73.46, H, 8.79, N, 5.31.

EXPERIMENTAL SECTION: CHAPTER II

General procedure for the preparation of 2,3,5,6-tetrafluoro-4-(5-*R*-1*H*-1,2,3-triazol-1-yl)benzenesulfonamide 6a-b.[73]

To a 1:$1_{v/v}$ solution of H_2O/*tert*-ButOH (2 mL), compound **12** (0.64 mmol) was added under stirring followed by the addition of the appropriate alkyne (**13a-b**, 0.64 mmol), nanosized activated powder Cu(0) (0.064 mmol) and triethylamine hydrochloride (0.64 mmol). The reaction mixture was stirred at room temperature for 16 h. After the addition of a further amount of alkyne (0.32 mmol) the reaction mixture was stirred for 24 h and then was diluted with water and extracted with ethyl acetate. The combined organic phases were washed with brine, dried over anhydrous sodium sulphate and evaporated. The obtained solid was purified by flash chromatography.

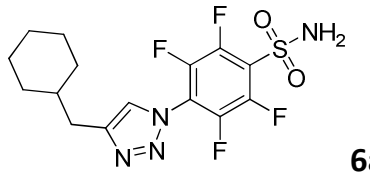

6a

4-(4-(cyclohexylmethyl)-1*H*-1,2,3-triazol-1-yl)-,3,5,6-tetrafluorobenzene

Sulfonamide

Yellow solid.

Yield: 60 %.

R*f* : 0.66 (ethyl acetate : petroleum ether = 1:1).

M.p.: 144-146 °C

^{1}H NMR 200 MHz (DMSO-d_6): δ 8.65 (bs, 2H, SO_2NH_2); 8.39 (s, 1H, Ar-H); 2.64 (d, 2H, CH_2); 1.71-0.96 (m, 11H).

MS: *m/z* 393 (M^+).

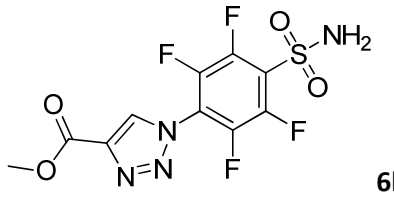

6b

Methyl1-(2,3,5,6-tetrafluoro-4-sulfamoylphenyl)-1*H*-1,2,3-triazol-4-carboxylate

White powder.

Yield: 60 %.

R*f* : 0.55 (ethyl acetate : petroleum ether = 1:1).

M.p.: 184-186 °C

^{1}H NMR 200 MHz (DMSO-d_6): δ 9.35 (s, 1H, Ar-H); 8.69 (bs, 2H, SO_2NH_2); 3.90 (s, 3H, OCH_3).

IR (nujol) *v* cm^{-1} = 1731.71 (O-C=O ester); 1376.93-1166.72 (SO_2NH_2); 3351.68-3249.47 (stretching NH);

MS: *m/z* 355 [M^+].

General procedure for the preparation of *N*,*N*-dimethyl arene aldehyde hydrazones 17a-f:[80,116]

To a well-stirred amount of the appropriate arene aldehyde **16a-f** (3.8 mmol, 1 equiv.), *N,N*-dimethyl-hydrazine (4.2 mmol, 1.1. equiv) was added dropwise. For liquid arene aldehydes the reaction was conducted without solvent, whilst CH_2Cl_2 (4 mL) was used in case of solid arene aldehydes. After being stirred for about 6 h, CH_2Cl_2 (5 mL) was added to the mixture, then it was dried over Na_2SO_4, and the solvent was evaporated under reduce pressure to afford the product as a pale yellow oil or white solid.

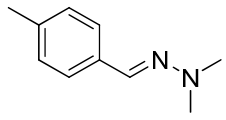

17a

(*E*)-1,1-dimethyl-2-(-methylbenzylidene)hydrazine[80]

Pale yellow oil.

Yield: 98 %.

R*f*: 0.66 (ethyl acetate : petroleum ether = 3:7).

^{1}H NMR 400 MHz ($CDCl_3$): δ 7.46 (d, *J* = 7.8 Hz, 2H, ArH), 7.25 (s. 1H, CH), 7.1 (d, *J* = 7.9 Hz, 2H, ArH), 2.94 (s, 6H, NCH_3), 2.33 (s, 3H, CH_3).

LC/MS: m/z 163.1 $[M+H]^+$.

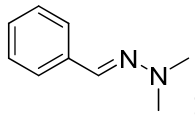

17b

(*E*)-2-benzylidene-1,1-dimethylhydrazine[80]

Pale yellow oil.

Yield: 98 %.

R*f*: 0.74 (ethyl acetate : petroleum ether = 2:8).

^{1}H NMR 400 MHz ($CDCl_3$): δ 7.56 (d, *J* = 7.6 Hz, 2H, ArH), 7.30 (t, *J* = 7.5 Hz, 2H, ArH), 7.23 (s, 1H, CH), 7.20 (m, 1H, ArH), 2.95 (s, 6H, NCH_3).

LC/MS: m/z 149.1 $[M+H]^+$.

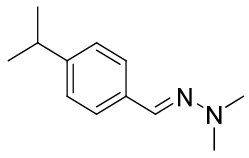

17c

(*E*)-2-(4-isopropylbenzylidene)-1,1-dimethylhydrazine

Pale yellow oil.

Yield: 96 %.

Rf: 0.73 (ethyl acetate : petroleum ether = 3:7).

^{1}H NMR 400 MHz ($CDCl_3$): δ 7.49 (d, *J* =8.1 Hz, 2H, ArH), 7.26 (s, 1H, CH), 7.18 (d, *J* = 7.9 Hz, 2H, ArH), 2.94 (s, 6H, NCH_3), 2.91-2.85 (m, 1H, CH), 1.24 (d, *J* = 6.9 Hz, 6H, CH_3).

^{13}C NMR 101 MHz ($CDCl_3$): δ 148.32, 134.48 (s, C=N), 133.57, 126.55, 125.66, 42.97, 33.91, 23.94.

LC/MS: m/z 190.1 $[M]^+$, 191.9 $[M+H]^+$.

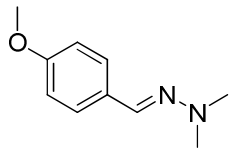

17d

(*E*)-2-(4-methoxybenzylidene)-1,1-dimethylhydrazine[80]

Pale yellow oil.

Yield: 83 %.

R*f*: 0.59 (ethyl acetate : petroleum ether = 2:8).

^{1}H NMR 400 MHz ($CDCl_3$): δ 7.51 (d, *J* = 9.0 Hz, 2H, ArH), 7.26 (s, 1H, CH), 6.87 (d, *J* = 8.8 Hz, 2H, ArH), 3.81 (s, 3H, CH_3), 2.92 (s, 6H, NCH_3).

LC/MS: m/z 179.1 $[M+H]^+$.

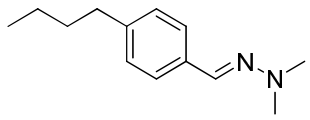

17e

(*E*)-2-(4-butylbenzylidene)-1,1-dimethylhydrazine

Pale yellow oil.

Yield: 97 %.

Rf: 0.71 (ethyl acetate : petroleum ether = 0.2:9.8).

^{1}H NMR 400 MHz ($CDCl_3$): δ 7.47 (d, *J* = 8.1 Hz, 2H, ArH), 7.26 (s, 1H, CH), 7.13 (d, *J* = 7.9 Hz, 2H, ArH), 2.94 (s, 6H, NCH_3), 2.59 (t, *J* =7.7 Hz, 2H, CH_2), 1.59 (m, 2H, CH_2), 1.35 (m, 2H, CH_2), 0.92 (t, *J* = 7.2 Hz, 3H, CH_3).

^{13}C NMR 101 MHz ($CDCl_3$): δ 142.36, 134.32 (s, C=N), 133.59, 128.58, 125.61, 42.97, 35.46, 33.60, 22.34, 13.98.

LC/MS: m/z 204.2 $[M]^+$, 226.8 $[M+Na]^+$.

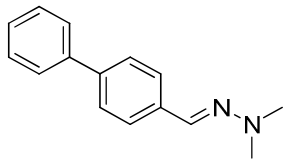

17f

(*E*)-2-(biphenyl-4-ylmethylene)-1,1-dimethylhydrazine

White solid.

M.p. 83-84 °C.

Yield: 93 %.

Rf: 0.77 (ethyl acetate : petroleum ether = 2:8).

^{1}H NMR 400 MHz ($CDCl_3$): δ 7.60 (overlapping, 6H, ArH), 7.43 (t, *J* = 7.4 Hz, 2H, ArH), 7.33 (t, *J* = 7.6 Hz, 1H, ArH), 7.28 (s, 1H, CH), 2.99 (s, 6H, NCH_3).

^{13}C NMR 101 MHz ($CDCl_3$): 140.9, 139.9, 136.0, 132.3 (s, CN), 128.8, 127.2, 126.9, 126.0, 42.9.

LC/MS: m/z 225.0 $[M+H]^+$, 247.1 $[M+Na]^+$.

General procedure for the trifluoroacetylation of *N*,*N*-dimethyl arene aldehyde hydrazones 18a-f:[80]

To an ice-cooled mixture of *N,N*-dimethyl arene aldehyde hydrazones **17a-f** (3.3 mmol, 1 equiv.) and 2,6-lutidine (2 equiv. for **17a,b** , 3 equiv. for **17c-e**, 4 equiv. for **17f**) in anhydrous dichloromethane (10 mL), a solution of trifluoroacetic anhydride (TFAA, 2 equiv. for **17a,b**, 6 equiv. for **17f** , 10

equiv. for **17d**) in dichloromethane (3 mL) was added dropwise with continuous stirring. The mixture was warmed to 20 °C and stirring was continued for about 6 hours. Then the reaction mixture was diluted with dichloromethane (5 mL), washed once with HCl 0.1N, once with H_2O and once with $Na_2CO_{3(aq)}$. The organic layer was dried over anhydrous Na_2SO_4 and the solvent was removed under reduced pressure to afford the crude product, which was purified by trituration with petroleum ether and diethyl ether.

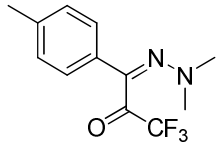

18a

(*Z*)-3-(2,2-dimethylhydrazono)-1,1,1-trifluoro-3-*p*-tolylpropan-2-one[80]

White solid.

M.p. 113-115 °C.

Yield: 50 %.

R*f*: 0.31 (ethyl acetate : petroleum ether = 2:8).

^{1}H NMR 400 MHz ($CDCl_3$): δ 7.17 (d, *J* = 7.9 Hz, 2H, ArH), 7.10 (d, *J* = 7.9 Hz, 2H, ArH), 3.05 (s, 6 H, NCH_3), 2.37 (s, 3H, CH_3).

^{13}C NMR 101 MHz ($CDCl_3$): δ 178.0 (q, *J* = 29.9 Hz, CO), 138.5, 131.9 (s, C=N), 130.3, 129.9, 128.5, 117.8 (q, *J* = 292.2 Hz, CF_3), 47.1, 21.3.

^{19}F NMR 376 MHz ($CDCl_3$): δ -68.8 (s, 3F, CF_3).

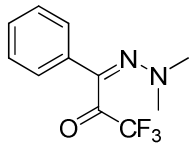

18b

(*Z*)-3-(2,2-dimethylhydrazono)-1,1,1-trifluoro-3-phenyl propan-2-one[80]

Pale yellow solid.

M.p. 71 °C.

Yield: 63 %.

R*f*: 0.27 (ethyl acetate : petroleum ether = 1:9).

^{1}H NMR 400 MHz ($CDCl_3$): δ 7.36 (overlapping, 3H, ArH), 7.21 (overlapping, 2H, ArH), 3.05 (s, 6H, NCH_3).

^{13}C NMR 101 MHz ($CDCl_3$): δ 177.9 (q, *J* = 30.3 Hz, CO), 133.0 (s, C=N), 130.5, 128.6, 127.7, 125.9, 118.0 (q, *J* = 292.3 Hz, CF_3), 47.1.

^{19}F NMR 376 MHz ($CDCl_3$): δ -68.8 (s, 3F, CF_3).

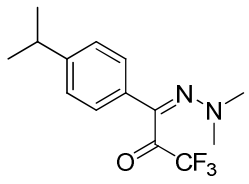

18c

(*Z*)-3-(2,2-dimethylhydrazono)-1,1,1-trifluoro-3-(4-isopropylphenyl)propan-2-one

White crystals.

M.p. 86-88 °C.

Yield: 30 %.

R*f*: 0.70 (ethyl acetate : petroleum ether = 2:8).

^{1}H NMR 400 MHz ($CDCl_3$): δ 7.21 (d, *J* = 7.9 Hz, 2H, ArH), 7.12 (d, *J* = 7.9 Hz, 2H, ArH), 3.05 (s, 6 H, NCH_3), 2.95-2.88 (m, 1H, CH), 1.25 (d, *J* = 7.2 Hz, 6H, CH_3).

^{13}C NMR 101 MHz ($CDCl_3$): δ 176.2 (q, *J* = 32.1 Hz, CO), 149.9, 149.4, 140.0, 131.5 (s, C=N), 130.4, 126.5, 125.9, 122.9 (q, *J* = 286.6 Hz, CF_3), 41.2, 33.9, 23.7.

^{19}F NMR 376 MHz ($CDCl_3$): δ - 68.8 (s, 3F, CF_3).

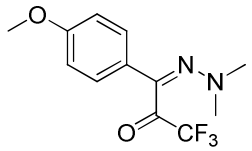

18d

(*Z*)-3-(2,2-dimethylhydrazono)-1,1,1-trifluoro-3-(4-methoxyphenyl)propan-2-one[80]

Beige solid.

M.p. 85 °C.

Yield: 35 %.

Rf: 0.30 (ethyl acetate : petroleum ether = 1.5:8.5).

^{1}H NMR 400 MHz ($CDCl_3$): δ 7.13 (d, *J* = 8.5 Hz, 2H, ArH), 6.89 (d, *J* = 8.5 Hz, 2H, ArH), 3.83 (s, 6 H, NCH_3), 3.06 (s, 3H, CH_3).

^{13}C NMR 101 MHz ($CDCl_3$): δ 190.8 (q, *J* =30.3 Hz, CO), 159.7, 131.7 (s, C=N), 127.4, 118.0 (q, *J* =292.2 Hz, CF_3), 113.8, 113.4, 52.2, 47.1.

^{19}F NMR 376 MHz ($CDCl_3$): δ -68.8 (s, 3F, CF_3).

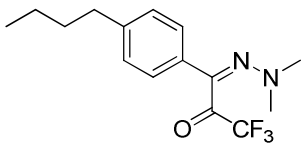

18e

(*Z*)-3-(4-butylphenyl)-3(2,2-dimethylhydrazono)-1,1,1-trifluoropropan-2-one

White crystals.

M.p. 86-88 °C.

Yield: 65 %.

R*f*: 0.48 (ethyl acetate : petroleum ether = 1:9).

^{1}H NMR 400 MHz ($CDCl_3$): δ 7.17 (d, *J* = 8.0 Hz, 2H, ArH), 7.11 (d, *J* = 7.9 Hz, 2H, ArH), 3.05 (s, 6 H, NCH_3), 2.62 (t, *J* = 8 Hz, 2H, CH_2), 1.65-1.57 (m, 2H, CH_2) 1.41-1.32 (m, 2H, CH_2), 0.93 (t, *J* = 7.4 Hz, 3H, CH_3).

^{13}C NMR 101 MHz ($CDCl_3$): δ 175.2 (q, *J* = 31.1 Hz, CO), 143.5, 130.3 (s, C=N), 127.9, 118.0 (q, *J* = 292.3 Hz, CF_3), 47.1, 35.5, 33.4, 22.4, 13.4.

^{19}F NMR 376 MHz ($CDCl_3$): δ -68.8 (s, 3F, CF_3).

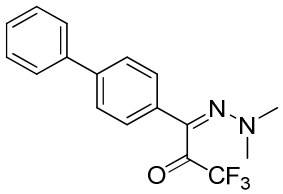

18f

(*Z*)-3-(biphenyl-4-yl)-3(2,2-dimethylhydrazono)-1,1,1-trifluoropropan-2-one

White solid.

M.p. 145 °C.

Yield: 89 %.

R*f*: 0.25 (ethyl acetate : petroleum ether = 2:9).

^{1}H NMR 400 MHz ($CDCl_3$): δ 7.62-7.59 (overlapping, 4H, ArH), 7.45 (t, *J* = 7.8 Hz, 2H, ArH), 7.36 (t, *J* = 7.1 Hz, 1H, ArH), 7.29 (d, *J* = 7.3 Hz, 2H, ArH), 3.10 (s, 6 H, NCH_3).

^{13}C NMR 101 MHz ($CDCl_3$): δ 178.0 (q, *J* = 32.4 Hz, CO), 141.4, 140.3, 131.9 (s, C=N), 130.9, 128.9, 127.1, 127.1, 126.5, 122.4, 118.0 (q, *J* = 292.6 Hz, CF_3), 47.3.

^{19}F NMR 376 MHz ($CDCl_3$): δ -68.8 (s, 3F, CF_3).

Hydrolysis of trifluoroacetylated *N*,*N*-dimethyl hydrazones 8 and IIIa-e:[80]

The opportune trifluoroacetylated hydrazone **18a-f** was dissolved in 5N H_2SO_4 and the solution was stirred for 24 h for compounds **18a,b**, 2.5 h for **18c** and 1 h for **18e** at room temperature (for **18d and 18f** the reaction mixture was heated at 60 °C for 24 hours). Then the product was extracted with diethyl ether and the organic layers were dried over Na_2SO_4, and the solvent was evaporated under reduced pressure. The product was then purified by trituration with petroleum ether and diethyl ether.

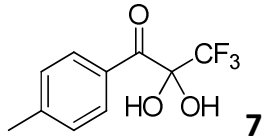

7

3,3,3-trifluoro-2,2-dihydroxy-1-*p*-tolylpropan-1-one[80]

White crystals.

M.p. 84-86 °C.

Yield: 60 %.

R*f*: 0.51 (ethyl acetate : petroleum ether = 2:8)

^{1}H NMR 400 MHz ($CDCl_3$): δ 8.23 (d, *J* = 8.6 Hz, 2H, ArH), 7.30 (d, *J* = 8.6 Hz, 2H, ArH), 4.79 (s, 2 H, OH), 2.45 (s, 3H, CH_3).

^{13}C NMR 101 MHz ($CDCl_3$): δ 191.4 (s, CO), 146.7, 132.0, 129.3, 128.9, 121 (q, *J* = 289.1 Hz, CF_3), 93 (q, *J* = 32.5 Hz, COH), 21.9.

^{19}F NMR 376 MHz ($CDCl_3$): δ -81.2 (s, 3F, CF_3).

ESI: m/z 231.0 $[M-2]^+$

Elemental analysis: $C_{10}H_9F_3O_3$. Calculated C 51.29, H 3.87. Found: C 51.73, H 3.78.

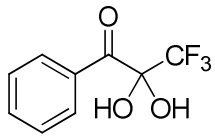

IIIa

3,3,3-trifluoro-2,2-dihydroxy-1-phenylpropan-1-one[80]

White crystals

M.p. 83 °C

Yield: 60 %

R*f*: 0.47 (ethyl acetate : petroleum ether = 2:8)

^{1}H NMR 400 MHz ($CDCl_3$): δ 8.33 (d, *J* = 8.1 Hz, 2H, ArH), 7.67 (t, *J* = 7.1 Hz, 1H, ArH), 7.51 (t, *J* = 7.8 Hz, 2H, ArH), 4.80 (s, 2 H, OH).

^{13}C NMR 101 MHz ($CDCl_3$): δ 191.2 (s, CO), 135.2, 131.8, 131.6, 128.5, 121.0 (q, *J* = 286.8 Hz, CF_3), 93.8 (q, *J* = 35.6 Hz, COH).

^{19}F NMR 376 MHz ($CDCl_3$): δ -81.1 (s, 3F, CF_3).

ESI: m/z 257.0 $[M+K-2]^+$

Elemental analysis: $C_9H_7F_3O_3$. Calculated C 49.10, H 3.20. Found: C 49.07, H 3.32.

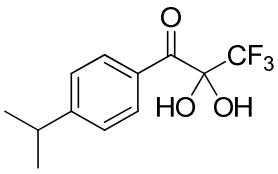

IIIb

3,3,3-trifluoro-2,2-dihydroxy-1-(4-isopropylphenyl)propan-1-one

Yellow oil

Yield: 82 %

R*f*: 0.25 (ethyl acetate : petroleum ether = 1:9)

^{1}H NMR 400 MHz ($CDCl_3$): δ 8.27 (d, *J* = 8.2 Hz, 2H, ArH), 8.35 (t, *J* = 8.6 Hz, 2H, ArH), 4.95 (s, 2 H, OH), 2.99 (m, 1H, CH), 1.29 (d, *J* = 7.0 Hz, 6H, CH_3).

^{13}C NMR 101 MHz ($CDCl_3$): δ 191.3 (s, CO), 157.2, 132.2, 129.2, 126.7, 121.5 (q, *J* = 286.1 Hz, CF_3), 93.8 (q, *J* = 35.4 Hz, COH), 34.4, 23.5.

^{19}F NMR 376 MHz ($CDCl_3$): δ -81.2 (s, 3F, CF_3).

ESI: m/z 299.0 $[M+K-2]^+$

Elemental analysis: $C_{12}H_{13}F_3O_3$. Calculated C 54.96, H 5.00. Found: C 53.67, H 5.34.

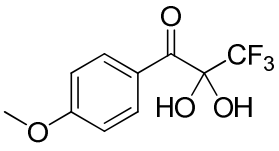

IIIc

3,3,3-trifluoro-2,2-dihydroxy-1-(4-methoxyphenyl)propan-1-one[80]

White crystals

M.p. 81 °C

Yield: 59 %

R*f*: 0.54 (ethyl acetate : petroleum ether = 3:7)

^{1}H NMR 400 MHz ($CDCl_3$): δ 8.34 (d, *J* = 9.2 Hz, 2H, ArH), 6.97 (d, *J* = 9.2 Hz, 2H, ArH), 4.81 (s, 2 H, OH), 3.91 (s, 3H, CH_3).

^{13}C NMR 101 MHz ($CDCl_3$): δ 189.8 (s, CO), 165.2, 134.7, 132.9, 121.0 (q, *J* =289.9 Hz, CF_3), 113.9, 93.7 (q, *J* = 34.1 Hz, COH), 55.7.

^{19}F NMR 376 MHz ($CDCl_3$): δ -81.4 (s, 3F, CF_3).

ESI: m/z 249 $[M-1]^-$

Elemental analysis: $C_{10}H_9F_3O_4$. Calculated C 48.01, H 3.63. Found: C 48.20, H 3.42.

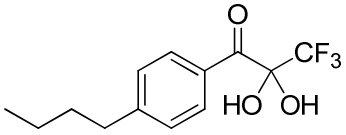

IIId

1-(4-butylphenyl)-3,3,3-trifluoro-2,2-dihydroxypropan-1-one

Yellow oil.

Yield: 74 %.

R*f*: 0.58 (ethyl acetate : petroleum ether = 2:8).

^{1}H NMR 400 MHz ($CDCl_3$): δ 8.25 (d, *J* = 8.3 Hz, 2H, ArH), 7.30 (d, *J* = 8.3 Hz, 2H, ArH), 4.86 (s, 2 H, OH), 2.69 (t, *J* = 7.7 Hz, 2H, CH_2), 1.63 (m, 2H, CH_2), 1.37 (m, 2H, CH_2), 0.94 (t, *J* = 7.4 Hz, 3H, CH_3).

^{13}C NMR 101 MHz ($CDCl_3$): δ 191.5 (s, CO), 151.4, 132.1, 129.1, 128.6, 121.0 (q, *J* = 288.1 Hz, CF_3), 94,1 (q, *J* = 38.4 Hz, COH), , 35.9, 32.9, 22.4, 13.9.

^{19}F NMR 376 MHz ($CDCl_3$): δ -81.2 (s, 3F, CF_3).

ESI: m/z 313.0 $[M+K-2]^+$

Elemental analysis: $C_{13}H_{15}F_3O_3$. Calculated C 56.52, H 5.47. Found: C 55.83, H 5.31.

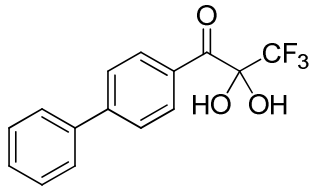

IIIe

1-(biphenyl-4-yl)-3,3,3-trifluoro-2,2-dihydroxypropan-1-one

White crystals.

M.p. 87-88 °C.

Yield: 85 %.

R*f*: 0.31 (ethyl acetate : petroleum ether = 2:8).

^{1}H NMR 400 MHz ($CDCl_3$): δ 8.41 (d, *J* = 8.8 Hz, 2H, ArH), 7.73 (d, *J* = 7.2 Hz, 2H, ArH), 7.65 (d, *J* =8.2 Hz, 2H, ArH), 7.51-7.43 (overlapping, 3H, ArH), 4.79 (s, 2 H, OH).

^{13}C NMR 101 MHz ($CDCl_3$): δ 191.3 (s, CO), 147.8, 139.4, 132.5, 130.2, 129.0, 128.7, 127.4, 127.1, 121.5 (q, *J* = 289.6 Hz, CF_3), 93.8 (q, *J* = 37.3 Hz, COH).

^{19}F NMR 376 MHz ($CDCl_3$): δ -81.2 (s, 3F, CF_3).

ESI: m/z 333 $[M+K-2]^+$

Elemental analysis: $C_{15}H_{11}F_3O_3$. Calculated C 60.82, H 3.74. Found: C 60.64, H 3.32.

General procedure for the preparation of *N*-alkyl-3-acetyl indoles 20a-c:

Anhydrous DMSO (25 mL) was added to KOH (50 mmol, 4 equiv., crushed pellets), and the mixture was stirred at room temperature for 5 min. 3-Acetylindole **19** (13 mmol, 1 equiv.) was then added, and the mixture was stirred at room temperature for 45 - 60 min. An appropriate alkyl halide (bromoethane, 2-iodo propane, 1-iodo butane, 26 mmol, 2 equiv.) was added, and the mixture was stirred at room temperature for 45-60 min. The progress of the reaction was monitored by TLC. Then, water was added and the white precipitate that formed was filtered under reduced pressure and washed with water. In case of compound 1-(1-butyl-1*H*-indol-3-yl)ethanone **20c**, product was extracted from the aqueous solution with

diethyl ether, the organic layer was washed with water and dried over Na_2SO_4, and the solvent was evaporated under reduced pressure to give the compound as a solid.

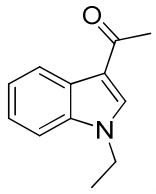

20a

1-(1-ethyl-1*H*-indol-3-yl)ethanone[87]

White crystals.

M.p. 87-89 °C.

Yield: 89 %.

R*f*: 0.28 (ethyl acetate: petroleum ether = 7:3).

^{1}H NMR 400 MHz ($CDCl_3$): δ 8.39-8.36 (m, 1H, ArH), 7.77 (s, 1H, ArH), 7.38-7.36 (m, 1H, ArH), 7.30 (overlapping, 2H, ArH), 4.21 (q, *J* = 7.4 Hz, 2H, CH_2), 2.53 (s, 3H, CH_3), 1.52 (t, *J* = 7.4 Hz, 3H, CH_3).

^{13}C NMR 101 MHz ($CDCl_3$): δ 192.91, 136.57, 133.9, 126.5, 123.20, 122.69, 122.50, 117.12, 109.68, 47.71, 27.66, 15.19.

LC/MS: m/z 188.1 $[M+H]^+$, 210.1 $[M+Na]^+$

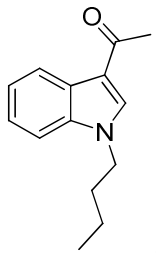

20b

1-(1-butyl-1*H*-indol-3-yl)ethanone

Pale yellow oil.

Yield: 91 %.

R*f*: 0.33 (ethyl acetate : petroleum ether = 7:3).

^{1}H NMR 400 MHz ($CDCl_3$): δ 8.39-8.36 (m, 1H, ArH), 7.73 (s, 1H, ArH), 7.37-7.35 (m, 1H, ArH), 7.30-7.28 (overlapping, 2 H, ArH), 4.15 (t, *J* = 7.15 Hz, 2H, CH_2), 2.53 (s, 3H, $COOCH_3$), 1.87 (m, 2H, CH_2), 1.37 (m, 2H, CH_2), 0.96 (t, 3H, CH_3).

^{13}C NMR 101 MHz ($CDCl_3$): δ 192.93, 136.81, 134.69,. 126.39, 123.16, 122.65, 122.46, 116.99, 109.81, 46.86, 31.94, 27.67, 20.12, 13.63

LC/MS: m/z 215.1 $[M+H]^+$

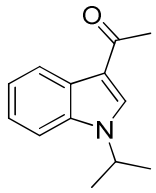

20c

1-(1-isopropyl-1*H*-indol-3-yl)ethanone

Beige solid.

M.p. 82-83 °C.

Yield: 50 %.

R*f*: 0.65 (ethyl acetate : petroleum ether = 8:2).

^{1}H NMR 400 MHz ($CDCl_3$): δ 8.38-7.36 (m, 1H, ArH), 7.86 (s, 1H, ArH), 7.41-7.39 (m, 1H, ArH), 7.31-7.29 (overlapping, 2H, ArH), 4.71 (m, 1H, CH), 2.55 (s, 3H, $COCH_3$), 1.60 (d, *J* = 6.6 Hz, 6H, CH_3).

^{13}C NMR 101 MHz ($CDCl_3$): δ 192.99, 136.84, 130.87, 126.44, 123.06, 122.62, 122.54, 117.23, 109.92, 47.84, 27.73, 22.65.

LC/MS: m/z 202.1 $[M+H]^+$.

General procedure for the preparation of *N*-alkyl-indoles β-diketoesters 21a-c:[87]

A solution of the appropriate 3-alkylacetylindole **20a-c** (3.8 mmol, 1 equiv.) and diethyl oxalate (1.3 equiv.) in methanol (7.45 mL) was added to a solution of sodium methoxide (3.2 equiv.), generated from sodium in methanol (3.2 equiv. of Na in 5.2 mL of MeOH). The mixture was refluxed under a nitrogen atmosphere for 4 h. Then 1.6 equiv. of MeONa and 0.65 equiv. of diethyl oxalate were added to the mixture and the mixture was refluxed for about 1 h. After starting material consumption, the reaction was quenched with water and acidified with HCl 1N. The product was then recovered by filtration under reduced pressure from water as yellow solid.

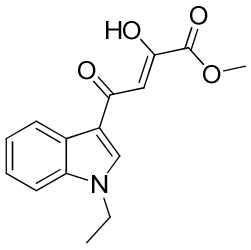

21a

(*Z*)-methyl 4-(1-ethyl-1*H*-indol-3-yl)-2-hydroxyoxobut-2-enoate[87]

Yellow solid.

M.p. 160 °C.

Yield: 85 %.

R*f*: 0.54 (ethyl acetate : petroleum ether = 1:1).

^{1}H NMR 400 MHz ($CDCl_3$): δ 8.40-8.36 (m, 1H, ArH), 7.93 (s, 1H, ArH), 7.42-7.40 (m, 1H, ArH), 7.36-7.34 (overlapping, 2H, ArH), 6.87 (s, 1H, ArH), 4.28 (q, *J* = 7.2 Hz, 2H, CH_2), 3.94 (s, 3H, $COOCH_3$), 1.58 (t, *J* = 7.2 Hz, 3H, CH_3).

^{13}C NMR 101 MHz ($CDCl_3$): δ 188.2 (s, COO), 163.6 (s, CO), 163.2 (s, COH), 137.0, 134.2, 126.3, 123.9, 123.2, 122.8, 116.3, 110.1, 100.4, 52.9, 42.1, 15.1.

LC/MS: m/z 296.1 $[M+Na]^+$.

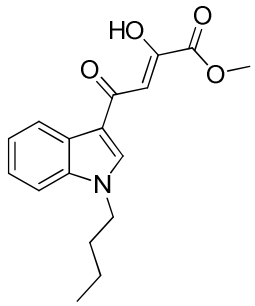

21b

(*Z*)-methyl 4-(1-butyl-1*H*-indol-3-yl)-2-hydroxyoxobut-2-enoate

Yellow solid.

M.p. 104-105 °C.

Yield: 54 %.

R*f*: 0.60 (ethyl acetate : petroleum ether = 4:6).

^{1}H NMR 400 MHz ($CDCl_3$): δ 8.39-8.37 (m, 1H, ArH), 7.90 (s, 1H, ArH), 7.41-7.39 (m, 1H, ArH), 7.36-7.33 (overlapping, 2H, ArH), 6.87 (s, 1H, ArH), 4.20 (t, *J* = 6.9 Hz, 2H, CH_2), 3.94 (s, 3H, $COOCH_3$), 1.90 (m, 2H, CH_2), 1.38 (m, 2H, CH_2), 0.98 (t, *J* = 7.2 Hz, 3H, CH_3).

^{13}C NMR 101 MHz ($CDCl_3$): δ 188.22 (s, COO), 163.61 (s, CO), 163.1 (s, COH), 137.22, 134.94, 126.25, 123.88, 123.17, 122.75, 114.84, 110.29, 100.41, 52.99, 47.21, 31.83, 20.10, 13.61.

LC/MS: m/z 301.1 $[M]^+$.

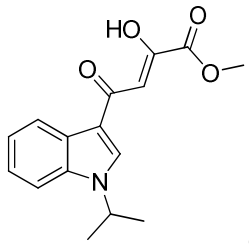

21c

(*Z*)-methyl 4-(1-isopropyl-1*H*-indol-3-yl)-2-hydroxyoxobut-2-enoate

Yellow solid.

M.p. 90-92 °C.

Yield: 93 %.

R*f*: 0.70 (ethyl acetate : petroleum ether = 6:4).

^{1}H NMR 400 MHz ($CDCl_3$): δ 8.40-8.38 (m, 1H, ArH), 8.00 (s, 1H, ArH), 7.45-7.43 (m, 1H, ArH), 7.36-7.33 (overlapping, 2H, ArH), 6.89 (s, 1H, ArH), 4.73 (m, 1H, CH), 3.95 (s, 3H, $COOCH_3$), 1.62 (d, *J* = 7 Hz, 6H, CH_3).

^{13}C NMR 101 MHz ($CDCl_3$): δ 188.1 (s, COO), 163.6 (s, CO), 163.2 (s, COH), 136.9, 131.3, 126.2, 123.7, 123.2, 122.7, 114.9, 110.3, 100.3, 52.9, 48.2, 22.6.

LC/MS: m/z 287.9 $[M]^+$, 310.1 $[M+Na]^+$.

General procedure for the preparation of *N*-alkyl-indoles-1*H*-pyrazole-5-carboxylates IVa,d,f:[90]

Hydrazine monohydrate 98% ((64-65% N_2H_4), 28.1 mmol, 8.8 equiv,) was added dropwise to a mixture of isopropyl alcohol (7.9 mL) and glacial acetic acid (3.4 mL) cooled at 0 °C. Then the appropriate *N*-alkyl-indoles β-diketoester **21a-c** (3.2 mmol, 1 equiv.) was added portionwise. After stirring for 2 h, the mixture was poured into water and ice to afford the product as a brown precipitate that was filtered under reduced pressure.

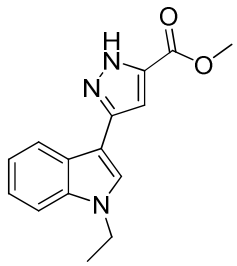

IVa

Methyl 3-(1-ethyl-1*H*-indol-3-yl)-1*H*-pyrazole-5-carboxylate[87]

Yellow solid.

M.p. 176-178 °C.

Yield: 93 %.

R*f*: 0.41 (ethyl acetate : petroleum ether = 5:5).

^{1}H NMR 400 MHz ($CDCl_3$): δ 8.37 (bs, 1H, NH) 7.95 (d, *J* = 6.1 Hz, 1H, ArH), 7.47 (s, 1H, ArH), 7.40 (d, *J* = 6.7 Hz, 1H, ArH), 7.32-7.21 (overlapping, 2H, ArH), 7.07 (s, 1H, ArH), 4.23 (q, *J* = 7.3 Hz, 2H, CH_2), 3.96 (s, 3H, $COOCH_3$), 1.52 (t, *J* = 7.5 Hz, 3H, CH_3).

^{13}C NMR 101 MHz ($CDCl_3$): δ 161.9, 146.6, 136.2, 132.2, 125.7, 125.3, 122.4, 120.6, 120.0, 109.8, 108.0, 105.3, 52.1, 41.2, 15.4.

LC/MS: m/z 270.2 $[M+H]^+$

Elemental analysis: $C_{15}H_{15}N_3O_2$. Calculated C 66.90, H 5.61, N 15.60. Found: C 66.86, H 5.57, N 15.02.

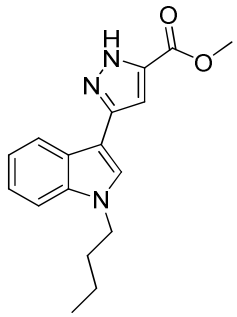

IVd

Methyl 3-(1-butyl-1*H*-indol-3-yl)-1*H*-pyrazole-5-carboxylate

Pale yellow solid.

M.p. 173-175 °C.

Yield: 46 %.

R*f*: 0.55 (ethyl acetate : petroleum ether = 6:4).

^{1}H NMR 400 MHz ($CDCl_3$): δ 10.45 (bs, 1H, NH), 7.95 (d, *J* = 7.9 Hz, 1H, ArH), 7. 44 (s, 1H, ArH), 7.40 (d, *J* = 7.9, Hz, 1H, ArH), 7.29 (t, *J* = 6.2 Hz, 1H, ArH), 7.23 (t, *J* = 6.2 Hz, 1H, ArH), 7.07 (s, 1H, ArH), 4.17 (t, *J* = 6.9 Hz, 2H, CH_2),

3.97 (s, 3H, $COOCH_3$), 1.87 (m, 2H, CH_2), 1.37 (m, 2H, CH_2), 0.96 (t, *J* = 7.5 Hz, 3H, CH_3).

^{13}C NMR 101 MHz ($CDCl_3$): δ 161.9, 149.1, 143.5, 136.5, 129.9, 126.1, 125.7, 122.3, 120.5, 120.0, 109.9, 105.2, 52.1, 46.3, 32.2, 20.2, 13.7.

MALDI: m/z 298.3 $[M+H]^+$.

Elemental analysis: $C_{17}H_{19}N_3O_2$. Calculated C 68.67, H 6.44, N 14.13. Found: C 70.03, H 6.51, N 12.32.

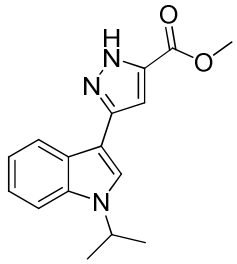

IVf

Methyl 3-(1-isopropyl-1*H*-indol-3-yl)-1*H*-pyrazole-5-carboxylate

Pale yellow solid.

M.p. 174-175 °C.

Yield: 66 %.

R*f*: 0.41 (ethyl acetate : petroleum ether = 5:5).

^1H NMR 400 MHz ($CDCl_3$): δ 10.71 (bs, 1H, NH), 7.94 (d, *J* = 7.5 Hz, 1H, ArH), 7.58 (s, 1H, ArH), 7.43 (d, *J* = 8 Hz, 1H, ArH), 7.29 (t, *J* = 8 Hz, 1H, ArH), 7.23 (t, *J* = 7.2 Hz, 1H, ArH), 7.09 (s, 1H, ArH), 4.73 (m, 1H, CH), 3.96 (s, 3H, $COOCH_3$), 1.58 (d, *J* = 7.8 Hz, 6H, $(CH_3)_2$).

^{13}C NMR 101 MHz ($CDCl_3$): δ 161.8, 143.7, 140.4, 136.1, 125.7, 122.3, 122.1, 120.6, 119.9, 109.9, 105.9, 105.3, 52.1, 47.4, 22.8.

LC/MS: m/z 284.3 $[M+H]^+$.

Elemental analysis: $C_{16}H_{17}N_3O_2$. Calculated C 67.83, H 6.05, N 14.83. Found: C 67.60, H 6.21, N 14.81.

Procedure for the alkylation of Methyl 3-(1-ethyl-1*H*-indol-3-yl)-1*H*-pyrazole-5-carboxylate IVb:[90]

To a solution of Methyl 3-(1-ethyl-1*H*-indol-3-yl)-1*H*-pyrazole-5-carboxylate (1.8 mmol, 1 equiv.) in anhydrous DMF (2.6 mL) under nitrogen atmosphere, NaH 60% oil dispersion (2.6 mmol, 1.5 equiv.) was added portionwise at 0 °C. The mixture thus obtained was stirred for 10 min at a 0 °C, then CH_3I (2.6 mmol, 1.5 mmol) was added dropwise, and the stirring was continued for another 1 h at room temperature. The mixture was poured into water and extracted with ethyl acetate. The combined organic layers were then washed with water, dried over Na_2SO_4 and evaporated under reduced pressure. The crude product was purified by flash chromatography (8:2 petroleum ether / ethyl acetate) to give the desired product.

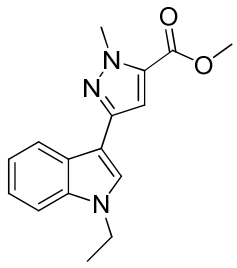

IVb

Methyl 3-(1-ethyl-1*H*-indol-3-yl)-1-methyl-1*H*-pyrazole-5-carboxylate

Pale brown solid.

M.p. 110 °C.

Yield: 39 %.

R*f*: 0.65 (ethyl acetate : petroleum ether = 5:5).

^{1}H NMR 400 MHz ($CDCl_3$): δ 8.09 (d, *J* = 7.8 Hz, 1H, ArH), 7.52 (s, 1H), 7.37 (d, *J* =8.2 Hz, 1H, ArH), 7.28-7.19 (overlapping, 2H, ArH), 7.11 (s, 1H, ArH), 4.24 (s, 3H, NCH_3), 4.21 (q, J =7.3 Hz, 2H, CH_2), 3.92 (s, 3H, $COOCH_3$), 1.50 (t, 3H, CH_3).

^{13}C NMR 101 MHz ($CDCl_3$): δ 160.5, 146. 0, 136.3, 132.7, 126.1, 124.1, 121.9, 120.8, 120.0, 109.4, 108.4, 107.9, 51.9, 41.1, 39.4, 15.4.

MALDI: m/z 284.3 $[M+H]^+$.

Elemental analysis: $C_{16}H_{17}N_3O_2$. Calculated C 67.83 H 6.05, N 14.83. Found: C 67.85, H 5.97, N 14.25.

General procedure for the preparation of *N*-alkyl-indoles-1*H*-pyrazole-5-carboxylic acids 8, IVc,e,g:[87,90]

To a solution of the appropriate ester **IVa,b,d,f** (0.5 mmol, 1 equiv.) and 20% NaOH (2 mmol, 4 equiv.) in ethanol (16 mL) was stirred under reflux for about 1.5 h. Then, the reaction mixture was poured into water and ice and acidified with 1N HCl to afford the product as a white precipitate that was filtered under reduced pressure.

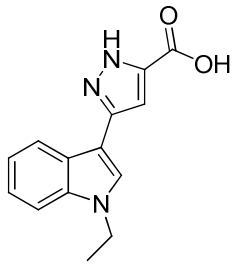

8

3-(1-ethyl-1*H*-indol-3-yl)-1*H*-pyrazole-5-carboxylic acid[87]

White solid.

M.p. 280-281 °C.

Yield: 30 %.

R*f*: 0.09 (petroleum ether : ethyl acetate = 5:5)

^{1}H NMR 400 MHz (DMSO-d_6): δ 7.99 (s, 1H, ArH), 7.88 (s, 1H, ArH), 7.54 (d, *J* = 8.1, Hz1H, ArH), 7.21 (t, *J* = 7.44 Hz, 1H, ArH), 7.15 (t, *J* = 7.44 Hz, 1H, ArH), 7.00 (s, 1H, ArH), 4.26 (q, *J* = 6.8 Hz, 2H, CH_2), 1.41 (t, *J* = 6.8 Hz, 3H, CH_3).

^{13}C NMR 101 MHz (DMSO-d_6): δ 168.4 (s, CO), 138.62, 135.8, 132.8, 126.1, 125.0, 121.7, 119.9, 117.9, 117.6, 110.1, 40.4, 15.3

MALDI: m/z 256.1 $[M+H]^+$

Elemental analysis: $C_{14}H_{13}N_3O_2$. Calculated C 65.87 H 5.13, N 16.46. Found: C 65.89 H 5.24, N 16.16

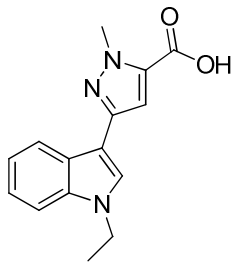

IVc

3-(1-ethyl-1*H*-indol-3-yl)-1-methyl-1*H*-pyrazole-5-carboxylic acid

White solid.

M.p. 224-225 °C.

Yield: 64 %.

Rf: 0.05 (ethyl acetate : petroleum ether = 2:8).

^{1}H NMR 400 MHz (DMSO-d_6): δ 8.14 (d, *J* = 7.9 Hz, 1H, ArH), 7.88 (s, 1H), 7.51 (d, *J* = 8.7 Hz, 1H, ArH), 7.20 (t, *J* = 8.2 Hz, 1H, ArH), 7.14-7.11 (overlapping, 2H, ArH), 4.24 (q, *J* = 7.2 Hz, 2H, CH_2), 4.14 (s, 3H, NCH_3), 1.41 (t, *J* = 7.2 Hz, 3H, CH_3).

^{13}C NMR 101 MHz (DMSO-d_6): δ 160.8, 145.6, 135.3, 133.7, 126.1, 125.2, 121.5, 120.9, 119.5, 109.8, 107.7, 107.1, 40.4, 38.9, 15.3.

MALDI: m/z 270 $[M+H]^+$

Elemental analysis: $C_{15}H_{15}N_3O_2$. Calculated C 66.90 H 5.61, N 15.60. Found: C 66.67, H 5.32, N 15.17.

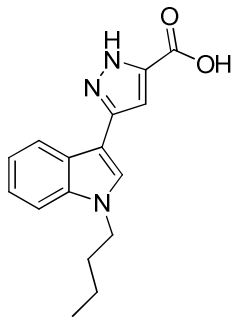

IVe

3-(1-butyl-1*H*-indol-3-yl)-1*H*-pyrazole-5-carboxylic acid

White solid.

M.p. 250-252 °C.

Yield: 86 %.

R*f*: 0.05 (ethyl acetate : petroleum ether = 6:4).

^{1}H NMR 400 MHz (DMSO-d_6): δ 8.01 (s, 1H, ArH), 7.85 (s, 1H, ArH), 7.53 (d, *J* =8.4 Hz, 1H, ArH), 7.21 (t, *J* = 8.4 Hz, 1H, ArH), 7.13 (t, *J* = 8.4 Hz, 1H, ArH), 6.97 (s, 1H, ArH), 4.22 (t, *J* = 6.0 Hz, 2H, CH_2), 1.79 (m, 2H, CH_2), 1.28 (m, 2H, CH_2), 0.91 (t, *J* = 5.4 Hz, 3H, CH_3).

^{13}C NMR 101 MHz (DMSO-d_6): δ 162.2, 136.2, 126.8, 124.9, 121.7, 119.8, 110.2, 104.1, 45.3, 31.8, 19.5, 13.5.

MALDI: m/z 284.1 $[M+H]^+$

Elemental analysis: $C_{16}H_{17}N_3O_2$. Calculated C 67.83 H 6.05, N 14.83 Found: C 66.15, H 6.05, N 14.01.

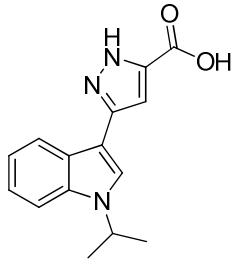

IVg

3-(1-isopropyl-1*H*-indol-3-yl)-1*H*-pyrazole-5-carboxylic acid

Yellow solid.

M.p. 287 °C dec.

Yield: 64 %.

R*f*: 0.03 (ethyl acetate : petroleum ether = 6:4).

^{1}H NMR 400 MHz (DMSO-d_6): δ 7.99 (overlapping, 2H, ArH), 7.57 (d, *J* = 7.3 Hz, 1H, ArH), 7.21 (t, J = 7.8 Hz, 1H, ArH), 7.13 (t, *J* = 7.8 Hz, 1H, ArH), 7.00 (s, 1H, ArH), 4.81 (m, 1H, CH), 1.50 (d, J = 6.9 Hz, 6H, CH_3).

^{13}C NMR 101 MHz (DMSO-d_6): δ 163.6, 140.9, 130.2, 128.3, 126.8, 125.5, 125.1, 115.4, 109.3, 51.9, 27.7.

MALDI: m/z 270.3 $[M+H]^+$

Elemental analysis: $C_{15}H_{15}N_3O_2$. Calculated C 66.90, H 5.61, N 15.60. Found: C 66.23, H 5.10, N 14.80.

Preparation of 6-nitrobenzo[c][1,2]oxaborol-1(3*H*)-ol 23:[94,104]

To 6.4 mL of fuming nitric acid (18.3 equiv.) cooled at -45/-40 °C was added 1 g (7.4 mmol, 1 equiv.) of commercially available benzoxaborole

with stirring. The addition was done portionwise and was complete in about 5 min. The mixture was stirred and maintained at -45 to -30 °C, and the progress of the reaction was monitored by TLC (ethyl acetate : petroleum ether = 7:3). After 20 min. the mixture was poured into water and ice and kept at 0-10 °C for 2 hours. The obtained white precipitate was then filtered *in vacuo*, washed with water and lyophilized to afford the compound as a white solid.

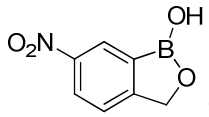

24

6-nitrobenzo[c][1,2]oxaborol-1(3H)-ol[94]

White solid.

M.p. 178-180 °C.

Yield: 80 %.

R*f*: 0.32 (ethyl acetate : petroleum ether = 7:3).

^{1}H NMR: δ 9.59 b(s, 1H, OH), 8.58 (ss, 1H, ArH), 8.33 (d, *J* = 1.7 Hz, 1H, ArH), 8.33 (dd, J^{1} = 8.3 Hz, J^{2} = 2.2 Hz, 1H, ArH), 7.69 (d, *J* = 8.5 Hz, 1H, ArH), 5.12 (s, 2H, CH_2).

^{13}C NMR: δ 160.6, 147.2, 140.7, 125.6, 123.1, 70.1 (s, CH_2).

MS: ESI: *m/z* 178.0 $[M]^{+}$.

Preparation of 6-aminobenzo[c][1,2]oxaborol-1(3H)-ol 24:[117]

To a solution of 6-nitrobenzo[c][1,2]oxaborol-1(3H)-ol **23** (2.8 mmol, 1 equiv.) in THF (12 mL) was added AcOH glacial (1.2 mL). The mixture was vacuum/N_2 purged three times and 10% Pd/C (82 mg) was added. The mixture was again vacuum/N_2 purged three times then vacuum purged again. H_2 was then introduced from a balloon and the reaction was stirred at room temperature for 2 hours. The reaction solution was filtered through a short pad of celite, washed with methanol, and the filtrate was evaporated to afford the product as a foamy orange solid.

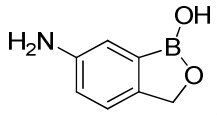

24

6-aminobenzo[c][1,2]oxaborol-1(3H)-ol[117]

Foamy orange solid.

Yield: 95 %.

R*f*: 0.46 (ethyl acetate).

^{1}H NMR 400 MHz (DMSO-d_6): δ 9.05 (bs, 2H, NH_2), 7.03 (d, *J* = 7.9 Hz, 1H, ArH), 6.89 (s, 1H, ArH), 6.71 (dd, J^1= 7.7 Hz, J^2= 2.0 Hz, 1H, ArH), 4.90 (s, 1H, OH), 4.81 (s, 2H, CH_2).

^{13}C NMR 101 MHz (DMSO-d_6): δ 172.1, 147.6, 141.5, 121.5, 117.6, 114.6, 69.7 (s, CH_2).

MS: ESI: m/z 148.0 $[M]^+$

General procedure for the synthesis of *N,N'*-disubstituted ureas 26a-j:

6-Amino benzoxaborole **24** (6-aminobenzo[c][1,2]oxaborol-1(3H)-ol) (0.67 mmol, 1 equiv.) was dissolved in acetone (1.5 mL) and the solution was stirred at room temperature. Then the opportune isocyanate **25a-j** (0.67 mmol, 1 equiv.) was added dropwise (or in portion) and the solution became pasty. When **24** was consumed, petroleum ether was added to the mixture, and the precipitate was filtered. The solid was washed with methanol to afford the desired product as a solid.

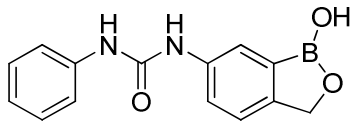

26a

1-(1-hydroxy-1,3-dihydrobenzo[c][1,2]oxaborol-6-yl)-3-phenylurea

Pale yellow solid.

Yield: 42 %.

R*f*: 0.70 (ethyl acetate : petroleum ether = 9:1).

M.p. 260 °C dec.

^{1}H NMR 400 MHz (DMSO-d_6): δ 9.18 (s, 1H, OH), 8.66 (s, 1H, NH), 8.64 (s, 1H, NH), 7.83 (d, *J* = 1.8 Hz, 1H, Ar), 7.53 (dd, J^{1} =8.2 Hz, J^{2} = 2.1 Hz, 1H, Ar), 7.46 (overlapping, 2H, Ar), 7.29 (overlapping, 3H, Ar), 6.97 (t, *J* = 7.3 Hz,1H, Ar), 4.92 (s, 2H, CH_2).

^{13}C NMR 101 MHz (DMSO-d_6):δ 140.1(s, CO), 128.4, 121.4, 121.2, 121.1, 119.5, 117.7, 69.3 (s, CH_2).

MS: ESI: m/z 269.1 $[M+H]^+$

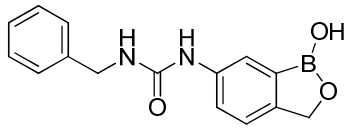

26b

1-benzyl-3-(1-hydroxy-1,3-dihydrobenzo[c][1,2]oxaborol-6-yl)urea

White solid.

Yield: 41 %.

R*f*: 0.48 (ethyl acetate).

M.p. 237-239 °C dec.

^{1}H NMR 400 MHz (DMSO-d_6): δ 9.13 (s, 1H, OH), 8.56 (s, 1H, NH), 7.78 (d, *J* = 1.7 Hz, 1H, NH), 7.49 (dd, J^1 = 2.1 Hz, J^2= 8.2 Hz , 1H, ArH), 7.35-7.30 (overlapping, 4H, ArH), 7.26-7.24 (overlapping, 2H, ArH), 6.60 (t, *J* = 5.9 Hz, 1H, ArH), 4.90 (s, 2H, CH_2), 4.31 (d, *J* = 5.9 Hz, 2H, CH_2).

^{13}C NMR 101 MHz (DMSO-d_6):δ 140.0 (s, CO), 127.9, 126.8, 126.3, 121.0, 120.7, 119.0, 69.2 (s, CH_2), 42.4 (s, CH_2).

MS: ESI: m/z 283.1 $[M+H]^+$.

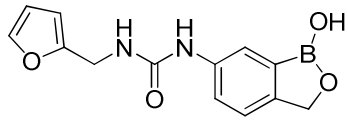

26c

1-(furan-2-ylmethyl)-3-(1-hydroxy-1,3-dihydrobenzo[c][1,2]oxaborol-6-yl)urea

Pale brown solid.

Yield: 28 %.

R*f*: 0.69 (ethyl acetate).

M.p. 270 °C.

^{1}H NMR 400 MHz (DMSO-d_6): δ 9.12 (s, 1H, OH), 8.50 (s, 1H, NH), 7.74 (s, 1H, NH), 7.58 (s, 1H, ArH), 7.48 (d, *J* = 8.3 Hz, 1H, ArH), 7.26 (d, *J* = 8.1 Hz, 1H,ArH), 6.51 (m, 1H, ArH), 6.39 (s, 1H, ArH), 6.26 (d, *J* =2.3 Hz, 1H, ArH), 4.89 (s, 2H, CH_2), 4.29 (d, J = 5.3 Hz, 2H, CH_2).

^{13}C NMR 101 MHz (DMSO-d_6): δ 141.6 (s,CO), 121.0, 120.7, 119.0, 110.1, 106.1, 69.2 (s, CH_2), 35.7 (s, CH_2).

MS: ESI: m/z 273.1 $[M+H]^{+,}$ 295.1 $[M+Na]^{+}$.

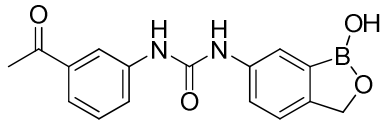

26d

1-(3-acetylphenyl)-3-(1-hydroxy-1,3-dihydrobenzo[c][1,2]oxaborol-6-yl)urea

White solid.

Yield: 23 %.

R*f*: 0.60 (ethyl acetate : petroleum ether = 9:1).

M.p. 235 °Cdec.

^{1}H NMR 400 MHz (DMSO-d_6): δ 9.19 (s, 1H, OH), 8.9 (s, 1H, NH), 8.73 (s, 1H, NH), 8.10 (d, *J* = 1.7 Hz, 1H, ArH), 7.86 (d, *J* = 0.5 Hz, 1H, ArH), 7.66 (d, *J* = 6.2 Hz, 1H, ArH), 7.57 (d, *J* = 6.2 Hz, 1H, ArH), 7.50 (d, *J* = 6.3 Hz, 1H, ArH), 7.43 (m, 1H, ArH), 7.33 (m, 1H, ArH), 4.93 (s, 2H, CH_2), 2.55 (s, 3H, CH_3).

^{13}C NMR 101 MHz (DMSO-d_6):δ 140.0 (s, CO), 128.8, 122.3, 121.5, 121.3, 119.7, 116.9, 69.3(s, CH_2), 26.4 (s, CH_3).

MS: ESI: m/z 311.1 $[M+H]^+$.

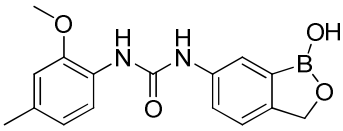

26e

1-(1-hydroxy-1,3-dihydrobenzo[c][1,2]oxaborol-6-yl)-3-(2-methoxy-4-methylphenyl)urea

Pale yellow solid.

Yield: 23 %.

R*f*: 0.85 (ethyl acetate).

M.p. 263 °C dec.

^{1}H NMR 400 MHz (DMSO-d_6): δ 9.31 (s, 1H, OH), 9.16 (s, 1H, NH), 8.16 (s, 1H, NH), 8.00 (s, 1H, Ar), 7.86 (s, 1H, Ar), 7.51 (d, *J* = 8.0 Hz, 1H, ArH), 7.31 (d, *J* = 8.0 Hz, 1H, ArH), 6.88(d, *J* = 8.1 Hz, 1H, ArH), 6.73 (d, *J* = 7.4 Hz,1H, ArH), 4.92 (s, 2H, CH_2), 3.83 (s, 3H, CH_3), 2.22 (s, 3H, CH_3).

^{13}C NMR 101 MHz (DMSO-d_6):δ (s, CO), 121.4, 121.2, 120.8, 119.2, 118.6, 110.2, 69.3(s, CH_2), 55.5(s, CH_3), 20.4 (s, CH_3).

MS: ESI: m/z 313.1 $[M+H]^+$,335.1 $[M+Na]^+$

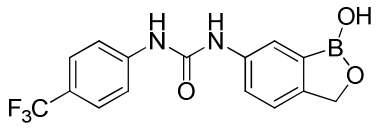

26f

1-(1-hydroxy-1,3-dihydrobenzo[c][1,2]oxaborol-6-yl)-3-(4-(trifluoromethyl)pheny)urea

Pale yellow solid.

Yield: 20 %.

R*f*: 0.63 (ethyl acetate).

M.p. 269-270 °C dec.

^{1}H NMR 400 MHz (DMSO-d_6):δ 9.19 (s, 1H, OH), 9.08 (s, 1H, NH), 8.82 (s, 1H, NH), 7.84 (d, *J* = 0.9 Hz, 1H, ArH), 7.65-7.64 (overlapping, 3H, Ar), 7.53 (dd, J^1 = 8.4 Hz, J^2 = 1.9 Hz, 1H, Ar), 7.33 (d, *J* = 8.2 Hz , 1H, Ar), 4.93 (s, 2H, CH_2).

^{13}C NMR 101 MHz (DMSO-d_6):δ 140.3 (s, CO), 125.7, 125.7, 121.4, 121.3, 119.8, 117.4, 69.3 (s, CH_2).

MS: ESI: m/z 337.1 $[M+H]^+$.

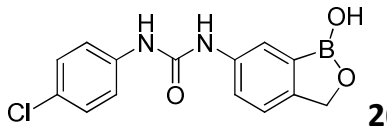

26g

1-(4-chlorophenyl)-3-(1-hydroxy-1,3-dihydrobenzo[c][1,2]oxaborol-6-yl)urea

Pale yellow solid.

Yield: 46 %.

R*f*: 0.66 (ethyl acetate : petroleum ether = 9:1).

M.p. 278 °C dec.

^{1}H NMR 400 MHz (DMSO-d_6):δ 9.16 (s, 1H, OH), 8.78 (s, 1H, NH), 8.70 (s, 1H, NH), 7.81 (s, 1H, ArH), 7.53-7.48 (overlapping, 3H, ArH), 7.32 (overlapping,3H, ArH), 4.93 (s, 2H, CH_2).

^{13}C NMR 101 MHz (DMSO-d_6):δ 140.1 (s, CO), 128.2, 121.3, 121.2, 119.7, 119.3, 69.3 (s, CH_2).

MS: ESI: m/z 303.1 $[M+H]^+$.

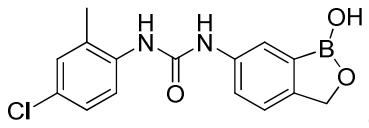

26h

1-(4-chloro-2-methylphenyl)-3-(1-hydroxy-1,3-dihydrobenzo[c][1,2] oxaborol-6-yl)urea

White solid.

Yield: 30 %.

R*f*: 0.45 (ethyl acetate).

M.p. 250-252 °C dec.

^{1}H NMR 400 MHz (DMSO-d_6):δ 9.18 (s, 1H, OH), 9.08 (s, 1H, NH), 7.98 (s, 1H, NH), 7.91 (d, *J* = 8.7 Hz, 1H, ArH), 7.84 (d, *J* =1.7 Hz ,1H, ArH), 7.53 (dd, J^1 = 8.2 Hz, J^2 = 2.0 Hz,1H, ArH), 7.32 (d, J = 8.2 Hz, 1H, ArH), 7.26 (d, J = 2.2

Hz, 1H, ArH), 7.20 (dd, J^1 = 8.7 Hz, J^2 = 2.4 Hz, 1H, ArH), 4.93 (s, 2H, CH_2), 2.25 (s, 3H).

^{13}C NMR 101 MHz (DMSO-d_6):δ 140.3(s, CO), 129.5, 125.8, 122.6, 121.9, 121.6, 121.3, 119.7, 69.6(s, CH_2), 17.6(s, CH_3).

MS: ESI: m/z 317.1 $[M+H]^+$

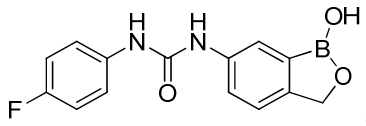

26i

1-(4-fluorophenyl)-3-(1-hydroxy-1,3-dihydrobenzo[c][1,2]oxaborol-6-yl)urea

Pale yellow solid.

Yield: 42 %.

R*f*: 0.48 (ethylAcetate).

M.p. 260 °C.

^{1}H NMR 400 MHz (DMSO-d_6):δ 9.17 (bs, 1H, OH), 8.68 (s,1H, NH), 8.67 (s, 1H, NH), 7.82 (d, *J* = 1.8 Hz, 1H, Ar), 7.53 (dd, J^1 = 8.2 Hz, J^2 = 2.0 Hz, 1H, Ar), 7.48-7.44 (overlapping, 2H, Ar), 7.32 (d, *J* = 8.2 Hz, 1H, Ar), 7.14-7.09 (overlapping, 2H, Ar), 4.93 (s, 2H, CH_2).

^{13}C NMR 101 MHz (DMSO-d_6): δ 140.5 (s, CO), 121.2, 119.6, 119.5, 119.4, 115.0, 114.8, 69.3 (s, CH_2).

MS: ESI: m/z 287.1 $[M+H]^+$

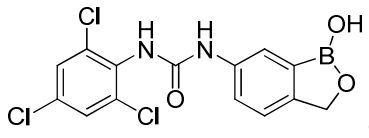

26j

1-(1-hydroxy-1,3-dihydrobenzo[c][1,2]oxaborol-6-yl)-3-(2,4,6-trichloro phenyl)urea

White solid.

Yield: 42 %.

R*f*: 0.71 (ethylAcetate).

M.p. 267 °C dec.

^{1}H NMR 400 MHz (DMSO-d_6): δ 9.18 (s, 1H, OH), 8.99 (s, 1H, NH), 8.24 (s, 1H, NH), 7.81 (d, *J* = 1.7 Hz, 1H, ArH), 7.75 (s, 2H, ArH), 7.51 (dd, J *J* = 8.2Hz, J^{2} = 2.0,1H, ArH), 7.31 (d, *J* = 8.2 Hz, 1H, ArH), 4.92 (s, 2H, CH_2).

^{13}C NMR 101 MHz (DMSO-d_6):δ (s, CO), 127.8, 121.2, 121.1, 119.7, 69.3 (s, CH_2).

MS: ESI: m/z 372.9 $[M+H]^{+}$

General procedure for the synthesis of *N,N*'-disubstituted thioureas 28a-j:

6-amino benzoxaborole **24** (0.67 mmol, 1 equiv.) was dissolved in acetone (1.5 mL) and the solution was stirred at room temperature. Then the opportune isothiocyanate (0.80 mmol, 1.2 equiv.) was added dropwise (or in portion). The solution was refluxed for about 2-6 hours and the progress of reaction was monitored by TLC (ethyl acetate). Then the solvent was

evaporated under reduce pressure, and the crude solid was washed with petroleum ether and n-pentane to afford the desired product as a pale yellow solid.

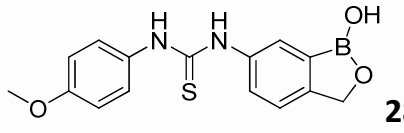

28a

1-(1-hydroxy-1,3-dihydrobenzo[c][1,2]oxaborol-6-yl)-3-(4-methoxy phenyl)thiourea

White solid.

Yield: 25 %.

R*f*: 0.46 (dichloromethane : methanol = 96:4).

M.p. 169-170 °C dec.

^{1}H NMR 400 MHz (DMSO-d_6): δ 9.71 (s, 1H, OH), 9.66 (s, 1H, NH), 9.23 (s, 1H, NH), 7.74 (s, 1H, ArH), 7.50 (d, *J* = 7.2 Hz, 1H, ArH), 7.35 (t, *J* = 7.2 Hz, 3H, ArH), 7.13 (d, *J* = 7.4 Hz, 2H, ArH), 4.96 (s, 2H, CH_2), 2.27 (s, 3H, CH_3).

^{13}C NMR 101 MHz (DMSO-d_6): δ 183.8, 126.7, 125.4, 125.4, 120.8, 113.2, 69.4, 54.9.

MS: ESI: m/z 315.1 $[M+H]^+$

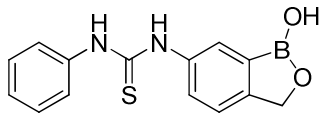

28b

1-(1-hydroxy-1,3-dihydrobenzo[c][1,2]oxaborol-6-yl)-3-phenylthiourea

Pale yellow solid.

Yield: 45 %.

R*f*: 0.33 (dichloromethane : methanol = 94:6).

M.p. 164-165 °C dec.

^{1}H NMR 400 MHz (DMSO-d_6):δ 9.83 (s, 1H, OH), 9.72 (s, 1H, NH), 9.23 (s, 1H, NH), 7.74 (d, *J* = 1.6, 1H, ArH), 7.51-7.45 (overlapping, 4H, ArH), 7.38 (d, *J* = 8.2, 1H, ArH),), 7.19-7.14 (overlapping, 2H, ArH), 4.96 (s, 2H, $CH_{2)}$.

^{13}C NMR 101 MHz (DMSO-d_6):δ 184.2, 140.7, 127.0, 125.9, 125.9, 125.7, 121.1, 114.8, 114.6, 99.2, 69.4.

MS: ESI: m/z 286.1 $[M+H]^+$

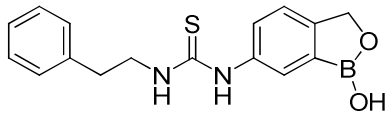

28c

1-(1-hydroxy-1,3-dihydrobenzo[c][1,2]oxaborol-6-yl)-3-phenetylthiourea

Pale yellow solid.

Yield: 20 %.

R*f*: 0.48 (dichloromethane : methanol = 94:6).

M.p. 173-174 °C dec.

^{1}H NMR 400 MHz (DMSO-d_6):δ 9.55 (bs, 1H, OH), 9.22 (s, 1H, NH), 7.64 (s, 1H, NH), 7.37-7.33 (overlapping, 5H, ArH), 7.31-7.19 (overlapping, 3H, ArH), 4.96 (s, 2H, CH_2), 3.68 (bs, 2H, CH_2), 2.86 (t, *J* = 7.7, 2H, CH_2).

^{13}C NMR 101 MHz (DMSO-d_6):δ 184.6, 128.3, 128.0, 125.8, 69.4 (s, CH_2), 45.1(s, CH_2), 34.2 (s, CH_2).

MS: ESI: m/z 313.1 $[M+H]^+$.

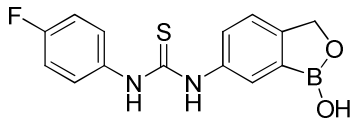

28d

1-(4-fluorophenyl)-3-(1-hydroxy-1,3-dihydrobenzo[c][1,2]oxaborol-6-yl)thiourea

Pale yellow solid.

Yield: 25 %.

R*f*: 0.44 (dichloromethane : methanol = 94:6).

M.p. 172 °C dec.

^{1}H NMR 400 MHz (DMSO-d_6): δ 9.81 (s, 1H, OH), 9.70 (s, 1H, NH), 9.2 (s, 1H, NH), 7.74 (d, *J* = 1.6 Hz, 1H, ArH), 7.47 (overlapping, 3H, ArH), 7.38 (d, *J* = 8.1 Hz, 1H, ArH), 7.16 (t, *J* = 8.8 Hz, 2H, ArH), 4.96 (s, 2H, CH_2).

^{13}C NMR 101 MHz (DMSO-d_6):δ 184.0 (s, CS),140.7, 127.0, 125.9, 125.9, 125.7, 121.4, 114.8, 114.6, 99.2, 69.4(s, CH_2).

MS: ESI: m/z 303.1 $[M+H]^+$.

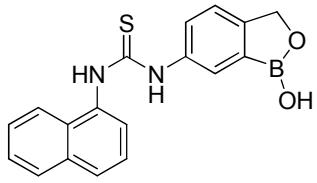

28e

1-(1-hydroxy-1,3-dihydrobenzo[c][1,2]oxaborol-6-yl)-3-(naphthalene-1-yl)thiourea

White solid.

Yield: 28 %.

R*f*: 0.53 (dichloromethane : methanol = 94:6).

M.p. 172-173 °C dec.

^{1}H NMR 400 MHz (DMSO-d_6): δ 9.84 (bs, 1H, OH), 9.72 (s, 1H, NH), 9.21 (s, 1H, NH), 7.99-7.95 (overlapping, 2H, ArH), 7.86 (t, *J* = 4.8, 1H, ArH), 7.78 (d, *J* = 1.4, 1H, ArH), 7.58-7.52 (overlapping, 5H, ArH), 7.36 (d, *J* = 8.2, 1H, ArH), 4.96 (s, 2H, CH_2).

^{13}C NMR 101 MHz (DMSO-d_6):δ 184.6, 140.9, 127.8, 127.5, 126.5, 126.4, 125.8, 125.7, 125.3, 125.1, 122.8, 120.9, 69.4

MS: ESI: m/z 335.1 $[M+H]^+$.

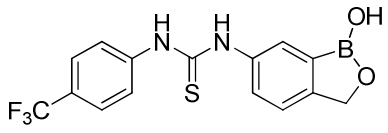

28f

1-(1-hydroxy-1,3-dihydrobenzo[c][1,2]oxaborol-6-yl)-3-(4-trifluoromethyl)phenyl)thiourea

White solid.

Yield: 40 %.

R*f*: 0.46 (dichloromethane : methanol = 94:6).

M.p. 179 °C dec.

^{1}H NMR 400 MHz (DMSO-d_6): δ 10.09 (s, 1H, OH), 10.08 (s, 1H, NH), 9.24 (s, 1H, NH), 7.76 (d, *J* = 7.4 Hz, 3H, ArH), 7.68 (d, *J* = 8.1 Hz, 2H, ArH), 7.52 (dd, J^1 = 7.8 Hz, J^2 = 1.3 Hz, 1H, ArH), 7.39 (d, *J* = 8.1 Hz, 1H, ArH), 4.97 (s, 2H, CH_2).

^{13}C NMR 101 MHz (DMSO-d_6): δ 183.3, 140.7, 126.9, 125.9, 125.8, 125.7, 121.1, 114.7, 114.5, 99.2, 69.4.

MS: ESI: m/z 353.1 $[M+H]^{+\cdot}$

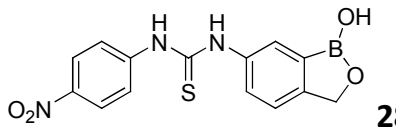

28g

1-(1-hydroxy-1,3-dihydrobenzo[c][1,2]oxaborol-6-yl)-3-(4-nitrophenyl)thiourea

Yellow solid.

Yield: 25 %.

R*f*: 0.63 (dichloromethane : methanol = 94:6).

M.p. 166 °C dec.

^{1}H NMR 400 MHz (DMSO-d_6): δ 10.39 (s, 1H, OH), 10.33 (s, 1H, NH), 9.26 (s, 1H, NH), 8.21 (d, *J* = 8.7, 2H, ArH), 7.84 (d, *J* = 8.7, 2H, ArH), 7.70-7.67 (s, 1H, ArH), 7.52 (d, *J* =7.5 Hz, 1H, ArH), 7.40 (d, J = 7.5 Hz,1H, ArH), 4.97 (s, 2H, CH_2).

^{13}C NMR 101 MHz (DMSO-d_6):δ 184.6, 140.9, 126.8, 125.6, 124.0, 121.3, 69.4.

MS: ESI: m/z 330.1 $[M+H]^{+\cdot}$

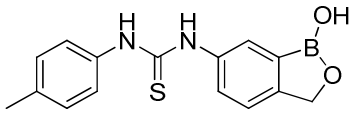

28h

1-(1-hydroxy-1,3-dihydrobenzo[c][1,2]oxaborol-6-yl)-3-(*p*-tolyl)thiourea

White solid.

Yield: 24 %.

R*f*: 0.30 (dichloromethane : methanol = 94:6).

M.p. 169-170 °C dec.

^{1}H NMR 400 MHz (DMSO-d_6): δ 9.71 (s, 1H, OH), 9.66 (s, 1H, NH), 9.23 (s, 1H, NH), 7.74 (s, 1H, ArH), 7.50 (d, *J* = 7.4, 1H, ArH), 7.36-7.33 (overlapping, 3H, ArH), 7.13 (d, *J* = 7.4, 2H, ArH), 4.96 (s, 2H, CH_2), 3.68 (bs, 2H, CH_2), 2.28 (s, 3H, CH_3).

^{13}C NMR 101 MHz (DMSO-d_6): δ 184.6, 128.5, 126.9, 125.7, 123.6, 121.0, 69.4, 20.1.

MS: ESI: m/z 299.1 $[M+H]^{+\cdot}$

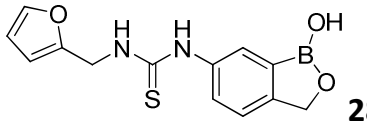

28i

1-(furan-2-ylmethyl)-3-(1-hydroxy-1,3-dihydrobenzo[c][1,2]oxaborol-6-yl)thiourea

Yellow solid.

Yield: 40 %.

R*f*: 0.47 (dichloromethane : methanol = 94:6).

M.p. 172 °C dec.

^{1}H NMR 400 MHz (DMSO-d_6):δ 9.58 (s, 1H, OH), 9.22 (s, 1H, NH), 8.02 (d, *J* = 4.9 Hz, 1H, NH), 7.69 (d, *J* = 1.7, 1H, ArH), 7.60 (m, *J* = 8.7, 1H, ArH), 7.46 (dd, *J* = 8.1 Hz, *J* = 1.9 Hz, 1 H, ArH), 7.35 (d, J =8.2 Hz, 1H, ArH), 7.42 (m, 1H, ArH), 6.32 (dd, J^1 = 3.1 Hz, J^2 = 0.7 Hz, 1 H, ArH), 4.96 (s, 2H, CH_2)., 4.70 (d, *J* = 5.2 Hz, 2H, CH_2).

^{13}C NMR 101 MHz (DMSO-d_6):δ 183.4 (s, CS), 141.7, 140.15, 121.1, 120.8, 119.1, 110.1, 106.2, 69.3, 35.8 (s, CH_2).

MS: ESI: m/z 289.1 $[M+H]^{+\cdot}$

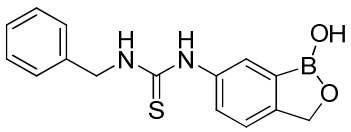

28j

1-benzyl-l-3-(1-hydroxy-1,3-dihydrobenzo[c][1,2]oxaborol-6-yl)thiourea

White solid.

Yield: 40 %.

R*f*: 0.47 (dichloromethane : methanol = 94:6).

M.p. 172 °C dec.

^{1}H NMR 400 MHz (DMSO-d_6):δ 9.61 (s, 1H, OH), 9.22 (s, 1H, NH), 8.11 (d, *J* = 4.9 Hz, 1H, NH), 7.71 (s, 1H, ArH), 7.48 (d, *J* = 8.0, 1H, ArH), 7.38-7.34 (overlapping, 5H, ArH), 7.25 (m, 1H, ArH), 4.97 (s, 2H, CH_2)., 4.74 (d, *J* = 4.8 Hz, 2H, CH_2).

^{13}C NMR 101 MHz (DMSO-d_6):δ 181.2 (s, CS), 150.2, 139.1, 137.9, 128.2, 127.4, 126.8, 121.6, 69.7 (s, CH_2), 47.2.

MS: ESI: m/z 299.1 $[M+H]^{+\cdot}$

Co-Crystallization and X-ray data collection of *h*CA II-ligand complexes.

Co-crystals for each of two sulfonamides reported here (**6a** and **6b**) with *h*CA II were obtained using the hanging drop vapor diffusion method as reported earlier.[118] Drops of 10 µL (0.3 mM hCA II; 0.7 mM drug 1; 0.1 % DMSO; 0.8 M Sodium Citrate; 50 mM Tris-HCl; pH 8.0) were equilibrated against the precipitant solution (1.6 M sodium citrate; 50 mM Tris-HCl; pH 8.0) at room temperature (~20 ºC), for all the three compounds. Crystals were observed after 5 days. Based of visual selection a crystal of each of the CA II - complexes were cryoprotected by quick immersion into 20% sucrose precipitant solution and flash-cooled by exposing to a gaseous stream of nitrogen at 100 K. The X-ray diffraction data was collected using an R-AXIS IV^{++} image plate system on a Rigaku RU-H3R Cu rotating anode operating at 50 kV and 22 mA, using Osmic Varimax HR optics. The detector-crystal distance was set to 80 mm. The oscillation steps were 1° with a 5 min exposure per image. Indexing, integration, and scaling were performed using HKL2000.[119]

Structure determination of CA II drug complexes.

Starting phases were Calculatedd from Protein Data Bank (PDB) entry 3KS3[120] with waters removed. Refinement using *Phenix* package,[121] with 5% of the unique reflections selected randomly and excluded from the refinement data set for the purpose of R_{free} calculations,[122] was alternated with manual refitting of the model in *Coot*.[123] The validity of the final model was assessed by *PROCHECK*.[124] Complete refinement statistics and model quality are included in Table S1. Figures were made in PyMOL.[125]

Table S1 Crystallographic data refinement and model quality statistics.

	PDB accesion codes	
	4DZ7 (Compound 5c)	**4DZ9 (Compound 5h)**
Data-collection statistics		
Temperature (K)	100	100
Wavelength (Å)	1.5418	1.5418
Space group	$P2_1$	$P2_1$
Unit-cell parameters (Å, °): *a, b, c, β*	42.3, 41.3, 72.0, 104.1	42.2, 41.3 72.0 104.1
Total theoretical reflections	39683	39669
Total measured reflections	38255	37765
Resolution (Å)	50.0 – 1.5 (1.54 – 1.49)	50.0 – 1.5 (1.54 – 1.49)
$^{a}R_{sym}$ (%)	7.0 (26.1)	4.6 (17.4)

I/σ(I)	14.0 (5.7)	27.6 (6.9)
Completeness (%)	96.4 (90.1)	95.2 (88.2)
Redundancy	5.4 (5.1)	4.7 (4.5)
Final Model Statistics		
[b]R_{cryst}, [c]R_{free} (%)	15.6, 17.8	21.1, 22.9
Residue numbers	4 - 261	4 - 261
[d]No. of atoms: *Protein, drug, water*	2275, 23, 208	2247, 25, 186
R.M.S.D.: *Bond lengths* (Å), *bond angles* (°)	0.010, 1.37	0.009, 1.35
Ramachandran statistics (%): *Most favored, allowed, outliers*	98.03, 1.97, 0.00	97.24, 2.76, 0.00
Average B-factors (Å^2): *Main chain, side chain, inhibitor, solvent*	12.9, 16.7, 19.7, 25.9	11.2, 14.6, 18.3, 21.9

[a]$R_{sym} = \Sigma |I - \langle I \rangle| / \Sigma \langle I \rangle$. [b]$R_{cryst} = (\Sigma ||Fo| - |Fc|| / \Sigma |F_{obs}|) \times 100$. [c]$R_{free}$ is Calculated in same manner as R_{cryst}, except that it uses 5% of the reflection data omitted from refinement. [d]Includes alternate conformations. *Values in parenthesis represent highest resolution bin.

CA inhibition studies.

An Applied Photophysics stopped-flow instrument has been used for assaying the CA catalysed CO_2 hydration activity.[126] Phenol red (at a concentration of 0.2 mM) has been used as indicator, working at the

absorbance maximum of 557 nm, with 20 mM Hepes (pH 7.4) and 20 mM $NaBF_4$ (for maintaining constant the ionic strength), following the initial rates of the CA-catalyzed CO_2 hydration reaction for a period of 10-100 s. The CO_2 concentrations ranged from 1.7 to 17 mM for the determination of the kinetic parameters and inhibition constants. For each inhibitor, at least six traces of the initial 5-10% of the reaction have been used for determining the initial velocity. The uncatalyzed rates were determined in the same manner and subtracted from the total observed rates. Stock solutions of inhibitor (10 mM) were prepared in distilled-deionized water and dilutions up to 0.01 nM were done thereafter with distilled-deionized water. Inhibitor and enzyme solutions were preincubated together for 15 min at RT prior to assay, in order to allow for the formation of the E-I complex. The inhibition constants were obtained by non-linear least-squares methods using PRISM 3, whereas the kinetic parameters for the uninhibited enzymes from Lineweaver-Burk plots, as reported earlier,[127] and represent the mean from at least three different determinations. All CAs were recombinant proteins obtained as reported earlier by these groups.[128]

Cell culture.

Human neuroblastoma SH-SY5Y cells (American Type Culture Collection number CRL-2266) were cultured in Dulbecco's Modified Eagle Medium F-12 (DMEM/F12) ground (Life Technologies, Carlsbad, CA, USA) in the presence of 10% fetal calf serum (Life Technologies) inactivated at 56 °C for 30 minutes. The cells are grown in an incubator at 37 °C in a humidified atmosphere containing 5% CO2. Stable clones expressing CFP-DEVD-YFP

(Addgene company code 24537) were obtained by transfecting cells with LipofectAMINE LTX and PLUS reagent (Life Technologies) using 1.5 μg DNA/5–7×105 cells according to the manufacturer's protocol. The different SH-SY5Y clones were maintained under selection by 400 μg/mL of G418. Individual clones expressing antibiotic resistance were picked after 14 days of selection, moved into a 48-well plate, and maintained in selective medium until confluence growth. Different individual clones were analyzed for CFP-DEVD-YFP expression upon treatment with the caspase-3 activator staurosporine (1 μg/mL).

Assessment of cell viability.

The viability of control SH-SY5Y-CFP-DEVD-YFP cells was Calculated after 72 hours through an MTS assay with and without overnight treatment of cell with $CoCl_2$. Cell viability was assessed by a colorimetric assay using the MTS assay (CellTiter 96 Aqueous One Solution Assay; Promega Corporation, Madison, WI, USA), according to the manufacturer's instructions. Absorbance at 490 nm was measured in a multilabel counter (Victor X5; Perkin Elmer, Waltham, MA, USA).

References and notes

[1] (a) Humphrey, J. M.; Chamberlin, A. R. Chemical Synthesis of Natural Product Peptides: Coupling Methods for the Incorporation of Noncoded Amino Acids into Peptides. *Chem. Rev.* **1997**, 97, 2243; (b) Carey, J. S.; Laffan, D.; Thomson, C.; Williams, M. T. Analysis of the reactions used for the preparation of drug candidate molecules. *Org. Biomol. Chem.* **2006**, 4, 2337; (c) Allen, C. L.; Williams, J. M. J. *Chem. Soc. Rev.* **2011**, 40, 3405.

[2] Ghose, A. K.; Viswanadhan, V. N.; Wendoloski, J. J. A knowledge-based approach in designing combinatorial or medicinal chemistry libraries for drug discovery. 1. A qualitative and quantitative characterization of known drug databases. *J. Comb. Chem*. **1999**, 1, 55.

[3] Jursic B.S. and Zdravkovdki, Z. A simple preparation of amides from acids and amines by heating of their mixture. *Synth. Commun*. **1993**, 23, 2761–2770.

[4] Valeur, E.; Bradley, M. Amide bond formation: beyond the myth of coupling reagents. *Chem. Soc. Rev*. **2009**, 38, 606–631.

[5] Saxo, E.; Bertozzi, C. Z. Cell surface engineering by a modified Staudinger reaction. Science **2000**, 287, 2007–2010.

[6] Owston, N.A.; Parker, A. J.; Williams, J.M.J. Highly efficient ruthenium-catalyzed oxime to amide rearrangement. *Org. Lett.* **2007**, 9, 3599–3601. (b) Hashimoto, M.; Obora, Y.; Sakaguchi, S; Ishii, Y. Beckmann rearrangement of ketoximes to lactams by triphosphazene catalyst. *J. Org. Chem.* **2008**, 73, 2894–2897.

[7] Martinelli, J. R.; Clark, T. p.; Watson, D. A.; Munday, R. H.; Buchwald, S. L. Palladium-Catalyzed Aminocarbonylation of Aryl Chlorides at Atmospheric Pressure: The Dual Role of Sodium Phenoxide. *Angew. Chem.* **2007**, 119, 8612–8615.

[8] Shen, B.; Makley, D. M.; Johnston, J. N. Umpolung reactivity in amide and peptide synthesis. *Nature* **2010**, 465, 1027–1032.

[9] (a) Gunanathan, C.; Ben-David, Y.; Milstein, D. Direct synthesis of amides from alcohols and amines with liberation of H_2. *Science* **2007**, 317, 790–792. (b) Nordstom, L. U.; Vogt, H.; MadsenR. Amide synthesis from alcohols and amines by the extrusion of dihydrogen. *J. Am. Chem. Soc*. **2008**, 130, 17672–17673. (c) Zweifel, T.; Naubron, J. V.; Grutzmacher, H. Catalyzed dehydrogenative coupling of primary alcohols with water, methanol, or amines. *Angew. Chem., Int. Ed*. **2009**, 48, 559–563. (d) Ghosh, S. C. Muthaiah, S.; Zhang, Y.; Xu, X.; Homg, S. H. Direct Amide Synthesis from Alcohols and Amines by Phosphine-Free Ruthenium Catalyst Systems. *Adv. Synth. Catal.* **2009**, 351, 2643–2649. (e) Zhang, Y.; Chen, C.; Ghosh, S. C.; Li, Y.; Hong, S. H. Well-Defined N-Heterocyclic Carbene Based Ruthenium Catalysts for Direct Amide Synthesis from Alcohols and Amines. *Organometallics* **2010**, 29, 1374–1378. (f) Cheng, C.; Hong, S. H. Oxidative amide synthesis directly from alcohols with amines. *Org. Biomol. Chem.* **2011**, 9, 20–26. (g) Wang, Y.; Zhu, D.; Tang, L.; Wang, S.; Wang, Z. Highly Efficient Amide Synthesis from Alcohols and Amines by Virtue of a Water-Soluble Gold/DNA Catalyst. *Angew. Chem., Int. Ed.* **2011**, 50, 8917–8921. (h) Soule, J.-F.; Miyamura, H.; Kobayashi, S. Powerful Amide Synthesis from Alcohols and Amines under Aerobic Conditions Catalyzed by Gold or Gold/Iron, -Nickel or -Cobalt Nanoparticles. *J. Am. Chem. Soc.* **2011**, 133, 18550–18553. (i) Kegnaes, S.; Mielby, J.; Mentzel, U. V.; Jensen, T.; Fristrup, P.; Riisager, A. One-pot synthesis of amides by aerobic oxidative coupling of alcohols or aldehydes with amines using supported gold and base as catalysts. *Chem. Commun*. **2012**, 48, 2427–2429. (j) Xiao, F.; Liu, Y.; Tang, C.; Deng, G. *J.* Peroxide-Mediated Transition-Metal-Free Direct Amidation of Alcohols with Nitroarenes. *Org. Lett*. **2012**, 14, 984–987 and references herein.

[10] (a) Cho, S.; Yoo, E.; Bae, I.; Chang, S. Copper-Catalyzed Hydrative Amide Synthesis with Terminal Alkyne, Sulfonyl Azide, and Water. *J. Am. Chem. Soc.* **2005**, 127, 16046–16047. (b) Chen, Z.W.; Jiang, H.F.; Pan, X.Y.; He, Z.J. Practical

synthesis of amides from alkynyl bromides, amines, and water. *Tetrahedron* **2011**, 67, 5920–5927.

[11] (a) Kolakowski, R. V.; Shangguan, N.; Sauers, R. R.; Williams, L. J. Mechanism of thio acid/azide amidation. *J. Am. Chem. Soc.* **2006**, 128, 5695–5702. (b) Zhang, X.; Li, F.; Lu, X. W.; Liu, C. F. Protein C-terminal modification through thioacid/azide amidation. Bioconjugate Chem. **2009**, 20, 197–200.

[12] (a) Dineen, T. A.; Zajac, M. A.; Myers, A. G. Exiguamine A, an indoleamine-2,3-dioxygenase (IDO) inhibitor isolated from the marine sponge Neopetrosia exigua. *J. Am. Chem. Soc*. **2006**, 128, 16046–16047. (b) Allen, C. L.; Atkinson, B. N.; Williams, J. M. J. Transamidation of primary amides with amines using hydroxylamine hydrochloride as an inorganic catalyst. *Angew. Chem., Int. Ed*. **2012**, 51, 1383–1386. (c) Tamura, M.; Tonomura, T.; Shimizu, K.-I.; Satsuma, A. Transamidation of amides with amines under solvent-free conditions using a CeO_2 catalyst. *Green Chem*. **2012**, 14, 717–724. (d) Zhang, M.; Imm, S.; Bahn, S.; Neubart, L.; Neumann, H.; Beller, M. Efficient copper(II)-catalyzed transamidation of non-activated primary carboxamides and ureas with amines. *Angew. Chem., Int. Ed*. **2012**, 51, 3905–3909

[13] (a) Chen, X.; Engle, K. M.; Wang D.H. and Yu, J.Q. Palladium(II)-catalyzed C-H activation/C-C cross-coupling reactions: versatility and practicality. *Angew. Chem. Int.Ed*. **2009**, 48, 5094; (b) Daugulis, O. Do H.Q. and Shabashov, D. Palladium- and copper-catalyzed arylation of carbon-hydrogen bonds. *Acc. Chem. Res*. **2009**, 42, 1074; (c) Ritleng, V. Sirlin C. and Pfeffer, M. Ru-, Rh-, and Pd-catalyzed C-C bond formation involving C-H activation and addition on unsaturated substrates: reactions and mechanistic aspects. *Chem. Rev.* **2002**, 102, 1731.

[14] Li, J. Cross-dehydrogenative coupling (CDC): exploring C-C bond formations beyond functional group transformations. *Acc. Chem. Res.* **2009**, 42, 335.

[15] (a) Li, Z.; Li, C.J. CuBr-catalyzed efficient alkynylation of sp3 C-H bonds

adjacent to a nitrogen atom. *J. Am. Chem. Soc.* **2004**, *126*, 11810–11811; (b) Li, Z.; Li, C.J. CuBr-catalyzed direct indolation of tetrahydroisoquinolines via cross-dehydrogenative coupling between sp3 C-H and sp2 C-H bonds. *J. Am. Chem. Soc.* **2005**, *127*, 6968–6969; (c) Basle, O.; Li, C.J. Copper catalyzed oxidative alkylation of sp^3 C–H bond adjacent to a nitrogen atom using molecular oxygen in water. *Green Chem.* **2007**, *9*, 1047–1050. (d) Zhang, Y.; Li, C.J. Highly Efficient Direct Alkylation of Activated Methylene by Cycloalkanes. *Eur. J. Org. Chem.* **2007**, 4654–4657.

[16] (a) Cai, G.; Fu, Y.; Li, Y.; Wan, X.; Shi, Z. Indirect ortho Functionalization of Substituted Toluenes through ortho Olefination of N,N-Dimethylbenzylamines Tuned by the Acidity of the Reaction Conditions. *J. Am. Chem. Soc.* **2007**, *129*, 7666–7673. (b) Stuart, D. R.; Fagnou, K. The catalytic cross-coupling of unactivated arenes. *Science* **2007**, *316*, 1172–1175. (c) Dwight, T. A.; Rue, N. R; Charyk, D.; Josselyn, R.; DeBoef, B. C-C bond formation via double C-H functionalization: aerobic oxidative coupling as a method for synthesizing heterocoupled biaryls. *Org. Lett.* **2007**, *9*, 3137–3139. (d) Hull, K. L.; Sanford, M. S. Catalytic and highly regioselective cross-coupling of aromatic C-H substrates. *J. Am. Chem. Soc.* **2007**, *129*, 11904–11905. (e) Xia, J.-B.; You, S.-L. Carbon−Carbon Bond Formation through Double sp^2 C−H Activations: Synthesis of Ferrocenyl Oxazoline Derivatives. *Organometallics* **2007**, *26*, 4869–4871. (f) Zhang, H.-B.; Liu, L.; Chen,Y.J.; Wang, D.; Li, C.J. "On Water"-Promoted Direct Coupling of Indoles with 1,4-Benzoquinones without Catalyst. *Eur. J. Org. Chem.* **2006**, 869–873. (g) Jia, C.; Kitamura, T.; Fujiwara, Y. Catalytic functionalization of arenes and alkanes via C-H bond activation. *Acc. Chem. Res.* **2001**, *34*, 633–639.

[17] Yoo, W. J.; Li, C. J. Highly stereoselective oxidative esterification of aldehydes with beta-dicarbonyl compounds. *J. Org. Chem.* **2006**, 71, 6266–6268.

[18] Möller, K.; Wienhöfer, G.; Schöder, K.; Join, B.; Junge K. and Beller, M. Selective

iron-catalyzed oxidation of phenols and arenes with hydrogen peroxide: synthesis of vitamin e intermediates and vitamin K(3). *Chem. Eur. J*. **2010**, 16, 10300.

[19] Kumar, G. S.; Maheswari, C. U.; Kumar, R. A.; Kantam M. L. and Reddy, K. R. Copper-catalyzed oxidative C-O coupling by direct C-H bond activation of formamides: synthesis of enol carbamates and 2-carbonyl-substituted phenol carbamates. *Angew. Chem., Int. Ed*. **2011**, 50, 11748–11751.

[20] (a) Sun, C.L.; Li, B.J.; Shi, Z. J. Direct C-H transformation via iron catalysis. *Chem. Rev*. **2011** , 111, 1293–1314. (b) Lyons, T. W.; Sanford, M. Palladium-catalyzed ligand-directed C-H functionalization reactions. *Chem. Rev*. **2011** , 110, 1147–1169. (c) Correa, A.; M Mancheno, O. G.; Bolm, C. Iron-catalysed carbon-heteroatom and heteroatom-heteroatom bond forming processes. *Chem. Soc. Rev*. **2008**, 37, 1108–1117.

[21] Wang, Z.; Zhang, Y.; Fu, H.; Jiang Y. and Zhao, Y. Efficient intermolecular iron-catalyzed amidation of C-H bonds in the presence of N-bromosuccinimide. *Org. Lett*. **2008**, 10, 1863.

[22] Cho, S. H.; Yoon J. and Chang, S. Intramolecular oxidative C-N bond formation for the synthesis of carbazoles: comparison of reactivity between the copper-catalyzed and metal-free conditions. *J. Am. Chem. Soc*. **2011**, 133, 5996–6005.

[23] Li, S. and Wu, J. Synthesis of H-pyrazolo[5,1-a]isoquinolines via copper(II)-catalyzed oxidation of an aliphatic C-H bond of tertiary amine in air. *Org. Lett*. **2011**, 13, 712–715.

[24] Yoo, W.; Li, C. Highly efficient oxidative amidation of aldehydes with amine hydrochloride salts. *J. Am. Chem. Soc*. **2006**, 128, 13064–13065.

[25] Tillack, A.; Rudloff, I.; Beller, M. Catalytic amination of aldehydes to amide. *Eur. J. Org. Chem*. **2001**, 66, 523–528.

[26] Naota, T.; Murahashi, S. Ruthenium-catalyzed transformations of amino alcohols to lactams. *Synlett* **1991**, 693–694.

[27] Tamaru, Y.; Yamada, Y.; Yoshida, Z. Direct oxidative transformation of aldehydes to amides by palladium catalysis. *Synthesis* **1983**, 474–476.

[28] Nakagawa, K.; Onoue, H.; Minami, K. Oxidation with nickel peroxide. a new synthesis of amides from aldehydes or alcohols. *Chem. Commun*. **1966**, 1, 17–18.

[29] Ghosh, S. C.; Ngiam, J. S. Y.; Chai, C. L. L.; Seayad, A. M. Dang, T. T.; Chen, A. Cu(I) Oxide-catalyzed Synthesis of primary amides by direct Oxidative Amidation of Aldehydes with Ammonium Chloride. *Adv. Synth. Catal.* **2012**, 354, 1407–1412.

[30] Ekoue-Kovi, K.; Wolf, C. Metal-free one-pot oxidative amination of aldehydes to amides. *Organic Letters* **2007**, 9, 3429-3432.

[31] Liu, Z.; Zhang, J.; Chen, S.; Shi, E.; Xu, Y.; Wan, X. Cross coupling of acyl and aminyl radicals: direct synthesis of amides catalyzed by Bu4NI with TBHP as an oxidant. *Angew. Chem. Int. Ed.* **2012**, 51, 3231–3235.

[32] Xu, K.; Hu, Y.; Zhang, S.; Zha, Z.; Wang, Z. Direct amidation of alcohols with N-substituted formamides under transition-metal-free conditions. *Chem. Eur. J.* **2012**, 18, 9793–9797.

[33] (a) Sibi, M. P.; Manyem, S.; Zimmerman, J. Enantioselective radical processes. *Chem. Rev*. **2003**, 103, 3263; (b) Renaud, P.; Sibi, M. P. *Radicals in Organic Synthesis*, Wiley-VCH, New York, **2001**; c) Gansuer, A. *Radicals in Synthesis*, Springer, Heidelberg, **2006**.

[34] Wei, W.; Zhang, C.; Xu, Y.; Wan, X. Synthesis of tert-butyl peresters from aldehydes by Bu4NI-catalyzed metal-free oxidation and its combination with the Kharasch-Sosnovsky reaction. *Chem. Commun*. **2011**, 47, 10827-10829.

[35] Cadoni, R.; Porcheddu, A.; Giacomelli, G.; De Luca, L. *Org. Lett*. **2012**, 14, 5414-5417.

[36] Rothenberg, G.; Feldberg, L.; Wiener, H.; Sasson, Y. Copper-catalyzed homolytic and heterolytic benzylic and allylic oxidation using *tert*-butyl

hydroperoxide. *J. Chem. Soc*., *Perkin Trans. 2* **1998**, 2429–2434.

[37] Kochi, J. K. The mechanism of the copper salt catalysed reactions of peroxides. *Tetrahedron* **1962**, 18, 483-497.

[38] *Minisci*, F. Novel application of free-radical reactions in preparative organic chemistry. *Synthesis **1973***, 1–24.

[39] Liu, W.; Li, Y.; Li, Z. Iron-catalyzed carbonylation-peroxidation of alkenes with aldehydes and hydroperoxides. *J. Am. Chem. Soc.* **2011**, 133, 10756–10759.

[40] (a) Supuran, C.T.; Scozzafava, A.; Conway, J., Carbonic Anhydrase—Its Inhibitors and Activators; Eds.; CRC Press:Boca Raton (FL), USA, **2004**, pp 1–363, and references cited therein. (b) Supuran, C.T.; Scozzafava, A. Carbonic anhydrase inhibitors and their therapeutic potential *Expert Opin. Ther. Pat.* **2000**, 10, 575-600. (c) Supuran, C.T.; Scozzafava, A.; Casini, A. Carbonic Anhydrase Inhibitors *Med. Res. Rev*. **2003**, 23, 1464. (d) Smith, K.S.; Ferry, J. G. Prokaryotic carbonic anhydrases. *FEMS Microbiol. Rev*. **2000**, 24, 335. (e) Liljas, A.; Kannan, K. K.; Bergsten, P.C.; Waara, I.; Fridborg, K.; Strandberg, B.; Carlbom, U.; Jarup, L.; Lovgren, S.; Petef, M. Crystal structure of human carbonic anhydrase C. Inhibition and catalysis of carbonic anhydrase. Recent crystallographic analyses. *Nat. New Biol*. **1972**, 235, 131-136. (f) Liljas, A.; Hakansson, K.; Jonsson, B. H.; Xue, Y. Inhibition and catalysis of carbonic anhydrase. Recent crystallographic analyses. *Eur. J.Biochem.* **1994**, 219, 1-7. (g) Lane, T.W.; Morel, F.M. A biological function for cadmium in marine diatoms. *Proc. Natl. Acad. Sci. U.S.A*. **2000**, 97, 4627-4627. (h) Hilvo, M.; Tolvanen, M.; Clark, A.; Shen, B.; Shah, G.N.; Waheed, A.; Halmi, P.; Hanninen, M.; Hamalainen, J.M.; Vihinen, M.; Sly, W. S.; Parkkila, S. Characterization of CA XV, a new GPI-anchored form of carbonic anhydrase. *Biochem. J*. **2005**, 392, 83. (i) Anthony K.C.; So, G.S.; Espie, E.B.; Williams, J.M.; Shively, S.H.; Gordon C. C. A Novel Evolutionary Lineage of Carbonic Anhydrase (ε Class) Is a Component of the Carboxysome *Shell Bacteriol*. **2004**, 186, 623-630.

[41] Alterio, V.; Di Fiore, A.; D'Ambrosio, K.; Supura, C.T.; De Simone, G. *Multiple* Binding Modes of Inhibitors to Carbonic Anhydrases: How to Design Specific *Drugs Targeting 15 Different Isoforms*? *Chem. Rev.* **2012**, 112, 4421-4468.

[42] Supuran, C.T. Carbonic anhydrases: novel therapeutic applications for inhibitors and activators. *Nature Reviews Drug Discovery* **2008**, 7, 168-181.

[43] (a) Whittington, D.A.; Waheed, A.; Ulmasov, B.; Shah, G.N.; Grubb, J.H.; Sly, W.S.; Christianson, D. W. Crystal structure of the dimeric extracellular domain of human carbonic anhydrase XII, a bitopic membrane protein overexpressed in certain cancer tumor cells. *Proc. Natl. Acad. Sci. U.S.A*. **2001**, 98, 9545. (b) Alterio, V.; Hilvo, M.; Di Fiore, A.; Supuran, C.T.; Pan, P.; Parkkila, S.; Scaloni,A.; Pastorek, J.; Pastorekova, S.; Pedone, C.; Scozzafava, A.; Monti, S. M.; De Simone, G. Crystal structure of the catalytic domain of the tumor-associated human carbonic anhydrase IX. *Proc. Natl. Acad. Sci. U.S.A*. **2009**, 106, 16233

[44] *Aggarwal*, M.; Boone, C.D.; Kondeti, B.; McKenna, R. Structural annotation of human carbonic anhydrases. *Jour. Enz. Inhib. Med. Chem.* **2013**, 28, 267–277.

[45] Hassan, I.; Shajee, B.; Waheed, A.; Ahmad, F. Sly, W.S. Structure, function and applications of carbonic anhydrase isozymes. *Bioorg. Med. Chem*. **2013**, 21, 1570-1582.

[46] Hassan, I.; Shajee, B.; Waheed, A.; Ahmad, F. Sly, W.S. Structure, function and applications of carbonic anhydrase isozymes. *Bioorg. Med. Chem*. **2013**, 21, 1570-1582.

[47] (a) Sjöblom, B.; Polentarutti, M.; Djinovic-Carugo, K. Structural study of X-ray induced activation of carbonic anhydrase. *Proc. Natl.Acad. Sci. U.S.A*. **2009**, 106, 10609. (b) Domsic, J. F.; Avvaru, B. S.; Kim, C. U.; Gruner, S. M.; Agbandje-McKenna, M.; Silverman, D. N.; McKenna, R. Entrapment of carbon dioxide in the active site of carbonic anhydrase II. *J. Biol. Chem*. **2008**, 283, 30766.

[48] Supuran C. T.; Scozzafava A. Carbonic anhydrases as targets for medicinal

chemistry. *Bioorg. Med. Chem.* **2007**, 15, 4336-4350.

[49] (a) Supuran C. T.; Winum J.Y. Drug Design of Zinc-Enzyme Inhibitors: Functional, Structural, and Disease Applications. Wiley: New York, **2009**. (b) Supuran, C.T.; Scozzafava, A. Applications of carbonic anhydrase inhibitors and activators in therapy. *Expert Opin Ther Patents* **2002**, *12*, 217-242. (c) Breton, S. The cellular physiology of carbonic anhydrases. *JOP* **2001**, *2*, 159-164. (d) Mincione, F.; Scozzafava, A.; Supuran, C. T. The development of topically acting carbonic anhydrase inhibitors as anti-glaucoma agents. *Curr Top Med Chem* **2007**, *7,* 9, 849-854

[50] Smith, C.E.; Nanci, A.; Moffatt, P. Evidence by signal peptide trap technology for the expression of carbonic anhydrase 6 in rat incisor enamel organs. *Eur. J. Oral. Sci.* **2006**, 114, 147.

[51] Nagelhus*,* A.*;* Mathiisen*,* T.M.*;* Bateman*,* A.C.*;* Haug*,* F.M.*;* Ottersen*,* *O*.P.*;* Grubb*,* J.H. et al. Carbonic anhydrase XIV is enriched in specific membrane domains of retinal pigment epithelium, Muller cells, and astrocytes. *Proc. Natl. Acad. Sci. USA* **2005**, 102, 8030–8035.

[52] Temperini, C.; Scozzafava, A.; Supuran, C.T. In Drug Design of Zinc-Enzyme Inhibitors: Functional, Structural, and Disease Applications; Supuran, C.T., Winum, J.Y., Eds.; Wiley: Hoboken, NJ, **2009**, p. 473.

[53] De Simone, G.; Supuran, C. T. Carbonic anhydrase IX: Biochemical and crystallographic characterization of a novel antitumor target. *Biochim. Biophys. Acta* **2010**, 1804, 404.

[54] Gambhir, K. K.; Ornasir, J.; Headings, V.; Bonar, A. Decreased total carbonic anhydrase esterase activity and decreased levels of carbonic anhydrase 1 isozyme in erythrocytes of type II diabetic patients. *Biochemical Genetics* **2007**, 45, 431-439.

[55] Gao, B. B.; Clermont, A.; Rook, S. Extracellular carbonic anhydrase mediates hemorrhagic retinal and cerebral vascular permeability through prekallikrein

activation. *Nature Medicine* **2007**, 13, 181-188.

[56] (a)Chang, X.; Zheng, Y.; and, Yang, Q. Carbonic anhydrase I (CA1) is involved in the process of bone formation and is susceptible to ankylosing spondylitis. *Arthritis Research & Therapy* **2012**, 14, 176. (b) Chang, X.; Han, J.; Zhao, Y.; Yan, X.; Sun, S.; and Cui, Y. Increased expression of carbonic anhydrase I in the synovium of patients with ankylosing spondylitis. *BMC Musculoskeletal Disorders* **2010**, 11, 279.

[57] Pala, N.; Cadoni, R.; Sechi, M. *Carbonic Anhydrase I* in Carbonic anhydrases as biocatalysts: from theory to medical and industrial applications. De Simone, G. and Supuran. C.T. Eds. Elsevier in press.

[58] (a)Hen, N.; Bialer, M.; Yagen, B.; Maresca, A.; Aggarwal, M.;Robbins, A. H.; McKenna, R.; Scozzafava, A.; Supuran, C. T. Anticonvulsant 4-aminobenzenesulfonamide derivatives with branched-alkylamide moieties: X-ray crystallography and inhibition studies of human carbonic anhydrase isoforms I, II, VII, and XIV. *J. Med. Chem.* **2011**, 54, 3977. (b) Mincione, F.; Scozzafava, A.; Supuran, C. T. The development of topically acting carbonic anhydrase inhibitors as antiglaucoma agents. *Curr. Pharm. Des*. **2008**, 14, 649. (c) Supuran, C. T. Diuretics: from classical carbonic anhydrase inhibitors to novel applications of the sulfonamides. *Curr. Pharm. Des.* **2008**, 14, 641. (d) De Simone, G.; Scozzafava, A.; Supuran, C. T. Which carbonic anhydrases are targeted by the antiepileptic sulfonamides and sulfamates? *Chem. Biol. Drug Des*. **2009**, 74, 317. (e) Basnyat, B.; Gertsch, J. H.; Johnson, E. W.; Castro-Marin, F.;Inoue, Y.; Yeh, C. High Efficacy of low-dose acetazolamide (125 mg BID) for the prophylaxis of acute mountain sickness: a prospective, double-blind, randomized, placebo-controlled trial. *Alt. Med. Biol*. **2003**, 4, 45. (f) Swenson, E. R.; Teppema, L. J. Prevention of acute mountain sickness by acetazolamide: as yet an unfinished story. *J. Appl. Physiol*. **2007**, 102, 1305.

[59] (a)Barreiro, E.; Hussain, S. N. A. Protein carbonylation in skeletal muscles:

impact on function. *Antioxid. Redox Signal.* **2010**, 12,417. (b) Brancaccio, P.; Lippi, G.; Maffulli, N. Biochemical markers of muscular damage. *Clin. Chem. Lab. Med*. **2010**, 48, 757. (36) Zimmerman, U. J.; Wang, P.; Zhang, X.; Bogdanovich, S.;Forster, R. Anti-oxidative response of carbonic anhydrase III in skeletal muscle. *IUBMB Life*. **2004**, 56, 343.

[60] Matsui, H.; Murakami, M.; Wynns, G. C.; Conroy, C. W.; Mead,A.; Maren, T. H.; Sears, M. L. Membrane carbonic anhydrase (IV) and ciliary epithelium. Carbonic anhydrase activity is present in the basolateral membranes of the non-pigmented ciliary epithelium of rabbit eyes. Exp. Eye Res. **1996**, 62, 409. (b)Datta, R.; Waheed, A.; Bonapace, G.; Shah, G. N.; Sly, W. S. Pathogenesis of retinitis pigmentosa associated with apoptosis-inducing mutations in carbonic anhydrase IV. *Proc. Natl. Acad. Sci. U.S.A.* **2009**, 106, 3437.

[61] De Simone, G.; Di Fiore, A.; Supuran, C. T. Are carbonic anhydrase inhibitors suitable for obtaining antiobesity drugs? *Curr. Pharm. Des.* **2008**, 14, 655. (21) De Simone, G.; Supuran, C. T. Antiobesity carbonic anhydrase inhibitors. *Curr. Top. Med. Chem*. **2007**, 7, 879.

[62] (a)Nishimori, I.; Minakuchi, T.; Onishi, S.; Vullo, D.; Scozzafava,A.; Supuran, C.T. Carbonic anhydrase inhibitors. DNA cloning, characterization, and inhibition studies of the human secretory isoform VI, a new target for sulfonamide and sulfamate inhibitors. *J. Med. Chem.* **2007**, 50, 381. (b) Kivelä, J.; Parkkila, S.; Parkkila, A. K.; Rajaniemi, H. A low concentration of carbonic anhydrase isoenzyme VI in whole saliva is associated with caries prevalence. *Caries Res***. 1999**, 33, 178.

[63] (a) Pastorekova, S.; Parkkila, S.; Zavada, J. Tumor-associated carbonic anhydrases and their clinical significance. *Adv. Clin. Chem*. **2006**, 42, 167. (b) Saarnio, J.; Parkkila, S.; Parkkila, A.K.; Pastorekova, S.; Haukipuro, K.; Pastorek, J.; Juvonen, T.; Karttunen, T.J. Transmembrane carbonic anhydrase, MN/CA IX, is a potential biomarker for biliary tumours. *J. Hepatol.* **2001,** 35, 643-649. (c)

Chia, S.K.; Wykoff, C.C.; Watson, P.H.; Han, C.; Leek, R.D.; Pastorek, J.; Gatter, K.C.; Ratcliffe, P.; Harris, A.L. Prognostic significance of a novel hypoxia-regulated marker, carbonic anhydrase IX, in invasive breast carcinoma. *J. Clin. Oncol.* ***2001,*** 19, 3660-3668. (d) Parkkila, S.; Parkkila, A.K.; Saarnio, J.; Kivela, J.; Karttunen, T.J.; Kaunisto, K.; Waheed, A.; Sly, W.S.; Tureci, O.; Virtanen, I.; Rajaniemi, H. Expression of the membrane-associated carbonic anhydrase isozyme XII in the human kidney and renal tumors. *J. Histochem. Cytochem.***2000**, 48, 1601-1608. (e) Dungwa, J.V.; Hunt, L.P.; Ramani, P. Carbonic anhydrase IX up-regulation is associated with adverse clinicopathologic and biologic factors in neuroblastomas. *Hum. Pathol*. **2012**, 43, 1651-60.

[64] Cianchi, F.; Vinci, M.C.; Supuran, C.T.; Peruzzi, B.; De Giuli, P.; Fasolis, G. et al. Selective inhibition of carbonic anhydrase IX decreases cellproliferation and induces ceramide-mediated apoptosis in humancancer cells. *J. Pharmacol. Exp. Ther.* **2010**, 334, 710–719.

[65] (a) Guler, O.O.; De Simone, G.; Supuran, C.T. Drug design studies of the novel antitumor targets carbonic anhydrase IX and XII. *Curr. Med. Chem.* **2010**, 17, 1516. (b) De Simone, G.; Supuran, C. T. Carbonic anhydrase IX: Biochemical and crystallographic characterization of a novel antitumor target. *Biochim. Biophys. Acta* **2010**, 1804, 404.

[66] (a) Battke, C.; Kremmer, E.; Mysliwietz, J.; Gondi, G.; Dumitru, C.;Brandau, S.; Lang, S.; Vullo, D.; Supuran, C. T; Zeidler, R. Generation and characterization of the first inhibitory antibody targeting tumour-associated carbonic anhydrase XII. *Cancer Immunol. Immunother*. **2011**, 60, 649. (b) Liao, S. Y.; Ivanov, S.; Ivanova, A.; Ghosh, S.; Cote, M. A.;Keefe, K.; Coca-Prados, M.; Stanbridge, E. J.; Lerman, M.I. Expression of cell surface transmembrane carbonic anhydrase genes CA9 and CA12 in the human eye: overexpression of CA12 (CAXII) in glaucoma. *J. Med.Genet*. **2003**, 40, 257.

[67] (a)Abbate, F.; Winum, J.Y.; Potter, B.V.; Casini, A.; Montero, J.L.; Scozzafava, A. *et al*. Carbonic anhydrase inhibitors: X-ray crystallographicstructure of the adduct of human isozyme II with EMATE,a dual inhibitor of carbonic anhydrases and steroid sulfatase. *Bioorg. Med. Chem. Lett.* **2004**, 14, 231-4. (b) Winum, J.Y.; Temperini, C.; El Cheikh, K,; Innocenti, A.; Vullo, D.; Ciattini, S. *et al*. Carbonic anhydrase inhibitors: clash with Ala65 as ameans for designing inhibitors with low affinity for the ubiquitousisozyme II, exemplified by the crystal structure of the topiramatesulfamide analogue. *J. Med. Chem.* **2006**, 49, 7024-31.

[68] Alterio, V.; Di Fiore, A.; D'Ambrosio, K.; Supuran, C. T.; De Simone, G. X-rayCrystallography of CA Inhibitors and Its Importance in Drug Design. In DrugDesign of Zinc-Enzyme Inhibitors: Functional, Structural, and Disease Applications; Supuran, C. T., Winum, J. Y., Eds.; Wiley: Hoboken, **2009**; pp 73–138.2. (b) Supuran, C.T. Carbonic anhydrase inhibitors. *Bioorg. Med. Chem. Lett*. **2010**, 20, 3467; (c) Santos, M. A.; Marques, S.; Vullo, D.; Innocenti, A.; Scozzafava, A.; Supuran, C.T. Carbonic anhydrase inhibitors: inhibition of cytosolic/tumor-associated isoforms I, II, and IX with iminodiacetic carboxylates/hydroxamates also incorporating benzenesulfonamide moieties. *Bioorg. Med. Chem. Lett*. **2007**, 17, 1538. (d) Supuran, C. T. Carbonic anhydrase inhibition/activation: trip of a scientist around the world in the search of novel chemotypes and drug targets. *Curr. Pharm. Des.* **2010**, 16, 3233.

[69] Dogne, J. M.; Hanson, J.; Supuran, C.; Pratico, D. Coxibs and cardiovascular side-effects: from light to shadow. *Curr. Pharm. Des.* **2006**, *12,* 8, 971-975.101. Knudsen, J. F.; Carlsson, U.; Hammarstrom, P.; Sokol, G. H.; Cantilena, L. R. Thecyclooxygenase-2 inhibitor celecoxib is a potent inhibitor of human carbonic anhydraseII. *Inflammation* **2004**, *28,* 5, 285-290.

[70] (a)Mocharla, V.P.; Colasson, B.; Lee, L.V.; Röper, S.; Sharpless, K.B.; Wong, C.H.; Kolb, H.C. In situ click chemistry: enzyme-generated inhibitors of carbonic anhydrase II. *Angew. Chem. Int. Ed. Engl*. **2004**, *44*, 116-120. (b) Wilkinson, B. L.;

Innocenti, A.; Vullo, D.; Supuran, C. T.; Poulsen, S.A. Inhibition of carbonic anahydrases with glycosyltriazole benzene sulfonamides. *J. Med. Chem.* **2008**, *51*, 1945-1953. (c) Wilkinson, B.L.; Bornaghi, L.F.; Houston, T.A.; Innocenti, A.; Vullo, D.; Supuran, C.T.; Poulsen, S.A. Carbonic anhydrase inhibitors: Inhibition of isozymes I, II and IX with triazole-linked O-glycosides of benzene sulfonamides. *J. Med. Chem*. **2007**, *50*, 1651-1657. (d) Morris, J. C.; Chiche, J.; Grellier, C.; Lopez, M.; Bornaghi, L. F.; Maresca, A.; Supuran, C. T.; Pouyssegur, J.; Poulsen, S.A. Targeting hypoxic tumor cell viability with carbohydrate-based carbonic anhydrase IX and XII inhibitors. *J. Med. Chem.* **2011,** *54*, 6905-6918.

[71] Saada, M.C.; Ombouma, J.; Montero, J.L.; Supuran, C.T.; Winum, J.Y. Thiol-ene click chemistry for the synthesis of highly effective glycosyl sulfonamide carbonic anhydrase inhibitors. *Chem. Commun*. *(Camb.)* **2013**, *49*, 5699-5701.

[72] Leitans, J.; Sprudza, A.; Tanc, M.; Vozny, I.; Zalubovskis, R.; Tars, K.; Supuran, C.T. 5-Substituted-(1,2,3-triazol-4-yl)thiophene-2-sulfonamides strongly inhibit human carbonic anhydrases I, II, IX and XII: solution and X-ray crystallographic studies. *Bioorg. Med. Chem.* **2013**, *21*, 5130-5138.

[73] Pala, N.; Micheletto, L.; Sechi, M.; Aggarwal, M.; Carta, F.; McKenna, R.; Supuran, C.T. Carbonic Anhydrase Inhibition with Benzene Sulfonamides and Tetrafluorobenzenesulfonamides Obtained via Click Chemistry. *ACS Med. Chem. Lett*. **2014**, 5, 927-30.

[74] Carta, F.; Garaj, V.; Maresca, A.; Wagner, J.; Avvaru, B. S.;Robbins, A. H.; Scozzafava, A.; McKenna, R.; Supuran, C. T. Sulfonamides incorporating 1,3,5-triazine moieties selectively andpotently inhibit carbonic anhydrase transmembrane isoforms IX, XIIand XIV over cytosolic isoforms I and II: solution and X-ray crystallographic studies. *Bioorg. Med. Chem*. **2011**, 19, 3105−3119. (c) Biswas, S.; Aggarwal, M.; Guzel, O.; Scozzafava, A.; McKenna,R.; Supuran, C. T. Conformational variability of different sulfonamide inhibitors with thienyl-acetamido moieties attributes to differential binding in the active site of

cytosolic human carbonic anhydrase isoforms. *Bioorg. Med. Chem.* **2011**, 19, 3732−3738.

[75] (a)Scozzafava, A.; Menabuoni, L.; Mincione, F.; Briganti, F.; Mincione, G.; Supuran, C. T. Carbonic anhydrase inhibitors: Perfluoroalkyl/aryl-substituted derivatives of aromatic/heterocyclicsulfonamides as topical intraocular pressure lowering agents withprolonged duration of action. *J. Med. Chem*. **2000**, 43, 4542−4551. (b) Avvaru, B. S.; Wagner, J. M.; Maresca, A.; Scozzafava, A.;Robbins, A. H.; Supuran, C. T.; McKenna, R. Carbonic anhydrase inhibitors. The X-ray crystal structure of human isoform II in adduct with an adamantyl analogue of acetazolamide resides in a new hydrophobic binding pocket. *Bioorg. Med. Chem. Lett.* **2010**, 20, 4376−4381. (c) Di Fiore, A.; Maresca, A.; Alterio, V.; Supuran, C. T.; DeSimone, G. Carbonic anhydrase inhibitors: X-ray crystallographic studies for the binding of N-substituted benzenesulfonamides tohuman isoform II. *Chem. Commun*. **2011**, 47, 11636−11638. (d) Pinard, M. A.; Boone, C. D.; Rife, B. D.; Supuran, C. T.;McKenna, R. Structural study of interaction between brinzolamide anddorzolamide inhibition of human carbonic anhydrases. *Bioorg. Med. Chem.* **2013**, 21, 7210−7215. (e) Marini, A. M.; Maresca, A.; Aggarwal, M.; Nencetti, S.;Orlandini, E.; Da Settimo, F.; Salerno, S.; Simorini, F.; La Motta, C.;Taliani, S.; Nuti, E.; McKenna, R.; Rossello, A.; Supuran, C.T. Tricyclic sulfonamides incorporating benzothiopyrano[4,3-c]pyrazoleand pyridothiopyrano[4,3-c]pyrazole effectively inhibit α- and β-carbonic anhydrase: X-ray crystallography and solution investigationson 15 isoforms. *J. Med. Chem.* **2012**, 55, 9619−9629.

[76] Pala, N.; Dallocchio, R.; Dessi, A.; Brancale, A.; Carta, F.; Ihm, S.; Maresca, A.; Sechi, M., Supuran, C.T. Virtual screening-driven identification of human carbonic anhydrase inhibitors incorporating an original, new pharmacophore. *Bioorg. Med. Chem. Lett*. **2011**, 21, 2515–2520.

[77] Ripphausen, P.; Nisius, B.; Peltason, L.; Bajorath, J. Quo vadis, virtual

screening? A comprehensive survey of prospective applications. *J. Med. Chem.* **2010**, 53, 8461.

[78] Barchi, J.J.Jr.; Neamati, N. New paradigms in drug design and discovery *Curr. Top. Med. Chem*. **2002**, 2, 211.

[79] Tedder, J.M. *Chem. Rev.* **1955**, *55*, 787–827.

[80] Kamitori, Y.; Hojo, M.; Mauda, R.; Fujitani, T.M Ohara, S.; Yokoyama, T. Electrophilic Substitution at Azomethine Carbon Atoms. Reaction of Aromatic Aldehyde Hydrazones with Trifluoroacetic Anhydride *J. Org. Chem. **1988**, 53, 129-335.*

[81] Snider, B.B.; Conn, R.S.E.; Sealfon, S. Reactions of Phenylhydrazones with Electron-. Deficient Alkenes. *J. Org. Chem.* **1979**, 44, 218.

[82] Grundemann, E.; Brehme, R.; Nikolajewski, H. E. *J. Prakt. Chem.* **1982, 324, 575** and references cited therein.

[83] Kallio, H.; Martinez, A. R.; Hilvo, M.; Hyrskyluoto, A.; Parkkila, S*. J. Canc. Molec*. **2010**, 5, 73-78.

[84] McDonald, P.C.; Winum, J.Y.; Supuran, C.T.; Dedhar, S. Recent Developments in Targeting Carbonic Anhydrase IX for Cancer Therapeutics. *Oncotarget* **2012**, 3, 84–97.

[85] Supuran, C.T. Inhibition of carbonic anhydrase IX as a novel anticancer mechanism. *World J. Clin. Oncol.* **2012**, 3, 98-103.

[86] (a) Parkkila, S.; Parkkila, A.K.; Saarnio, J.; Kivela, J.; Karttunen, T.J.; Kaunisto, K.; Waheed, A.; Sly, W.S.; Tureci, O.; Virtanen, I.; Rajaniemi, H. Expression of the membrane-associated carbonic anhydrase isozyme XII in the human kidney and renal tumors. *J. Histochem. Cytochem.* **2000***,* 48, 1601-1608. (b) Kivela, A.; Parkkila, S.; Saarnio, J.; Karttunen, T.J.; Kivela, J.; Parkkila, A.K.; Waheed, A.; Sly, W.S.; Grubb, J.H.; Shah, G.; Tureci, O.; Rajaniemi, H. Expression of a novel transmembrane carbonic anhydrase

isozyme XII in normal human gut and colorectal tumors. *Am. J. Pathol.* **2000**, 156, 577-584. (c) Kivela, A.J.; Parkkila, S.; Saarnio, J.; Karttunen, T.J.; Kivela, J.; Parkkila, A.K.; Bartosova, M.; Mucha, V.; Novak, M.; Waheed, A.; Sly, W.S.; Rajaniemi, H.; Pastorekova, S.; Pastorek, J. Expression of von Hippel-Lindau tumor suppressor and tumor-associated carbonic anhydrases IX and XII in normal and neoplastic colorectal mucosa. *World J. Gastroenterol.* **2005**, 11, 2616-2625. (d) Kivela, A.J.; Parkkila, S.; Saarnio, J.; Karttunen, T.J.; Kivela, J.; Parkkila, A.K.; Pastorekova, S.; Pastorek, J.; Waheed, A.; Sly, W.S.; Rajaniemi, H. Expression of transmembrane carbonic anhydrase isoenzymesIX and XII in normal human pancreas and pancreatic tumours. *Histochem. Cell. Biol.* **2000**, 114: 197-204.

[87]Sechi, M.; Innocenti, A.; Pala, N.; Rogolino, D.; Carcelli, M.; Scozzafava, A.; Supuran, C.T. Inhibition of α-class cytosolic human carbonic anhydrases I, II, IX and XII, and β-class fungal enzymes by carboxylic acids and their derivatives: new isoform-I selective nanomolar inhibitors. *Bioorg. Med. Chem. Lett*. **2012**, 22, 5801–5806.

[88] De Simone, G.; Supuran, C.T. (In)organic anions as carbonic anhydrase inhibitors. *J. Inorg. Biochem*. **2012**, 111, 117.

[89] Sechi, M.; Derudas, M.; Dallocchio, R.; Dessì, A.; Bacchi, A.; Sannia, L.; Carta, F.; Palomba, M.; Ragab, O.; Chan, C.; Shoemaker, R.; Sei, S.; Dayam, R.; Neamati, N. Design and synthesis of novel indole beta-diketo acid derivatives as HIV-1 integrase inhibitors. *J. Med. Chem.* **2004**, 47, 5298-5310.

[90] Zhang, D.; Wang, G.; Tan, C.; Xu, W.; Pei, Y.; Huo, L. Synthesis and biological evaluation of 3-(1H-indol-3-yl)pyrazole-5-carboxylic acid derivatives. *Arch. Pharm. Res.* **2011**, 34, 343-355.

[91] Okail, M.A. Cobalt chloride, a chemical inducer of hypoxia-inducible factor-1a in U251 human glioblastoma cell line. Jour. Saudi Chem. Soc. 2010, 14, 197–201.

[92]Adamczyk-Woźniak A, Cyrański MK, Żubrowska A, Sporzyński A.Benzoxaboroles—Old compounds with new applications. *J. Organomet. Chem*, **2009**, 694: 3533–3541.

[93] (a)Liu, C. T.; Tomshon, J.W.; Benkovic, S.J. The unique chemistry of benzoxaboroles: current and emerging applications in biotechnology and therapeutic treatments. *Bioorganic & Medicinal Chemistry* **2014**, 22, 4462-4473.; (b) Zhang, J.; Zhu, M.Y.; Lin, Y.N.; Zhou, H.C. The synthesis of benzoxaboroles and their application in medicinal chemistry. *Science China* **2013**, 56, 1372–1381.

[94] Lennarz, W.J.; Snyder, H.R. Arylboronic acids. IV. Reactions of boronophthalide. *J. Am. Chem. Soc*. **1960**, 82, 2172–2175.

[95] Akama, T.; Baker, S.J.; Zhang, Y.K.; Hernandez, V.; Zhou, H.C.; Sanders, V.; Freund, Y.; Kimura, R.; Maples, K.R.; Plattner, J.J. Discovery and structure-activity study of a novel benzoxaborole anti-inflammatory agent (AN2728) for the potential topical treatment of psoriasis and atopicdermatitis. *Bioorg. Med. Chem. Lett.* **2009**, 19, 2129–2132.

[96] Ding, C.Z.; Zhang, Y.K.; Li, X.F.; Liu, Y.; Zhang, S. M.; Zhou, Y. S.; Plattner, J.J.; Baker, S. J.; Liu, L.A.; Duan, M.S.; Jarvest, R.L.; Ji, J.J.; Kazmierski, W. M.; Tallant, M.D.; Wright, L.L.; Smith, G.K.; Crosby, R.M.; Wang, A.A.; Ni, Z.J.; Zou, W.X.; Wright, J. Synthesis and biological evaluations ofP4-benzoxaborole-substituted macrocyclic inhibitors of HCV NS3protease. *Bioorg. Med. Chem. Lett.* **2010**, 20,

7317–7322.

[97] Hall, D.G.; Pal, A.; Bérubé, M. Design, synthesis, and screening of a library of peptidyl bis(boroxoles) as oligosaccharide receptors in water: identification of a receptor for the tumor marker TF-antigen disaccharide. *Angew. Chem. Int. Ed*., **2010**, 49, 1492-1495.

[98] Li, H.Y.; Wang, H.Y.; Liu, Y.C.; Liu, Z. A benzoboroxole-functionalized monolithiccolumn for the selective enrichment and separation of cis-diol containing biomolecules. *Chem. Commun*. **2012**, 48, 4115-4117.

[99] (a)Adamczyk-Wozniak, A.; Cyranski, M.K.; Zubrowska, A.; Sporzynski, A. Benzoxaboroles-Old compounds with new applications. *J. Organomet. Chem.* **2009**, 694, 3533-3541; (b) Baker, S.J.; Tomsho, J.W.; Benkovic, S.J. Boron-containing inhibitors of synthetases. *Chem. Soc. Rev.* **2011**, 40, 4279-4285; (c) Adamczyk-Wozniak, A.; Komarovska-Porokhnyavets, O.; Misterkiewicz, B.; Novikov, V.P.; Sporzynski, A. Biological activity of selected boronic acids and their derivatives. *Appl. Organomet. Chem*. **2012**, 26, 390-393. (d) Rock, F.L.; Mao, W.; Yaremchuk, A.; Tukalo, M.; Crepin, T.; Zhou, H.; Zhang, Y.K.; Hernandez, V.; Akama, T.; Baker, S.J.; Plattner, J.J. Shapiro, L.; Martinis, S.A.; Benkovic, S.J.; Cusack, S.; Alley, M.R. An antifungal agent inhibits an aminoacyl-tRNA synthetase by trappingtRNA in the editing site. *Science*. **2007**, 316, 1759-1761. (e) Hall, D. G. Boronic Acids: Preparation and Applications in Organic Synthesis, Medicineand Materials, Wiley-VCH Verlag & Co., Weinheim, **2011**. (f) Zhang, J.; Zhu, M.; Lin, Y.; Zhou, H. The synthesis of benzoxaboroles and their applicationsin medicinal chemistry. *Science China* **2013**, 56, 1372-1381.

[100] (a)D. Ding, Q. Meng, G. Gao, Y. Zhao, Q. Wang, B. Nare, R. Jacobs, F. Rock, M. R. Alley, Plattner, J.J.; Chen, G.; Li, D.; Zhou, H. Design, synthesis, and structure-activity relationship of Trypanosoma brucei leucyl-tRNA synthetase inhibitors as antitrypanosomal agents. *J. Med. Chem.* **2011**, 54, 1276-1287. (b) Jacobs, R.T.; Plattner, J.J.; Nare, B.; Wring, S.A.; Chen, D.T.; Freund, Y.; Gaukel, E.G.; Orr,

M.D.; Perales, J.B.; Jenks, M.; Noe, R.A.; Sligar, J.M.; Zhang, Y.K.; Bacchi, C.J.; Yarlett, N.; Don, R. Benzoxaboroles: a new class of potential drugs for human African trypanosomiasis. *Future Med. Chem*. **2011**, 3, 1259-1278. (c) Jacobs, R.T.; Nare, B.; Wring, S.A.; Orr, M.D.; Chen, D.; Sligar, J.M.; Jenks, M.X.; Noe, R.A.; Bowling, T.S.; Mercer, L.T.; Rewerts, C.; Gaukel, E.; Owens, J.; Parham, R.; Randolph, R.; Beaudet, B.; Bacchi, C.J.; Yarlett, N.; Plattner, J.J.; Freund, Y.; Ding, C.; Akama, T.; Zhang, Y.K.; Brun, R.; Kaiser, M.; Scandale, I.; Don, R. SCYX-7158, an Orally-Active Benzoxaborole for the Treatment of Stage 2 Human African Trypanosomiasis. *PLoS Negl. Trop. Dis.* **2011**, 5, 1151.

[101] Anacor Pharmaceuticals, http://www.anacor.com/ (Feb 27, **2014**).

[102] (a) Zhang, Y.K.; Plattner, J.J.; Freund, Y.R.; Easom, E.E.; Zhou, Y.; Ye, L.; Zhou, H.; Waterson, D.; Gamo, F.J.; Sanz, L.M., Ge, M.; Li, Z.; Li, L.; Wang, H.; Cui, H. Benzoxaborole antimalarial agents. Part 2: Discovery of fluoro-substituted 7-(2-carboxyethyl)-1,3-dihydro-1-hydroxy-2,1-benzoxaboroles. *Bioorg. Med. Chem. Lett*. **2012**, 22, 1299-1307.

[103] Data not published.

[104] Zhengyan F., Jiangpeng H., Aiping T., Yongmei X., Yuquan W. A Convenient and Efficient Synthesis of Dipeptidyl Benzoxaboroles and Their Peptidomimetics. Synthesis **2013**, 45, 2843–2852.

[105] Yasui, Y.; Tsuchida, S.; Miyabe, H.; Takemoto, Y. One-Pot Amidation of Olefins through Pd-Catalyzed Coupling of Alkylboranes and Carbamoyl Chlorides *J. Org. Chem.* **2007**, 72, 5898-5900.

[106] White, J.M.; Tunoori, A.R.; Turunen, B.J.; Georg, G.I. [Bis(2-methoxyethyl)amino]sulfur Trifluoride, the Deoxo-Fluor Reagent: Application toward One-Flask Transformations of Carboxylic Acids to Amides. *J. Org. Chem.* **2004**, 69, 2573-2576.

[107] Sawant, D.N.; Wagh, Y.S.; Bhatte, K.D.; Bhanage, B.M. Palladium-Catalyzed

Carbon-Monoxide-Free Aminocarbonylation of Aryl Halides Using N-Substituted Formamides as an Amide Source. *J. Org. Chem.* **2011**, 76, 5489-5494.

[108] Shroeder, N.; Wencel-Delord, J.; Glorius, F. High-yielding, versatile, and practical [Rh(III)Cp*]-catalyzed ortho bromination and iodination of arenes. *J. Am. Chem. Soc.* **2012**, 134, 8298-8301.

[109] Ekoue-Kovi, K.; Wolf, C. One-pot oxidative esterification and amidation of aldehydes. *Org. Lett*. **2007**, 9, 3429-3432.

[110] Bahrami, K.; Khodaei, M.M.; Tajik, M. Trimethylsilyl Chloride Promoted Selective Desulfurization of Thiocarbonyls to Carbonyls with Hydrogen Peroxide. *Synthesis* **2010**, 4282-4286.

[111] Angelastro, M.R.; Baugh, L.E.; Bey, P.; Burkhart, J. P.; Chen, T.M.; Durham S.L.; Hare, C.M.; Huber, E. W.; Janusz, M. J. Inhibition of human neutrophil elastase with peptidyl electrophilic ketones. 2. Orally active PG-Val-Pro-Val pentafluoroethyl ketones. *J. Med. Chem.* **1994**, 37, 4538-4553.

[112] Fujita, H.; Kanai, T.; Imai, S. Novel five-membered ring compound EP Patent 2272835A1, **2011.**

[113] Zhou, S.; Junge, K.; Addis, D.; Das, S.; Beller, M. A Convenient and General Iron-Catalyzed Reduction of Amides to Amines. *Angew. Chem. Int. Ed. Engl.* **2009**, 48, 9507-9510.

[114] Das, S; Join, B.; Junge, K.; Beller, M. A general and selective copper-catalyzed reduction of secondary amides. *Chem. Commun.* **2012**, 48, 2683-2685.

[115] Wu, X.; Larhed, M. Microwave-enhanced aminocarbonylations in water. *Org. Lett*. **2005**, 7, 3327-3329.

[116] Kamitori, Y.; Hojo, M.; Msuda, R.; Yoshida, T.; Ohara, S.; Yamada, K.; Yoshikawa, N. Electrophilic Substitution Reaction at Azomethine Carbon Atom. Acylation of Aliphatic Aldehyde Hydrazones *J. Org. Chem.* **1988**, 53, 519.

[117] Chen, D.; Orr, M.; Sligar, J.; Jacobs, R.; Plattner, J. *J. Assignee Anacor Pharmaceuticals*, Inc., USA **2011**.

[118] Pacchiano, F.; Aggarwal, M.; Avvaru, B.S.; Robbins, A.H.; Scozzafava, A.; McKenna, R.; Supuran, C.T. Selective hydrophobic pocket binding observed within the carbonic anhydrase II active site accommodate different 4-substituted-ureido-benzenesulfonamides and correlate to inhibitor potency. *Chem Commun (Camb).* **2010**, *46*, 8371-8373.

[119] Otwinowski, Z.; Minor, W. Processing of x-ray diffraction data collected in oscillation mode, *Methods Enzymol.* **1997**, *276*, 307–326.

[120] Avvaru, B. S.; Kim C. U.; Sippel K. H.; Gruner S. M.; Agbandje-McKenna M.; Silverman D. N.; McKenna R. A short, strong hydrogen bond in the active site of human carbonic anhydrase II. *Biochemistry* **2010**, *49*, 249-251

[121] Adams, P.D.; Afonine, P.V.; Bunkóczi, G.; Chen, V.B.; Davis, I.W.; Echols, N.; Headd, J.J.; Hung, L.W.; Kapral, G.J.; Grosse-Kunstleve, R.W.; McCoy, A.J.; Moriarty, N.W.; Oeffner, R.; Read, R.J.; Richardson, D.C.; Richardson, J.S.; Terwilliger, T.C.; Zwart, P.H PHENIX: a comprehensive Python-based system for macromolecular structure solution. *Acta Cryst. D* **2010**, *66*, 213-221.

[122] Brunger, A. T. Free R value: a novel statistical quantity for assessing the accuracy of crystal structures. *Nature* **1992**, *355*, 472-475.

[123] Emsley, P.; Cowtan, K. Coot: model-building tools for molecular graphics, *Acta Crystallogr. D* **2004**, *60*, 2126–2132.

[124] Laskowski, R. A.; MacArthur, M. W.; Moss, D. S.; Thornton, J. M. PROCHECK: a program to check the stereochemical quality of protein structures, *J. Appl. Cryst.* **1993**, *26*, 283–291.

[125] The PyMOL Molecular Graphics System, Version 1.2r3pre, Schrödinger, LLC.

[126] Khalifah, R. G. The Carbon Dioxide Hydration Activity of Carbonic Anhydrase. I. Stop-Flow Kinetic Studies on the Native Human Isoenzymes B and C. *J. Biol.*

Chem. **1971**, *246*, 2561-2573.

[127] (a) Neri, D.; Supuran, C. T. Interfering with pH Regulation in Tumors as a Therapeutic Strategy. *Nat. Rev. Drug Discov.* **2011**, *10*, 767-777. (b) Supuran, C.T. Carbonic anhydrase inhibitors and activators for novel therapeutic applications. *Future Med. Chem*. **2011**, *3*, 1165-1180.

[128] (a) Neri, D.; Supuran, C. T. Interfering with pH Regulation in Tumors as a Therapeutic Strategy. *Nat. Rev. Drug Discov.* **2011**, *10*, 767-777. (b) Supuran, C.T.; Mincione, F.; Scozzafava, A.; Briganti, F.; Mincione, G.; Ilies, M.A. Carbonic anhydrase inhibitors. Part 52. Metal complexes of heterocyclic sulfonamides: A new class of strong topical intraocular pressure-lowering agents with potential use as antiglaucoma drugs. *Eur. J. Med. Chem.* **1998**, *33*, 247-254.

Ringraziamenti

Desidero esprimere un sincero ringraziamento al Dott. Mario Sechi, Tutore di questo mio Dottorato, per i consigli, espressi sempre con grande competenza e rigore scientifico, e per l'aiuto e il sostegno che mi ha sempre offerto in ogni fase del lavoro sperimentale e durante la stesura di questa Tesi.

Ringrazio la Dott.ssa Lidia De Luca, Tutore della prima parte di questo importante percorso, per avermi dato la possibilità di svolgere una parte del Dottorato presso il suo Laboratorio, inserendomi nelle sue linee di ricerca che mi hanno stimolato per il tempo in cui me ne sono occupata.

Desidero anche ringraziare coloro che hanno contribuito alla realizzazione della presente tesi:

Il Dott. Pala, per avermi dedicato tempo prezioso, insegnandomi tecniche di lavoro che non conoscevo, e discutendo con me le problematiche attinenti ai vari progetti di ricerca per trovare risposte ai miei interrogativi.

Il Prof. Jean-Yves Winum dell'Institute des Biomoleculés Max Mousseron dell'Università di Montpellier II in Francia per avermi accolto nel suo laboratorio e avermi dato la possibilità di svolgere il periodo di soggiorno all'estero, dal quale è nata un'interessante collaborazione scientifica tra gruppi di ricerca;

Il Prof Claudiu Supuran e la Dott.ssa Daniel Vullo dell'Università di Firenze per i saggi enzimatici;

La Dott.ssa Dominga Rogolino dell'Università di Parma per gli esperimenti di spettroscopia di massa;

I Sig.ri Alessandro Dessì e Roberto Dallocchio per la loro disponibilità per i lavori di *Molecular Modelling*;

Il Dott. Ciro Iaccarino del Dipartimento di Scienze Biomediche dell'Università di Sassari per i saggi di citotossicità;

Il Prof. Robert McKenna dell'Università della Florida per gli esperimenti di cristallografia ai raggi X;

Un ringraziamento speciale va ai colleghi e amici che hanno speso parte del proprio tempo per leggere e discutere con me le bozze del lavoro.

Un ringraziamento anche a Irene e Simona, che mi hanno accolto a Montpellier, rendendosi parte di un'esperienza che non scorderò mai.

Ringrazio ancora i miei colleghi Manuel, Caterina L., Giammario, Silvia, Suvi, Salvatore e Caterina C. con i quali ho condiviso questi tre anni di dottorato. Con la vostra compagnia dalla mattina alla sera, dal pranzo alla cena, dal primo al dolce, dai caffè alle torte e gossip su Grey's Anatomy, avete addolcito la pillola del Dottorato.

Esprimo infine il mio ringraziamento più sentito a Pietro, perché questo Dottorato ha assorbito tutte le mie energie e la mia mente per tutto il tempo, e chi ci ha rimesso più di tutti, è lui. Lo ringrazio quindi per la sua pazienza, per la comprensione, per la voglia di rendersi utile in ogni modo e ad ogni costo, per il suo incoraggiamento costante e disinteressato, per la sua stima e il suo apprezzamento.